THE FLORIDA STATE UNIVERSITY

COLLEGE OF ARTS AND SCIENCES

ENERGY SOURCES FOR SOME TROPICAL WAVES

By
JACOB PADRO

A Dissertation submitted to
the Department of Meteorology
in partial fulfillment of the
requirements for the degree of
Doctor of Philosophy

Approved:

James J. O'Brien
Professor Directing Dissertation

T. N. Krishnamurti

C. L. Jordan

Robert C. Harriss

December, 1971

December, 1971

ABSTRACT

A non-linear, three-dimensional spectral model on a β-plane is developed to study the relative roles of some energy sources for tropical waves. In particular, both the north-south shear of the zonal wind and CISK (conditional instability of the second kind) are included. Energy exchanges, growth rates of waves and pressure levels of maximum wave activity in the presence of various specified vertical profiles of latent heat are studied. Radiative effects are included in the form of Newtonian cooling; they play a minor role. Latent heat is parameterized in terms of boundary layer convergence of moisture. Dissipation is also included.

The quasi-geostrophic model includes four layers, three in the troposphere and one in the stratosphere. The top of the boundary layer is taken at the 900-mb level and its effect is described by frictionally induced vertical velocity and surface dissipation. The initial state is an idealized form of observations taken in the Marshall Islands.

Important results show that when latent heat release decreases with height and is maximum at low tropospheric levels, the eddies initially are generated and maintained barotropically and then CISK assumes a dominating role. When heat release increases with height, whether or not it is large at the lower troposphere, CISK dominates at all stages of the wave development; the barotropic mechanism, however, is still important.

of the wave development; the barotropic mechanism, however, is still important.

In the absence of sources and sinks, the most unstable wave is of scale 3000-km with an initial growth rate in e-folding time of 5.5 days. This is found at the lower troposphere, while the larger scales of 5000-km and 10000-km dominate at the upper troposphere. These results are, in some important ways, modified when various vertical profiles of latent heat are applied. In particular, the initial growth rate of the low tropospheric 3000-km wave in e-folding time is three days when latent heat release is maximum at the low levels.

ACKNOWLEDGMENTS

I would like to acknowledge assistance and encouragement from Professor J. J. O'Brien throughout the preparation of this manuscript. Professors T. N. Krishnamurti and C. L. Jordan provided useful aid in some phases of this research. Expert typing is the product of Mrs. Janina Richards and drafting of the diagrams is the contribution of Mr. Dewey L. Rudd.

Financial support for this work was provided by the Department of Defense THEMIS Contract No.DAAB07-69-C-0062.

All computations were performed at the Florida State University Computing Center.

TABLE OF CONTENTS

REFERENCES	101
VITA	104

LIST OF TABLES

LIST OF ILLUSTRATIONS

LIST OF ILLUSTRATIONS - Continued

CHAPTER I

INTRODUCTION

The present investigation of energy sources and some properties of waves in the tropics is mainly theoretical and has been motivated by a number of recent theoretical and numerical studies on tropical motions. The objective is to use a theoretical model which can combine a number of possible energy sources for tropical disturbances and study their relative roles under imposed time-dependent external sources and sinks. First, a review of the relevant background will be presented.

Essential problems in the tropics deal with the explanation of the mean zonal motions (e.g., easterlies, ITCZ, jets) and the generation and maintenance of tropical asymmetries on all scales. The latter, no doubt, interacts non-linearly with the zonal mean motion and quite possibly with mid-latitude systems. Dickinson (1971), in a theoretical model, studied the maintenance of the zonal wind distribution by momentum and heat sources. He also explained some aspects of the coupling between the tropical and extratropical symmetric circulations. Charney (1968), on the other hand, concentrated on the generation and maintenance of the zonally symmetric ITCZ which is the primary source for the tropical Hadley circulation. He attributed the source of energy to latent heat release in narrow zones which parallel the equator and are about 5° to 15° away from it.

Concerning tropical waves, four possibilities of energy sources exist: (1) baroclinic instability which depends upon the vertical shear

Concerning tropical waves, four possibilities of energy sources exist: (1) baroclinic instability which depends upon the vertical shear of the zonal wind, (2) barotropic instability of the zonal easterlies

which depends upon the north-south shear of the zonal wind, (3) CISK mechanism which depends upon the release of latent heat and (4) forcing from mid-latitude motions. No theoretical model has yet been constructed to include all these mechanisms in an organized manner and study their relative importance in the evolution of tropical waves. However, progress has been made in numerical simulations of tropical flows which include some or all of these mechanisms (see Manabe et al., 1970; Krishnamurti, 1969; and Pike, 1971). Also, theories concerning the possibility of each of these sources in exciting some tropical waves have been developed.

Barotropic exchange of energy between the zonal easterlies and the waves has been suggested quite early by Palmer (1951) and Yanai (1961), but a theoretical linearized model was not presented until 1969 by Nitta and Yanai. They showed that small perturbations superimposed upon a realistic profile of surface zonal easterlies can be more unstable than waves embedded in the westerlies and there exists no upper limit to the wavelength scale which can become unstable (see Kuo, 1949). The most unstable wave with respect to a mean zonal current in the Western Pacific has a wavelength of 2000 km and an e-folding growth rate of 5.2 days. No CISK mechanism was allowed in this study.

The possibility of exciting tropical waves by latent heat has been demonstrated by Yamasaki (1969) and later by Holton (1971). In a multi-layer linearized model with fixed vertical shear of the zonal wind and various vertical latent heat profiles, Yamasaki (1969) has demonstrated the possibility of exciting waves of 2000 to 4000 km and waves of 6000 to 12000 km. The first group is induced by the combined effect

of 6000 to 12000 km. The first group is induced by the combined effect

of heat, vertical wind shear and surface friction. The second group of

larger scale waves depends largely upon heat released in the upper troposphere and can exist in the absence of vertical wind shear. The amplitude of the larger scale wave is largest in the lower stratosphere. In the smaller wavelength group he finds that for vertical heat profiles in which heat release is small in the lower troposphere and large in the upper troposphere, a wave of 2000 to 3000 km with a steering level (ES) is excited and it can grow with little vertical wind shear. In contrast to mode (ES), a mode without a steering level (E) has a smaller growth rate for large values of vertical wind shear. The model is two-dimensional and excludes a barotropic mechanism.

The possibility of forcing from extratropical motions has been presented by Mak (1969). A relative comparison of this mechanism with any of the above has not yet been made.

In an effort to study the role of asymmetries upon the zonally symmetric ITCZ of Charney's (1968) model, Bates (1970) devised a two-level non-linear model. He pointed out the importance of waves in a description of the general circulation. In particular, he introduced the possibility of the existence of a correlation between the perturbation part of the latent heat parameter η' and the perturbation Ekman vertical velocity ω' (i.e., $\overline{\eta'\omega'}$). The correlation of the zonal asymmetries η' and ω' can maintain the north-south shear of the zonal current which in turn allows for barotropic exchange of energy. He found the most unstable wave to have a wavelength of 2000 km and an e-folding growth rate of 3 days. In the two-level model, it was not possible to study the effect of various vertical profiles of latent heat upon the stability of the various scales. Neither was it possible to study the dependence of wave instability at different vertical regions in the troposphere.

In the present model, three sources of energy will be studied in a non-linear four-layer model. These consist of the barotropic and CISK mechanisms in the presence of time-dependent vertical shear of the zonal wind which evolves with the dynamics of the model. The relative importance of the north-south shear of the zonal wind and of latent heat release in generating and maintaining tropical waves will be discussed. Most unstable waves and their growth rates will be investigated at various pressure levels. These will be done in a number of experiments which exclude sources and sinks and some which include different vertical profiles of latent heat. Wave-wave interaction is also allowed.

Results from the present investigation apply only to regions in the tropics which possess similar initial basic structure as selected here. To describe such a structure, a brief review of observational studies in the tropics will be given.

Observations in the tropics are limited to certain areas. Sufficient data have been accumulated in the western parts of the Pacific and Atlantic and some studies were done with data from the Caribbean Islands and the Marshall Islands. Two approaches of analysis have been used and the results do not always agree. The best known synoptic models are the equatorial wave model of Palmer (1952) and easterly wave model of Riehl (1954). Both Palmer and Riehl concluded that the wavelength of tropical disturbances in the lower troposphere is about 2000 km and their westward phase speed is 13 kt. The maximum amplitude of the easterly wave found by Riehl is found at about the 600 mb level. Using time series approaches, Wallace and Chang (1969) found the wavelength to be of scale 3000 km. Nitta (1970) and Yanai et al. (1968) found it to be 5000-6000 km in western

Pacific and 8000-10,000 in eastern Pacific. More observations are needed to resolve such disagreements. However, there is agreement that larger scale waves dominate at higher levels and smaller scale waves at the lower troposphere.

What types of basic (zonal) flows exist in the tropics which can become unstable with respect to perturbations? A number of these have been presented, but here we shall focus our efforts on the structure of the zonal wind and zonal potential temperature which are sometimes found in regions of the ITCZ (Nitta and Yanai, 1969; Pike, 1971).

Fig. 1a (Nitta and Yanai, 1969) illustrates an average latitudinal distribution of zonal velocity and absolute vorticity at the surface, 1000, 850, 700 and 600 mb levels for Marshall Islands during June 1958. At the surface and at the 1000 mb level, the gradient of absolute vorticity changes its sign at about 8°N and disturbances are expected to amplify barotropically at these levels.

Fig. 1b, taken from a numerical experiment by Pike (1971), shows the latitudinal temperature profile. Features of utmost importance are the maximum in temperature at about 8°N and the minimum at the equator, which is attributed to upwelling and vertical mixing in the ocean's surface layer. Saha (1971) and others before him have noticed a maximum sea surface temperature in the vicinity of the ITCZ and lower temperatures near the equator. Manabe et al. (1970) concluded from their numerical experiment that a continuous supply of energy from the warm sea surface influences the location and intensity of the ITCZ. Further details of an idealized initial state suitable for the present problem will be presented in a subsequent chapter.

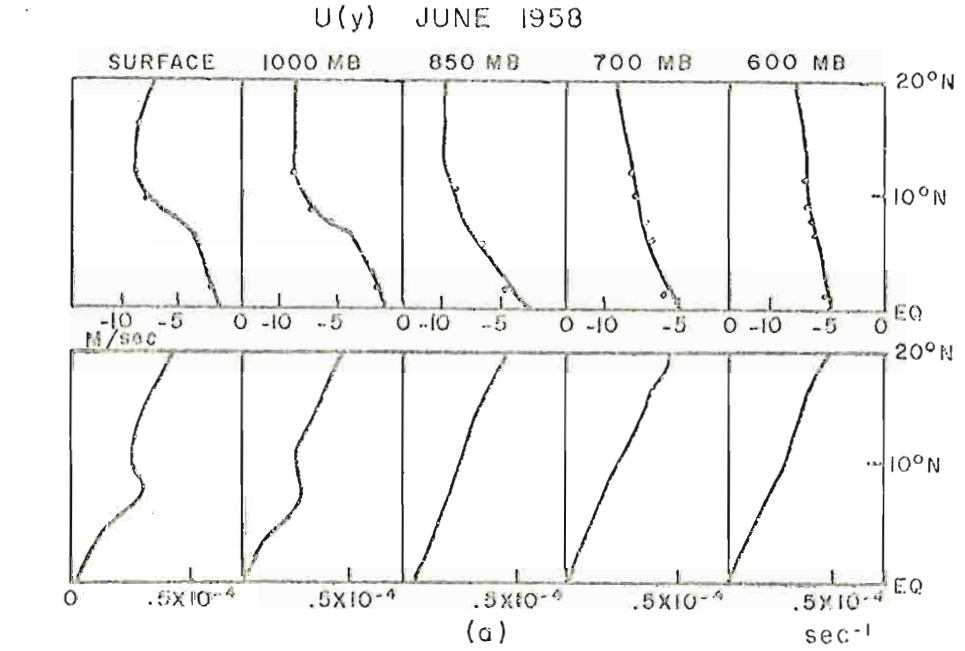

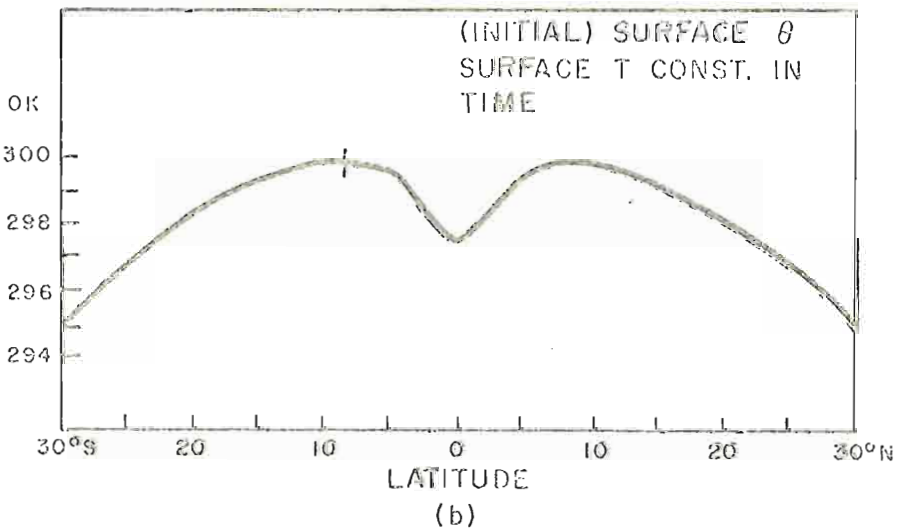

Fig. 1.-(a) The mean zonal current and the corresponding absolute vorticity observed over the Marshall Islands at various levels for June 1958 (Nitta and Yanai, 1959), (b) surface initial potential temperature profile, cold equator case II (Pike, 1971).

1958 (Nitta and Yanai, 1959), (b) surface initial potential temperature profile, cold equator case II (Pike, 1971).

CHAPTER II

THEORY

A quasi-geostrophic theory on a β-plane will be assumed to govern the motions of tropical disturbances. This balance is justified so long as the dynamics under consideration occur at latitudes sufficiently away from the equator. Validity of quasi-geostrophy is determined by a small Rossby number and a small ratio of north-south scale of motion to the planetary radius as explained by Phillips (1963). The theory is not adequate to explain properly the dynamics of the symmetric state or the maintenance of a narrow zonally symmetric ITCZ. Since our efforts will be focused upon the dynamics of the asymmetries in the basic state, the zonally symmetric basic state which will be selected here will be idealized to include the important energy sources which exist in the ITCZ. The location of the ITCZ and its detailed structure will not be studied.

When heating and dissipation are included, the governing equations take the form presented by Lorenz (1960):

vorticity equation,

$$\frac{\partial}{\partial t} \nabla^2\psi = - J (\psi, \nabla^2\psi + f) + f_0 \frac{\partial \omega}{\partial p} + A\nabla^4\psi - g\hat{k} \cdot \nabla x \frac{\partial \bar{\tau}}{\partial p} ; \qquad (1)$$

thermodynamic equation,

$$\frac{\partial \theta}{\partial t} = - J (\psi, \theta) + \sigma (P)\, \omega + \frac{1}{c_p} (P_0/p)^{\kappa} H ; \qquad (2)$$

$$\frac{\partial}{\partial t} \qquad c_p \qquad ; \qquad (2)$$

balance equation,

$$\nabla^2\theta = -\frac{p_0^{\kappa}}{c_p} f_0 \nabla^2 \frac{\partial \psi}{\partial p^{\kappa}} \quad . \tag{3}$$

An ω-equation will be subsequently presented (see Appendix). The static stability is a function of pressure only and is given by

$$\sigma = -\left(\frac{\partial \theta}{\partial P} \right)$$

This allows the use of available potential energy in place of potential energy. Definitions of other quantities are listed in Table 2 of Chapter IV. Typical summer values for σ are taken from Jordan (1958).

These equations are energetically consistent in the sense that the sum of available potential energy and kinetic energy is conserved. For a proper investigation of the basic state, a different balance of terms exists in the equations of motion where in particular the Coriolis parameter f must be kept variable everywhere it appears. This is of crucial importance in the generation and maintenance of a realistic zonally symmetric ITCZ (see Charney, 1969).

Using scale analysis concepts, Charney (1968) and Wallace (1971) have shown that the main balance in the thermodynamic equation exists between cooling by adiabatic ascent and warming by release of latent heat. Radiation plays a minor role. Holton (1971) has verified this in a linearized numerical model. It is with such notions that the present study will proceed. Krishnamurti (1971a) however, in a study of a more extensive area for the summer season in the tropics concludes from observations of 200-mb summer data that radiation can play a significant role. Frank (1970) in-

for the summer season in the tropics concludes from observations of 200-mb summer data that radiation can play a significant role. Frank (1970) in-

vestigated the maintenance of upper tropospheric cold cyclones and

speculated that radiational cooling in the cyclone center was important in order to convert potential energy to kinetic energy of the cyclone, i.e., for a direct circulation to occur.

The ω-equation, besides its importance in providing vertical-motion fields, serves the purpose of keeping the potential temperature field in quasi-geostrophic balance with the streamfunction field.

The vertical continuous structure of the atmosphere is replaced by a discrete number of layers; all variables and operators are subscripted with j increasing upward. The equations take the form

$$\frac{\partial}{\partial t}\nabla^2\psi_j = -J(\psi_j,\nabla^2\psi_j+f) + \frac{f_0}{(P_{j-1}-P_{j+1})}(\omega_{j-1}-\omega_{j+1}) + A\nabla^4\psi_j - g\hat{k}\cdot\nabla\times\frac{\bar{\tau}_{j-1}-\bar{\tau}_{j+1}}{(P_{j-1}-P_{j+1})}, \quad j = 1, 3, 5, 7; \tag{4}$$

$$\frac{\partial}{\partial t}\theta_j = -J(\psi_j,\theta_j) + \sigma_j\omega_j + \frac{1}{c_p}(P_0/P_j)^{\kappa}H_j, \quad j = 2, 4, 6; \tag{5}$$

$$\nabla^2\theta_j = -\frac{P_0^{\kappa}}{c_p}f_0\nabla^2\frac{(\psi_{j-1}-\psi_{j+1})}{(P_{j-1}^{\kappa}-P_{j+1}^{\kappa})}, \quad j = 2, 4, 6. \tag{6}$$

The streamfunctions for even j are assumed to be linear functions of pressure,

$$\psi_j = \tfrac{1}{2}(\psi_{j-1}+\psi_{j+1}), \quad j = 2;$$

$$\psi_j = \tfrac{1}{3}(2\psi_{j+1}+\psi_{j-1}), \quad j = 4, 6;$$

and $\psi_{-1} = \psi_9 = 0.$

and $\psi_{-1} = \psi_9 = 0.$

Parameterization of heating

The heating function is divided into a latent heat part H_L and radiation part H_R.

(i) Radiation is incorporated through Newton's law of cooling. This assumes the atmosphere to be in radiative equilibrium with the earth's surface which is taken to be a uniform ocean. Thus,

$$\frac{1}{c_p}(P_0/P_j)^{\kappa}H_R = h_j(\theta^*_j - \theta_j), \qquad j = 2, 4, 6;$$

where values for the radiative relaxation time are taken from Peng (1965) and are presented in Table 2 of Chapter IV. The forcing potential temperatures θ^* in radiative equilibrium are computed from a latitudinally varying sea-surface temperature in radiative equilibrium given in a formula by Charney (1969).

(ii) Latent heat is parameterized in a simple linear fashion after the ideas introduced by Ooyama (1969) in hurricane models. Rosenthal (1967) was the first to incorporate such parameterization in synoptic-scale studies of tropical disturbanes. In the present model we use

$$\frac{1}{c_p}(P_0/P_j)^{\kappa}H_L = -\sigma_j \eta_j \omega^*, \qquad j = 2, 4, 6;$$

where η_j has no horizontal variation, i.e., the heating is unconditional. This implies heating in regions of ascent and cooling in regions of descent and hence larger horizontal temperature gradients than would otherwise result. This can be reconciled by selecting regions of descent and hence larger horizontal temperature gradients than would otherwise result. This can be reconciled by selecting smaller values of η than have been used in other studies such as

Bates (1970). Thus, computations of available potential energy due to latent heat which depend upon horizontal temperature gradients can become meaningful. The time-independece of η_j is more serious because it does not include an inhibitive factor in the release of latent heat; i.e., when environmental temperature becomes that of the convective element, no more heat should be released. This limitation will not allow a proper investigation of the dissipative stages of tropical disturbances, but is not serious for many aspects of the growing stages. It also eliminates a source for the maintenance of the basic state which can become important in the study of the ITCZ (see the term $\overline{\eta'\omega^{*'}}$ in Bates, 1970).

The importance of linear heating depends most upon pumping of moisture from the Ekman boundary layer. This is done through an Ekman-suction formula derived by Charney and Eliassen (1949)

$$\omega^* = - g \rho_0 \frac{\sin 2\alpha}{f} \sqrt{\frac{A_V f_0}{2}} \nabla^2 \psi_1$$

where $\alpha = 22.5^\circ$, cross isobaric flow, $A_V = 10^5$ cm^2 sec^{-1}, kinematic eddy viscosity coefficient.

The convergence of moisture in the planetary boundary layer is proportional to the curl of the surface geostrophic wind stress. The largest amounts of moisture and potential buoyancy occur in the boundary layer and hence latent heat release depends largely upon suction of moisture through the top of the boundary layer.

We may remark that η is allowed to vary in the vertical. This is a key feature in studying energy changes of waves.

We may remark that η is allowed to vary in the vertical. This is a key feature in studying energy changes of waves.

Dissipation

(i) Surface friction is proportional to surface vorticity, i.e.,

$$\frac{g}{P_0 - P_2} \hat{k} \cdot \nabla x \, \bar{\tau}_0 = K_1 \nabla^2 \psi_1$$

K_1 is given in Table 2 of Chapter IV.

(ii) At higher levels, internal vertical dissipation is parameterized in the conventional manner.

$$\left(\frac{\partial \bar{\tau}}{\partial p} \right)_j = \mu_j \frac{\partial}{\partial p} \left(\frac{\partial \bar{v}}{\partial z} \right)_j = \mu_j \, g \, \rho_j \left(\frac{\partial^2 \bar{v}}{\partial p^2} \right)_j$$

where ρ_j is density of air at level j and is computed from the equation of state,

$$\rho = \frac{P}{RT}$$

and mean temperatures are selected following Peng (1965).

If $\bar{V}_j = k \times \nabla \psi_j$, then

$$g\hat{k} \cdot \nabla x \, \frac{(\bar{\tau}_{j-1} - \bar{\tau}_{j+1})}{(P_{j-1} - P_{j+1})} = K_{1,j} \nabla^2 (\psi_j - \psi_{j-2}) - K_{2,j} \nabla^2 (\psi_{j+2} - \psi_j),$$

$$j = 1, 3, 5, 7;$$

where $K_{2,j}$ is computed from μ_j, P_j, T_j, and μ_j is assumed to be inversely proportional to the static stability σ_j.

Also

$$K_{1,j} = K_{2,j+2} \frac{(P_{j+1} - P_{j+3})}{(P_{j-1} - P_{j+1})}$$

(iii) Horizontal diffusion is represented by $A \nabla^4 \psi_j$ and A is assumed to be independent of height.

The ω-equation can now be written in full, including dissipative and heating terms and in vertical finite-differenced form,

$$c_p\sigma_j \frac{(P_{j-1}^\kappa - P_{j+1}^\kappa)}{P_0^\kappa} \nabla^2\omega_j + f_0^2 \left[\frac{\omega_{j-2}}{(P_{j-2}-P_j)} - \frac{(P_{j-2}-P_{j+2})}{(P_{j-2}-P_j)(P_j-P_{j+2})}\omega_j + \frac{\omega_{j+2}}{(P_j-P_{j+2})}\right]$$

$$= f_0 \left| J(\psi_{j-1}, \nabla^2\psi_{j-1}) - J(\psi_{j+1}, \nabla^2\psi_{j+1}) \right| + \beta f_0 \left(\frac{\partial \psi_{j-1}}{\partial x} - \frac{\partial \psi_{j+1}}{\partial x}\right)$$

$$+ \frac{c_p}{P_0^\kappa}(P_{j-1}^\kappa - P_{j+1}^\kappa)\nabla^2 J(\psi_j, \theta_j) + f_0 A \nabla^4(\psi_{j-1} - \psi_{j+1}) + f_0 \left[K_{1,j-1}\nabla^2(\psi_{j-1} - \psi_{j-3})\right.$$

$$\left. - K_{1,j+1}\nabla^2(\psi_{j+1} - \psi_{j-1}) \frac{(P_{j-2}-P_{j+2})}{(P_{j-2}-P_j)} + K_{1,j+3} \frac{(P_{j+2}-P_{j+4})}{(P_j-P_{j+2})} \nabla^2(\psi_{j+3} - \psi_{j+1})\right]$$

$$- c_p \frac{(P_{j-1}^\kappa - P_{j+1}^\kappa)}{P_0^\kappa} \nabla^2\left(h(\theta^* - \theta) - \sigma\eta\omega^*\right) .$$

The finite difference set of equations, in absence of dissipation and heating also conserves the sum of available potential energy and kinetic energy. The vertical differencing consists of 4 layers, with one layer in the stratosphere (Fig. 2). Streamfunction ψ is described at odd levels and ω, θ, τ at even levels. The boundary conditions for the vertical motion are

$$\omega_0 = \omega_8 = 0.$$

Spectral equations

The horizontal dependence of the variables ψ, θ and ω is expressed in terms of truncated series of double-Fourier functions.

The horizontal dependence of the variables ψ, θ and ω is expressed in terms of truncated series of double-Fourier functions.

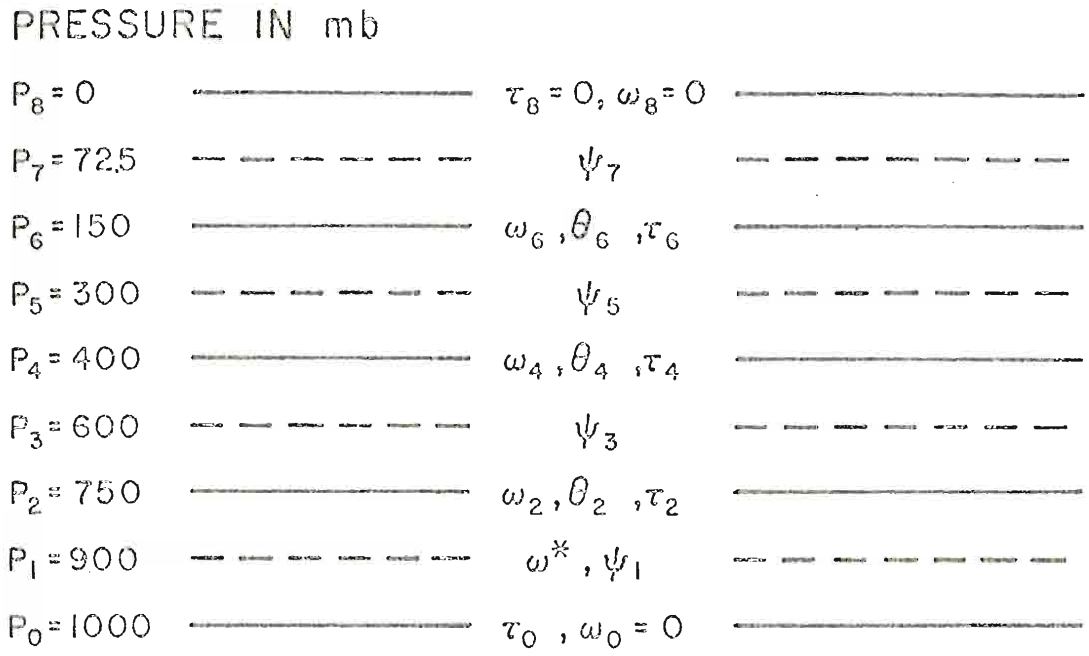

Fig. 2-Vertical resolution of the model.

$$\psi = \sum_{m=-3}^{3} \sum_{n=-1}^{1} \psi_n^m (t) F_n^m$$

$$\nabla^2\psi = \sum_{m'=-3}^{3} \sum_{n'=-1}^{1} (m'^2 k^2 + n'^2\ell^2) \psi_{n'}^{m'} (t) F_{n'}^{m'}$$

$$\theta = \sum_{m=-3}^{3} \sum_{n=-1}^{1} \theta_n^m (t) F_n^m$$

$$\omega = \sum_{m=-3}^{3} \sum_{n=-1}^{1} \omega_n^m (t) F_n^m$$

where

$$F_n^m = e^{i(mkx+n\ell y)}, \qquad F_{n'}^{m'} = e^{i(m'kx+n'\ell y)}$$

and m, n, m', n' are dummy indices which represent east-west and north-south wave numbers, respectively, and

$$k = \frac{2\pi}{K}, \qquad \ell = \frac{2\pi}{L}$$

where K, L are dimensions of the bounded region of the β-plane given by (0,K), (0,L). They are also the fundamental wavelengths in this domain. The complex coefficients of ψ_n^m, θ_n^m, and ω_n^m are given as in the following example, by the transform of $\psi(x,y,t)$,

$$\psi_n^m(t) = \frac{1}{KL} \int_0^K \int_0^L \psi(x,y,t)\, e^{-i(mkx+n\ell y)} dx\, dy = \psi_{1\ n}^{\ m}(t) - i\, \psi_{2\ n}^{\ m}(t)$$

and $\psi_{1\ n}^{\ m}$, $\psi_{2\ n}^{\ m}$ are the real and imaginary parts of ψ_n^m. We should also note that not all equations, in spectral form are independent because of the properties of conjugates, i.e.,

$$\psi_{1\ -n}^{\ -m} = \psi_{1\ n}^{\ m}, \qquad \psi_{2\ -n}^{\ -m} = -\psi_{2\ n}^{\ m}$$

These functions are periodic and orthogonal over the fundamental domain, i.e.,

$$\int_0^K \int_0^L F_n^m \, F_{-n''}^{-m''} \, dx \, dy = 0 \quad \text{if} \quad m \neq m'', \; n = n''$$

$$= KL \quad \text{if} \quad m = m'', \; n = n''$$

Expressed in terms of time-dependent spectral coefficients, the governing equations become, after separation into real and imaginary parts,

$$\text{(i)} \quad \dot{\psi}_{1\ n''}^{j\ m''} = \sum_{m'} \sum_{n'} C(m'',n'',m',n') \left(\psi_{1\ n''-n'}^{j\ m''-m'} \, \psi_{1\ n'}^{j\ m'} - \psi_{2\ n''-n'}^{j\ m''-m'} \, \psi_{2\ n'}^{j\ m'}\right)$$

$$- f_0 \, D(m'',n'') \, \frac{\left(\omega_{1\quad n''}^{j-1\ m''} - \omega_{1\quad n''}^{j+1\ m''}\right)}{\left(P_{j-1} - P_{j+1}\right)} + \beta_0 m'' k \, D(m'',n'') \, \psi_{2\ n''}^{j\ m''}$$

$$- K_{1,j} \left(\psi_{1\ n''}^{j\ m''} - \psi_{1\quad n''}^{j-2\ m''}\right) - K_{2,j} \left(\psi_{1\ n''}^{j\ m''} - \psi_{1\quad n''}^{j+2\ m''}\right)$$

$$- \frac{A}{D\,(m'',n'')} \, \psi_{1\ n''}^{j\ m''}$$

$$\text{(ii)} \quad \dot{\psi}_{2\ n''}^{j\ m''} = \sum_{m'} \sum_{n'} C(m'',n'',m',n') \left(\psi_{2\ n''-n'}^{j\ m''-m'} \, \psi_{1\ n'}^{j\ m'} + \psi_{1\ n''-n'}^{j\ m''-m'} \, \psi_{2\ n'}^{j\ m'}\right)$$

$$- f_0 \, D(m'',n'') \, \frac{\left(\omega_{2\quad n''}^{j-1\ m''} - \omega_{2\quad n''}^{j+1\ m''}\right)}{\left(P_{j-1} - P_{j+1}\right)} - \beta_0 \, m'' k \, D(m'',n'') \, \psi_{1\ n''}^{j\ m''}$$

$$- K_{1,j} \left(\psi_{2\ n''}^{j\ m''} - \psi_{1\quad n''}^{j-2\ m''}\right) - K_{2,j} \left(\psi_{2\ n''}^{j\ m''} - \psi_{2\quad n''}^{j+2\ m''}\right)$$

$$- K_{1,j} \left(\psi_{2\ n''}^{j\ m''} - \psi_{1\quad n''}^{j-2\ m''}\right) - K_{2,j} \left(\psi_{2\ n''}^{j\ m''} - \psi_{2\quad n''}^{j+2\ m''}\right)$$

$$- \frac{A}{D\,(m'',n'')} \, \psi_{2\ n''}^{j\ m''} \qquad (1)$$

where,

$$C(m'',n'',m',n') = k\ell\,(m'^2k^2+n'^2\ell^2)(m''n'-m'n'')/(m''^2k^2+n''^2\ell^2)$$

and

$$D(m'',n'') = 1/(m''^2k^2+n''^2\ell^2)$$

(i) $$\dot{\theta}_{1\ n''}^{j\ m''} = \sum_{m'}\sum_{n'} A(m'',n'',m',n')\left(\psi_{1\ n''-n'}^{j\ m''-m'}\ \theta_{1\ n'}^{j\ m'} - \psi_{2\ n''-n'}^{j\ m''-m'}\ \theta_{2\ n'}^{j\ m'}\right)$$

$$+ \sigma_j\ \omega_{1\ n''}^{j\ m''} + h_j\left(\theta^{*j\ m''}_{1\ n''} - \theta_{j\ n''}^{j\ m''}\right) - \frac{\eta_j\sigma_j Q}{D(m'',n'')}\ \psi_{1\ n''}^{1\ m''}$$

(ii) $$\dot{\theta}_{2\ n''}^{j\ m''} = \sum_{m'}\sum_{n'} A(m'',n'',m',n')\left(\psi_{1\ n''-n'}^{j\ m''-m'}\ \theta_{2\ n'}^{j\ m'} + \psi_{2\ n''-n'}^{j\ m''-m'}\ \theta_{1\ n'}^{j\ m'}\right)$$

$$+ \sigma_j\ \omega_{2\ n''}^{j\ m''} + h_j\left(\theta^{*j\ m''}_{2\ n''} - \theta_{2\ n''}^{j\ m''}\right) - \frac{\eta_j\sigma_j Q}{D(m'',n'')}\ \psi_{2\ n''}^{1\ m''}$$

$$j = 2,\ 4,\ 6 \qquad (2)$$

where

$$A(m'',n'',m',n') = k\ell\,(m''n' - n''m')$$

and

$$Q = g\,\rho_0\,\frac{\sin 2\alpha}{f}\sqrt{\frac{A_V\ f_0}{2}}$$

(i) $$\theta_{1\ n''}^{j\ m''} = -\,f_0/c_p\ \frac{\left(P^K_{j-1} - P^K_{j+1}\right)}{P^K_0}\left(\psi_{1\ \ n''}^{j-1\ m''} - \psi_{1\ \ n''}^{j+1\ m''}\right)$$

$$j = 2,\ 4,\ 6 \qquad (3)$$

(i) $$- \frac{c_p \sigma_j \left(P^{\kappa}_{j-1} - P^{\kappa}_{j+1}\right)}{D(m'',n'')\, P^{\kappa}_0} \omega_1^{j\ m''}_{\ \ n''} + f_0^2 \left[\frac{\omega_1^{j-2\ m''}_{\ \ \ n''}}{(P_{j-2} - P_j)} - \left[\frac{(P_{j-2} - P_{j+2})}{(P_{j-2} - P_j)(P_j - P_{j+2})} \right] \omega_1^{j\ m''}_{\ \ n''} \right.$$

$$\left. + \frac{\omega_1^{j+2\ m''}_{\ \ \ n''}}{(P_j - P_{j+2})} \right] = f_0 \sum_{m'} \sum_{n'} F(m'',n'',m',n') \left[\left(\psi_1^{j+1\ m''-m'}_{\ \ \ n''-n'} \psi_1^{j-1\ m'}_{\ \ \ n'} - \right. \right.$$

$$\left. \left. - \psi_2^{j-1\ m''-m'}_{\ \ \ n''-n'} \psi_2^{j-1\ m'}_{\ \ \ n'} \right) - \left(\psi_1^{j+1\ m''-m'}_{\ \ \ n''-n'} \psi_1^{j+1\ m'}_{\ \ \ n'} - \psi_2^{j+1\ m''-m'}_{\ \ \ n''-n'} \psi_2^{j+1\ m'}_{\ \ \ n'} \right) \right] +$$

$$+ \beta_0 f_0 m'' k \left(\psi_2^{j-1\ m''}_{\ \ n''} - \psi_2^{j+1\ m''}_{\ \ n''} \right) - \frac{c_p \left(P^{\kappa}_{j-1} - P^{\kappa}_{j+1}\right)}{P^{\kappa}_0} \sum_{m'} \sum_{n'} L(m'',n'',m',n')$$

$$\left(\psi_1^{j\ m''-m'}_{\ \ n''-n'} \theta_1^{j\ m'}_{\ \ n'} - \psi_2^{j\ m''-m'}_{\ \ n''-n'} \theta_2^{j\ m'}_{\ \ n'} \right) - \frac{f_0 A}{D(m'',n'')^2} \left(\psi_1^{j-1\ m''}_{\ \ \ n''} - \psi_1^{j+1\ m''}_{\ \ \ n''} \right) +$$

$$+ \frac{f_0 K_{1,j-1}}{D(m'',n'')} \psi_1^{j-3\ m''}_{\ \ \ n''} - \frac{f_0}{D(m'',n'')} \left(K_{1,j-1} + K_{1,j+1} \frac{(P_{j-2} - P_{j+2})}{(P_{j-2} - P_j)} \right) \psi_1^{j-1\ m''}_{\ \ \ n''}$$

$$+ \frac{f_0}{D(m'',n'')} \left[K_{1,j+1} \frac{(P_{j-2} - P_{j+2})}{(P_{j-2} - P_j)} + K_{1,j+2} \frac{(P_{j+2} - P_{j+4})}{(P_j - P_{j+2})} \right] \psi_1^{j+1\ m''}_{\ \ \ n''}$$

$$- \frac{f_0}{D(m'',n'')} K_{1,j+3} \frac{(P_{j+2} - P_{j+4})}{(P_j - P_{j+2})} \psi_1^{j+3\ m''}_{\ \ \ n''} + \frac{c_p (P^{\kappa}_{j-1} - P^{\kappa}_{j+1})}{D(m'',n'') P^{\kappa}_0}$$

$$\left[h_j \left(\theta^{*j\ m''}_{1\ n''} - \theta_1^{j\ m''}_{\ \ n''} \right) \eta_j \sigma_j Q \psi_1^{1\ m''}_{\ \ n''} \right] \qquad (4)$$

For more detail on this equation reference is made to the Appendix.

(ii) A similar equation exists for the imaginary part of $\omega_2^{j\ m''}_{\ \ n''}$, where

(ii) A similar equation exists for the imaginary part of $\omega_2^{j\ m''}_{\ \ n''}$, where

$$F(m'',n'',m',n') = (m'^2 k^2 + n'^2 \ell^2)(m''n' - n''m')$$

$$L(m'',n'',m',n') = (m''^2 k^2 + n''^2 \ell^2)(n''m' - m''n')$$

As was done for ψ_0^0, isobaric means θ_0^0 and ω_0^0 are also omitted. When we use the concept of available potential energy, the isobaric mean potential temperature is not required. The total number of first order coupled and non-linear differential equations is 140 and the number of algebraic equations for ω reduces to 20 matrices of order 3 by 3 each.

The north-south resolution is given by

$$\psi^j(y,t) = 2(\psi_{1\ 1}^{j\ 0}(t) \cos \ell y + \psi_{2\ 1}^{j\ 0}(t) \sin \ell y)$$

and the east-west number of waves is 3. We group these components in the form,

ultra-long wave	(1,0), (1,1), (1,-1)
long wave	(2,0), (2,1), (2,-1)
short wave	(3,0), (3,1), (3,-1)

This allows a north-south variation of the trough lines. When the scale of domain is selected, the wavelength scales are then determined from wave numbers m and n. The spectral equations, in the absence of sources and sinks, conserve the sum of kinetic and available potential energies.

CHAPTER III

ENERGY AND ENERGY CONVERSIONS

Energies of the various waves at various levels comprise an essential part of the present investigation. Wave instabilities in the linear sense (when the perturbation amplitude is very small) and energy conversions in the nonlinear sense can determine the most unstable modes, energy sources and sinks, and the pressure levels at which they exist. To achieve this end, we present a schematic energy diagram and formulate the necessary energy expressions (Fig. 3).

In the energy schematic diagram, the objective is to determine the directions of energy flow and, in particular, the relative magnitudes and directions of $[A_E \cdot K_E]$ and $[K_Z \cdot K_E]$ which represent, respectively, the conversion from eddy available potential energy to eddy kinetic energy and zonal kinetic energy to eddy kinetic energy. The former, in the non-conservative set of equations is primarily maintained by eddy conversion from latent heat to A_E, i.e., $L\,[H_E \cdot A_E]$, and hence represents part of the CISK mechanism. The latter is a barotropic conversion. Other symbols in the diagram are described in Table 1.

(1) The definition of available potential energy as formulated by Lorenz (1960) can be written as

$$A = \frac{\kappa c_p}{2p_0^{\kappa}} \int_M P^{\kappa-1} \frac{(\theta - \bar{\theta})^2}{\sigma(P)} \, dM$$

$$A = \frac{\kappa c_p}{2P_0^{\kappa}} \int_M P^{\kappa-1} \frac{(\theta - \bar{\theta})^2}{\sigma(P)} \, dM$$

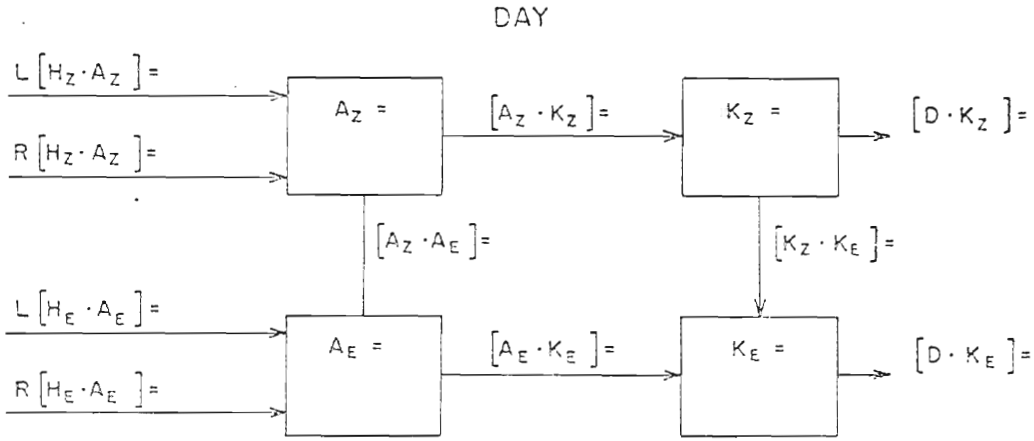

Fig. 3-Schematic energy cycle for the troposphere.

Table 1.-Energy quantities

Quantity	Definition
A_Z	Zonal available potential energy
A_E	Eddy available potential energy
K_E	Eddy kinetic energy
K_Z	Zonal kinetic energy
$[A_Z \cdot K_Z]$	Conversion from A_Z to K_Z
$[K_Z \cdot K_E]$	Conversion from K_Z to K_E
$[A_E \cdot K_E]$	Conversion from A_E to K_E
$[A_Z \cdot A_E]$	Conversion from A_Z to A_E
$L[H_Z \cdot A_Z]$	Zonal latent heat conversion to A_Z
$R[H_Z \cdot A_Z]$	Zonal radiation heat conversion to A_Z
$L[H_E \cdot A_E]$	Eddy latent heat conversion to A_E
$R[H_E \cdot A_E]$	Eddy radiation heat conversion
$[D \cdot K_E]$	Dissipation of eddy kinetic energy
$[D \cdot K_Z]$	Dissipation of zonal kinetic energy
$[K_Z \cdot K_Z]_F$	Transfer to stratosphere of energy flux
$[K_Z \cdot K_Z]_D$	Transfer of K_Z to stratosphere by shear drag
$[K_E \cdot K_E]_F$	Transfer to stratosphere of K_E flux
$[K_E \cdot K_E]_D$	Transfer to stratosphere of K_E flux by shear drag

or when P is expressed discretely and dM is expressed in terms of pressure, by using the hydrostatic equation, the expression reduces to

$$A_{Z,j} = \frac{c_p}{2g\sigma_j} \frac{\left(P_{j-1}^{\kappa} - P_{J+1}^{\kappa}\right)}{P_0^{\kappa}} \int_0^K \int_0^L \bar{\theta}_j^2 \, dx \, dy$$

$$A_{E,j} = \frac{c_p}{2g\sigma_j} \frac{\left(P_{j-1}^{\kappa} - P_{j+1}^{\kappa}\right)}{P_0^{\kappa}} \int_0^K \int_0^L \theta_j'^2 \, dx \, dy$$

where the overbar denotes zonal average and the prime denotes a deviation from it. In spectral form, after applying the orthogonality property, the expression becomes

$$A_{Z,j} + A_{E,j} = \frac{c_p}{2g\sigma_j} \frac{P_{j-1}^{\kappa} - P_{j+1}^{\kappa}}{P_0^{\kappa}} \sum_{m=-3}^{3} \sum_{n=-1}^{1} \theta_{j\,n}^{\,m} \theta_{j\,-n}^{\,-m}$$

A_j represents the quantity for the layer between P_{j-1} and P_{j+1} per unit area.

(2) The definition of kinetic energy is given by

$$E = \frac{1}{2} \int_M \left[\left(\frac{\partial \psi}{\partial x}\right)^2 + \left(\frac{\partial \psi}{\partial y}\right)^2 \right] dM$$

or

$$E_j = \frac{\left(P_{j-1} - P_{j+1}\right)}{2g} \int_0^K \int_0^L \left[\left(\frac{\partial \psi}{\partial x}\right)^2 + \left(\frac{\partial \psi}{\partial y}\right)^2 \right] dx \, dy$$

when expressed in vertical finite-difference form. The spectral form of the kinetic energy between the levels P_{j-1} and P_{j+1} takes the form,

form of the kinetic energy between the levels P_{j-1} and P_{j+1} takes the form,

$$E_j = K_{Z,j} + K_{E,j} = \frac{1}{2g} \sum_{m=-3}^{3} \sum_{n=-1}^{1} (m^2k^2 + n^2\ell^2)\psi_{j\,n}^{\,m} \psi_{j\,-n}^{\,-m}$$

(3) Time rate of change of available potential energy is given by

$$\frac{dA_Z}{dt} = \frac{c_p}{g\sigma_j} \frac{P^K_{j-1} - P^K_{j+1}}{P^K_0} \int_0^K \int_0^L \left(\overline{\theta}_j \frac{\partial \overline{\theta}_j}{\partial t} \right) dx\, dy$$

$$\frac{dA_E}{dt} = \frac{c_p}{g\sigma_j} \frac{P^K_{j-1} - P^K_{j+1}}{P^K_0} \int_0^K \int_0^L \left(\theta' \frac{\partial \theta'}{\partial t} \right) dx\, dy$$

The derivation of the expression is straightforward and makes use of the thermodynamic equation. The final results become,

$$\frac{dA_{Z,j}}{dt} = \frac{c_p}{g\sigma_j} \frac{P^K_{j-1} - P^K_{j+1}}{P^K_0} \left[\int - \overline{\theta}_j \overline{J(\psi'_j, \theta'_j)}\, dy + \int \int \left(\sigma_j \overline{\omega}_j \overline{\theta}_j + \overline{H}_j \overline{\theta}_j \right) dx\, dy \right]$$

and

$$\frac{dA_{E,j}}{dt} = \frac{c_p}{g\sigma_j} \frac{P^K_{j-1} - P^K_{j+1}}{P^K_0} \left[\int \overline{\theta}\, \overline{J(\psi'_j, \theta'_j)}\, dy + \int_0^K \int_0^L \left(\overline{\sigma\omega'\theta'} + \overline{H'\theta'} \right) dx\, dy \right]$$

The various terms in the integrands represent the following energy conversions,

$$[A_Z \cdot A_E] = \sum_j \frac{c_p}{g\sigma_j} \frac{P^K_{j-1} - P^K_{j+1}}{P^K_0} \int_0^L \overline{\theta}_j \overline{J(\psi'_j, \theta'_j)}\, dy$$

$$= \sum_j \frac{c_p}{g\sigma_j} \frac{P^K_{j-1} - P^K_{j+1}}{P^K_0} \sum_{n''} \sum_{m'} \sum_{n'} m'n'' k\ell\, \psi_{j\ -(n''+n')}^{\ -m'}\, \theta_{j\ n'}^{\ m'}\, \theta_{j\ n''}^{\ 0}$$

$$= \sum_j \frac{c_p}{g\sigma_j} \frac{P^K_{j-1} - P^K_{j+1}}{P^K_0} \sum_{n''} \sum_{m'} \sum_{n'} m'n'' k\ell\, \psi_{j\ -(n''+n')}^{\ -m'}\, \theta_{j\ n'}^{\ m'}\, \theta_{j\ n''}^{\ 0}$$

$$R[H_Z \cdot A_Z] = \sum_j \int_0^L \frac{c_p}{g\sigma_j} \frac{(P_{j-1}^\kappa - P_{j+1}^\kappa)}{P_0^\kappa} h_j \bar{\theta}_j (\bar{\theta}_j^* - \bar{\theta}_j)\, dy$$

$$= \sum_j \frac{c_p}{g\sigma_j} \frac{(P_{j-1}^\kappa - P_{j+1}^\kappa)}{P_0^\kappa} \left[h_j \sum_{n'} \theta^0_{j-n'} (\theta^{*\,0}_{j\,n'} - \theta^{\,0}_{j\,n'}) \right]$$

$$L[H_Z \cdot A_Z] = \sum_j \int_0^L \frac{c_p}{g} \frac{(P_{j-1}^\kappa - P_{j+1}^\kappa)}{P_0^\kappa} \eta_j Q \bar{\theta}_j \nabla^2 \bar{\psi}_j\, dy$$

$$= - \sum_j \frac{c_p}{g} \frac{(P_{j-1}^\kappa - P_{j+1}^\kappa)}{P_0^\kappa} \eta_j Q \sum_{n'=-1}^{1} n'^2 \ell^2 \theta^{\,0}_{j\,-n'} \psi^{\,0}_{1\,n'}$$

$$R[H_E \cdot A_E] = \sum_j \int \frac{c_p}{g\sigma_j} \frac{(P_{j-1}^\kappa - P_{j+1}^\kappa)}{P_0^\kappa} h_j \overline{\theta_j' (\theta_j^{*\prime} - \theta_j')}\, dy$$

$$= \sum_j \frac{c_p}{g\sigma_j} \frac{(P_{j-1}^\kappa - P_{j+1}^\kappa)}{P_0^\kappa} h_j \sum_{m'} \sum_{n'} \theta^{\,-m'}_{j\,-n'} (\theta^{*\,m'}_{j\,n'} - \theta^{\,m'}_{j\,n'})$$

$$L[H_E \cdot A_E] = \sum_j \int \frac{c_p}{g} \frac{(P_{j-1}^\kappa - P_{j+1}^\kappa)}{P_0^\kappa} \eta_j Q \overline{\theta_j' \nabla^2 \psi_1'}\, dy$$

$$= - \sum_j \frac{c_p}{g} \frac{(P_{j-1}^\kappa - P_{j+1}^\kappa)}{P_0^\kappa} \eta_j Q \sum_{m'} \sum_{n'}$$

$$(m'^2 k^2 + n'^2 \ell^2)\, \theta^{\,-m'}_{j\,-n'}\, \psi^{\,m'}_{1\,n'}$$

The quantities $\sigma\, \bar{\omega}\, \bar{\theta}$ and $\sigma\, \overline{\omega'\theta'}$ are baroclinic terms and will be discussed in a subsequent section.

(4) The time rate of change of kinetic energy in the troposphere is discussed in a subsequent section.

(4) The time rate of change of kinetic energy in the troposphere is given by

$$\frac{dK_Z}{dt} = -\frac{1}{g}\sum_j (P_{j-1} - P_{j+1}) \int \bar{\psi}_j \nabla^2 \frac{\partial \bar{\psi}}{\partial t}\, dy$$

$$\frac{dK_E}{dt} = -\frac{1}{g}\sum_j (P_{j-1} - P_{j+1}) \int \overline{\psi'_j \nabla^2 \frac{\partial \psi'_j}{\partial t}}\, dy$$

From the vorticity equation we obtain

$$\frac{dK_Z}{dt} = \frac{1}{g}\sum_{j=1,3}^{5} (P_{j-1} - P_{j+1}) \int \bar{\psi}_j \overline{J(\psi'_j, \nabla^2\psi'_j)}\, dy$$

$$+ \frac{f}{g}\sum_{j=2}^{4} \int (\bar{\psi}_{j-1} - \bar{\psi}_{j+1})\, \bar{\omega}_j\, dy + \frac{f}{g}\int \bar{\psi}_5\, \bar{\omega}_6\, dy$$

$$- \frac{A}{g}\sum_{j=1,3}^{5} \int (P_{j-1} - P_{j+1})\, \bar{\psi}_j \nabla^4 \bar{\psi}_j\, dy + \frac{1}{g}(P_0 - P_2) K_{1,1}$$

$$\int \bar{\psi}\nabla^2 \bar{\psi}_1\, dy + \frac{1}{g}\sum_{j=1}^{3} \int K_{2,j}\, (P_{j-1} - P_{j+1})(\bar{\psi}_{j+2} - \bar{\psi}_j)\nabla^2$$

$$(\bar{\psi}_{j+2} - \bar{\psi}_j)\, dy + K_{2,5}\, \frac{(P_4 - P_6)}{2g} \int (\bar{\psi}_7 - \bar{\psi}_5)\, \nabla^2\, (\bar{\psi}_7 - \bar{\psi}_5)\, dy$$

$$- K_{2,5}\, \frac{(P_4 - P_6)}{2g} \int (\bar{\psi}_7 - \bar{\psi}_5)\, \nabla^2\, (\bar{\psi}_7 + \bar{\psi}_5)\, dy$$

where the last term represents the vertical transport of zonal kinetic energy across level 6 due to shear drag.

kinetic energy across level 6 due to shear drag.

$$\frac{dK_E}{dt} = \frac{1}{g} \sum_{j=1,3}^{5} (P_{j-1} - P_{j+1}) \int \bar{\psi}_5 J \overline{(\psi'_5, \nabla^2 \psi'_5)}\, dy$$

$$+ \frac{f}{g} \sum_{j=2}^{4} \int \overline{(\psi'_{j-1} - \psi'_{j+1})\omega'_j}\, dy + \frac{f}{g} \int \overline{\psi'_5 \omega'_6}\, dy$$

$$- \frac{A}{g} \sum_{j=1,3}^{5} \int (P_{j-1} - P_{j+1}) \overline{\psi'_j \nabla^4 \psi'_j}\, dy + \frac{1}{g} (P_0 - P_2) K_{1,1}$$

$$\int \overline{\psi'_1 \nabla^2 \psi'_1}\, dy + \frac{1}{g} \sum_{j=1}^{3} \int K_{2,j} (P_{j-1} - P_{j+1}) \overline{(\psi'_{j+2} - \psi'_j)(\psi'_{j+2} - \psi'_j)} dy$$

$$+ K_{2,5} \frac{(P_4 - P_6)}{2g} \int \overline{(\psi'_7 - \psi'_5) \nabla^2 (\psi'_7 - \psi'_5)}\, dy$$

$$- K_{2,5} \frac{(P_4 - P_6)}{2g} \int \overline{(\psi'_7 - \psi'_5) \nabla^2 (\psi'_7 + \psi'_5)}\, dy$$

The last term represents vertical transport of eddy kinetic energy across level 6 due to shear drag.

In the above expressions a number of terms have a dual function when computed at level 6; this level separates the troposphere from the stratosphere. They allow for kinetic energy flux across level 6 and a partition of baroclinic energy conversion into the levels below and above level 6. These terms assume the following form when the thermal wind equation and the linear interpolation of stream functions are used,

$$f \int \bar{\psi}_7 \bar{\omega}_6\, dy \qquad f \int \bar{\psi}_7 \bar{\omega}_6\, dy \qquad 1\ c_p (P_5^\kappa - P_7^\kappa) \int \bar{\theta} \bar{\omega}_6\, dy$$

$$- \frac{f}{g} \int \bar{\psi}_7 \bar{\omega}_6\, dy = - \frac{f}{g} \int \bar{\psi}_6 \bar{\omega}_6\, dy - \frac{1}{3} \frac{c_p}{g} \frac{(P_5^\kappa - P_7^\kappa)}{P_0^\kappa} \int \bar{\theta}_6 \bar{\omega}_6\, dy$$

$$-\frac{f}{g}\int \overline{\psi_7'\omega_6'}\,dy = -\frac{f}{g}\int \overline{\psi_6'\omega_6'}\,dy - \frac{1}{3}\frac{c_p}{g}\frac{(P_5^\kappa - P_7^\kappa)}{P_0^\kappa}\int \overline{\theta_6'\omega_6'}\,dy$$

$$\frac{f}{g}\int \overline{\psi}_5\overline{\omega}_6\,dy = \frac{f}{g}\int \overline{\psi}_6\overline{\omega}_6\,dy - \frac{2}{3}\frac{c_p}{g}\frac{(P_5^\kappa - P_7^\kappa)}{P_0^\kappa}\int \overline{\theta}_6\overline{\omega}_6\,dy$$

$$\frac{f}{g}\int \overline{\psi_5'\omega_6'}\,dy = \frac{f}{g}\int \overline{\psi_6'\omega_6'}\,dy - \frac{2}{3}\frac{c_p}{g}\frac{(P_5^\kappa - P_7^\kappa)}{P_0^\kappa}\int \overline{\theta_6'\omega_6'}\,dy$$

The first terms on the right-hand sides are the flux terms and the second terms are the baroclinic conversions. Their spectral form is similar to some of the previous expressions.

By comparing the signs of integrands in the above list of integrals, the following are found to be the appropriate energy conversion formulae. The subscript S refers to stratosphere and T refers to troposphere,

$$[K_E \cdot K_Z]_S = \frac{(P_6 - P_8)}{g}\int \overline{\psi}_7\,\overline{J(\psi_7', \nabla^2\psi_7')}\,dy$$

$$= \frac{(P_6 - P_8)}{g}\sum_{n''=-1}^{1}\sum_{m'=-1}^{3}\sum_{n'=-1}^{1}[k\ell m'n''(m'^2k^2 + n'^2\ell^2)]$$

$$\psi_{7\ n''}^{0}\psi_{7-(n'+n'')}^{-m'}\psi_{7\ (n'+n'')}^{m'} \qquad m' \neq 0,\ n'' \neq 0$$

$$[K_E \cdot K_Z]_T = \frac{1}{g}\sum_{j=1,3}^{5}\sum_{n''}\sum_{m'}\sum_{n'}[(P_{j-1} - P_{j+1})k\ell m'n''$$

$$(m'^2k^2 + n'^2\ell^2)]\,\psi_{j\ n''}^{0}\,\psi_{j\ -(n'+n'')}^{-m'}\,\psi_{j\ n'}^{m'}$$

$$m' \neq 0,\ n'' \neq 0$$

$$m' \neq 0,\ n'' \neq 0$$

$$[A_Z \cdot K_Z]_S = -\frac{1}{3}\frac{c_p}{g}\frac{(P_5^K - P_7^K)}{P_0^K}\int \bar{\theta}_6\bar{\omega}_6\, dy$$

$$= \frac{1}{3}\frac{c_p}{g}\frac{(P_5^K - P_7^K)}{P_0^K}\sum_{n'} \theta_{6\ -n'}^{\ 0}\ \omega_{6\ n'}^{\ 0} \qquad n \neq 0$$

$$[A_Z \cdot K_Z]_T = \frac{f}{g}\sum_{j=2}^{4}\int (\bar{\psi}_{j-1} - \bar{\psi}_{j+1})\,\bar{\omega}_j - \frac{2}{3}\frac{c_p}{g}\frac{(P_5^K - P_7^K)}{P_0^K}\int \bar{\theta}_6\bar{\omega}_6\, dy$$

$$= \frac{f}{g}\sum_{j=2}^{4}\sum_{n'} (\psi_{1\ -n'}^{\ 0} - \psi_{3\ -n'}^{\ 0})\ \omega_{2\ n'}^{\ 0} - \frac{2}{3}\frac{c_p}{g}$$

$$\frac{(P_5^K - P_7^K)}{P_0^K}\sum_{n'} \theta_{6\ -n'}^{\ 0}\ \omega_{6\ n'}^{\ 0} \qquad n' \neq 0$$

$$[A_E \cdot K_E]_S = -\frac{1}{3}\frac{c_p}{g}\frac{(P_5^K - P_7^K)}{P_0^K}\int \overline{\theta'_6\,\omega'_6}\, dy$$

$$= -\frac{1}{3}\frac{c_p}{g}\frac{(P_5^K - P_7^K)}{P_0^K}\sum_{m'}\sum_{n'} \theta_{6\ -n'}^{\ -m'}\ \omega_{6\ n'}^{\ m'} \qquad m' \neq 0$$

$$[A_E \cdot K_E]_T = \frac{f}{g}\sum_{j=2}^{4}\int\overline{(\psi'_{j-1} - \psi'_{j+1})\,\omega'_j}\, dy - \frac{2}{3}\frac{c_p}{g}\frac{(P_5^K - P_7^K)}{P_0^K}$$

$$\int \overline{\theta'_6\,\omega'_6}\, dy = \frac{f}{g}\sum_{j=2}^{4}\sum_{m'}\sum_{n'} (\psi_{j-1\ -n'}^{\ -m'} - \psi_{j+1\ -n'}^{\ -m'})$$

$$\omega_{j\ n'}^{\ m'} - \frac{2}{3}\frac{c_p}{g}\frac{(P_5^K - P_7^K)}{P_0^K}\sum_{m'}\sum_{n'} \theta_{6\ -n'}^{\ -m'}\ \omega_{6\ n'}^{\ m'}$$

$$\omega_{j\ n'} - \overline{\frac{2}{3}\frac{c_p}{g}\frac{}{P_0^K}}\ \sum_{m'}\sum_{n'} \sigma_{6\ -n'}\ \omega_{6\ n'}^{\ m'} \qquad m' \neq 0$$

$$m' \neq 0$$

$$[D \cdot K_Z]_S = K_{2,5} \frac{(P_4 - P_6)}{2g} \int (\bar{\psi}_7 - \bar{\psi}_5) \nabla^2 (\bar{\psi}_7 - \bar{\psi}_5)\, dy$$

$$- \frac{A}{g} (P_6 - P_8) \int \bar{\psi}_7 \nabla^4 \bar{\psi}_7\, dy$$

$$= - K_{2,5} \frac{(P_4 - P_6)}{2g} \sum_{n'} n'^2 \ell^2 (\psi_{7\ -n'}^{\ 0} - \psi_{5\ -n'}^{\ 0})$$

$$(\psi_{7\ n'}^{\ 0} - \psi_{5\ n'}^{\ 0}) - A \frac{(P_6 - P_7)}{g} \sum_{n'} n'^4 \ell^4 \psi_{7\ -n'}^{\ 0} \psi_{7\ n'}^{\ 0}$$

$$[D \cdot K_Z]_T = K_{1,1} \frac{(P_0 - P_2)}{g} \int \bar{\psi}_1 \nabla^2 \bar{\psi}_1\, dy + \frac{1}{g} \sum_{j=1}^{3} (P_{j-1} + P_{j+1})$$

$$K_{2,1} \int (\bar{\psi}_{j+2} - \bar{\psi}_j)(\bar{\psi}_{j+2} - \bar{\psi}_j)\, dy + K_{2,5} \frac{(P_4 - P_6)}{2g}$$

$$\int (\bar{\psi}_7 - \bar{\psi}_5) \nabla^2 (\bar{\psi}_7 - \bar{\psi}_5)\, dy - \frac{A}{g} \sum_{j=1,3}^{5} (P_{j-1} - P_{j+1})$$

$$\int \bar{\psi}_j \nabla^4 \bar{\psi}_j\, dy = - K_{1,1} \frac{(P_0 - P_2)}{g} \sum_{n'} n'^2 \ell^2$$

$$\psi_{1\ -n'}^{\ 0} \psi_{1\ n'}^{\ 0} - \frac{1}{g} \sum_{j=1}^{3} (P_{j-1} - P_{j+1}) K_{2,j} \sum_{n'} n'^2 \ell^2$$

$$(\psi_{j+2\ -n'}^{\ 0} - \psi_{j\ -n'}^{\ 0})(\psi_{j+2\ n'}^{\ 0} - \psi_{j\ n'}^{\ 0}) - K_{2,5} \frac{(P_4 - P_6)}{2g}$$

$$\sum_{n'} n'^2 \ell^2 (\psi_{7\ -n'}^{\ 0} - \psi_{5\ -n'}^{\ 0})(\psi_{7\ n'}^{\ 0} - \psi_{5\ n'}^{\ 0})$$

$$- \frac{A}{g} \sum_{j=1,3}^{5} (P_{j-1} - P_{j+1}) \sum_{n'} n'^4 \ell^4 \psi_{j\ -n'}^{\ 0} \psi_{j\ n'}^{\ 0}$$

$$[D \cdot K_E]_S = K_{2,5} \frac{(P_4 - P_6)}{2g} \int \overline{(\psi_7' - \psi_5')\nabla^2(\psi_7' - \psi_5')}\, dy - \frac{A}{g} (P_6 - P_8)$$

$$\int \overline{\psi_7' \nabla^4 \psi_7'}\, dy = - K_{2,5} \frac{(P_4 - P_6)}{2g} \sum_{m'} \sum_{n'}$$

$$(m'^2 k^2 + n'^2 \ell^2)(\psi_{7\ -n'}^{\ -m'} - \psi_{5\ -n'}^{\ -m'})(\psi_{7\ n'}^{\ m'} - \psi_{5\ n'}^{\ m'})$$

$$\frac{(P_4 - P_6)}{(m'^2 k^2 + n'^2 \ell^2)}(\psi_{7\ -n'}^{\ -m'} - \psi_{5\ -n'}^{\ -m'})(\psi_{7\ n'}^{\ m'} - \psi_{5\ n'}^{\ m'})$$

$$- \frac{A}{g} \frac{(P_6 - P_8)}{g} \sum_{m'} \sum_{n'} (m'^2 k^2 + n'^2 \ell^2) \psi_{7\ -n'}^{\ -m'} \psi_{7\ n'}^{\ m'}$$

$$m \neq 0$$

$$[D \cdot K_E]_T = K_{1,1} \frac{(P_0 - P_2)}{g} \int \overline{\psi_1' \nabla^2 \psi_1'}\, dy + \frac{1}{g} \sum_{j=1}^{3} (P_{j-1} - P_{j+1})$$

$$K_{2,j} \int \overline{(\psi_{j+2}' - \psi_j') \nabla^2 (\psi_{j+2}' - \psi_j')}\, dy + K_{2,5}$$

$$\frac{(P_4 - P_6)}{2g} \int \overline{(\psi_7' - \psi_5') \nabla^2 (\psi_7' - \psi_5')}\, dy - \frac{A}{g} \sum_{j=1,3}^{5}$$

$$(P_{j-1} - P_{j+1}) \int \overline{\psi_j' \nabla^4 \psi_j'}\, dy = - K_{1,1}$$

$$\frac{(P_0 - P_2)}{g} \sum_{m'} \sum_{n'} (m'^2 k^2 + n'^2 \ell^2)\, \psi_{1\ -m'\ -n'}\, \psi_{1\ m'\ n'}$$

$$- \frac{1}{g} \sum_{j=1}^{3} (P_{j-1} - P_{j+1})\, K_{2,j} \sum_{m'} \sum_{n'} (m'^2 k^2 + n'^2 \ell^2)$$

$$(\psi_{j+2\ -m'\ -n'} - \psi_{j\ -m'\ -n'})(\psi_{j+2\ m'\ n'} - \psi_{j\ m'\ n'}) - K_{2,5} \frac{(P_4 - P_6)}{2g}$$

$$\sum_{m'} \sum_{n'} (m'^2 k^2 + n'^2 \ell^2)(\psi_{7\ -m'\ -n'} - \psi_{5\ -m'\ -n'})(\psi_{7\ m'\ n'} - \psi_{5\ m'\ n'})$$

$$- \frac{A}{g} \sum_{j=1,3}^{5} (P_{j-1} - P_{j+1}) \sum_{m'} \sum_{n'} (m'^2 k^2 + n'^2 \ell^2)$$

$$\psi_{j\ -m'\ -n'}\, \psi_{j\ m'\ n'} \qquad m \neq 0$$

The remaining expressions represent flux terms through the tropopause and will be discussed briefly in Chapter V. The subscript F will refer to energy flux and D to energy flux through shear drag.

$$[K_Z \cdot K_Z]_F = - \frac{f}{g} \int \overline{\psi}_6\, \overline{\omega}_6\, dy = - \frac{f}{g} \sum_{n'} \psi_{6\ n'}^{\ 0}\, \omega_{6\ n'}^{\ 0} \qquad m \neq 0$$

$$[K_Z \cdot K_Z]_D = K_{2,5} \frac{(P_4 - P_6)}{2g} \int (\overline{\psi}_7 - \overline{\psi}_5) \nabla^2 (\overline{\psi}_7 + \overline{\psi}_5)\, dy$$

$$= K_{2,5} \frac{(P_4 - P_6)}{2g} \sum n'^2 \ell^2 (\psi_{-\ n'}^{\ 0} - \psi_{-\ n'}^{\ 0})$$

$$= K_{2,5} \frac{(P_4 - P_6)}{2g} \sum_{n'} n'^2 \ell^2 (\psi_{7\ n'}^{\ 0} - \psi_{5\ -n'}^{\ 0})$$

$$(\psi_{7\ n'}^{\ 0} + \psi_{5\ n'}^{\ 0}) \qquad n' \neq 0$$

$$[K_E \cdot K_E]_F = -\frac{f}{g}\int \overline{\psi_6' \omega_6'}\, dy = -\frac{f}{g}\sum_{m'}\sum_{n'} \psi_{6\ -n'}^{-m'}\ \omega_{6\ n'}^{m'} \qquad m \neq 0$$

$$[K_E \cdot K_E]_D = K_{2,5}\frac{(P_4 - P_6)}{2g}\int \overline{(\psi_7' - \psi_5')\,\nabla^2\,(\psi_7' + \psi_5')}\, dy$$

$$= -K_{2,5}\frac{(P_4 - P_6)}{2g}\sum_{m'}\sum_{n'} (m'^2 k^2 + n'^2 \ell^2)$$

$$(\psi_{7\ -n'}^{-m'} - \psi_{5\ -n'}^{-m'})(\psi_{7\ n'}^{m'} + \psi_{n'}^{m'}) \qquad n' \neq 0$$

Further decomposition of various quantities of energy into ultralong, long, and short waves have been done for separate layers. These are computed and compared at various stages of wave evolution.

CHAPTER IV

PROCEDURE AND METHOD OF SOLUTION

In this chapter descriptions will be given concerning the method of numerical integration, initial analytic fields, details of eight experiments and values of necessary constants.

The numerical scheme selected for integration of the equations in the present model is the fourth-order Runge-Kutta method. Details about the scheme are given in standard textbooks on numerical analysis and its application in meteorology has been demonstrated by Young (1968) and Clark (1969). In the present investigation its application is somewhat unconventional because the variable ω is solved from a set of algebraic equations rather than a set of differential equations. Tests were performed to determine its accuracy and ability to conserve the sum of available potential energy and kinetic energy when dissipation and heating were set equal to zero. In the latter case, the energy sum was computed to the accuracy of four decimal figures for 30 days and showed no change at all; the scheme conserves the energy sum very accurately. This test was repeated for different initial conditions with similar results. To determine the accuracy of the scheme, the equations were integrated three different times for three different time intervals, Δt = 30, 48, 60 min. Energy of various wave components were computed in each case and the results did not differ markedly from one another. The method is therefore accurate, but somewhat slow because four steps are

needed to integrate one step forward in time. The time interval that was used for the final computations was $\Delta t = 48$ minutes.

Initial fields

The type of basic state under consideration is one which includes the essential features of the tropical state presented in the introduction. To simulate the exact N-S fields, a high order spectral formulation would be necessary. A low order N-S resolution in terms of wave components includes the details of the inflection point in the zonal wind profile, a maximum in zonal easterly winds, and a low temperature in the southernmost latitude to retain the effect of oceanic equatorial upwelling. The initial streamfunction field and its associated amplitudes at each level are as follows,

$$\psi^j(y) = 2\,(\psi^{j\ 0}_{1\ 1}\,(t=0)\cos \ell y + \psi^{j\ 0}_{2\ 1}\,(t=0)\sin \ell y)$$

$$\psi^{1\ 0}_{1\ 1} = -0.4, \qquad \psi^{1\ 0}_{2\ 1} = -1.5$$

$$\psi^{3\ 0}_{1\ 1} = -0.3 \qquad \psi^{3\ 0}_{2\ 1} = -1.0$$

$$\psi^{5\ 0}_{1\ 1} = -0.2 \qquad \psi^{5\ 0}_{2\ 1} = -0.3$$

$$\psi^{7\ 0}_{1\ 1} = -0.2 \qquad \psi^{7\ 0}_{2\ 1} = -0.7$$

The basic streamfunction in units of 10^{10} cm^2 sec^{-1}, was chosen to yield a maximum zonal easterlies of 6 m sec^{-1} at the 900 mb level. Any larger value would not change the fundamental results of the investigation, but merely give larger values for certain energy conversion terms. The intensity of ψ and the zonal wind were chosen to decrease with height except for the uppermost level. The corresponding initial potential temperatures

were computed from the balance equation and the ω-values from the ω-equation. In subsequent stages of the integrations, the potential temperature is computed from the thermodynamic equation rather than the balance equation.

The geometry of the region under consideration is rectangular, and the β-plane is centered at 18°N. The east-west extent varies from experiment to experiment to allow for different scales of waves, but the north-south extent is always 3141.5 km (i.e., proportional to π). This leads to a region of 28° in latitudinal extent. It is convenient to refer to such features as the inflection point and maximum zonal easterlies in terms of coordinates (x,y). Abscissa x increases from west to east and y from south to north. The southernmost boundary is taken at 4°N, and the northernmost boundary is at 32°N, so that the motions under consideration are confined to a region where the dynamic equations are valid.

Fig. 4 shows respectively the zonal distribution of ψ and u at level 1 and θ at level 2. Features to be noted are the inflection point of u_z at $y = 4$ ($\sim$ 9°N), maximum easterlies at $y = 7$ ($\sim$ 17°N), a cold southernmost potential temperature and a maximum potential temperature at $y = 4$, a latitude where an ITCZ may be expected to exist. This initial streamfunction field consists of a zonal low in low latitudes and a zonal high in northern latitudes. The area mean ψ_0^0 which has been omitted in the series expansion, accounts for the negative values of ψ in Fig. 4. In other general circulation problems, it is sometimes desirable to start integrations with an atmosphere at relative rest and possessing uniform temperature; this approach is computationally inefficient.

atmosphere at relative rest and possessing uniform temperature; this approach is computationally inefficient.

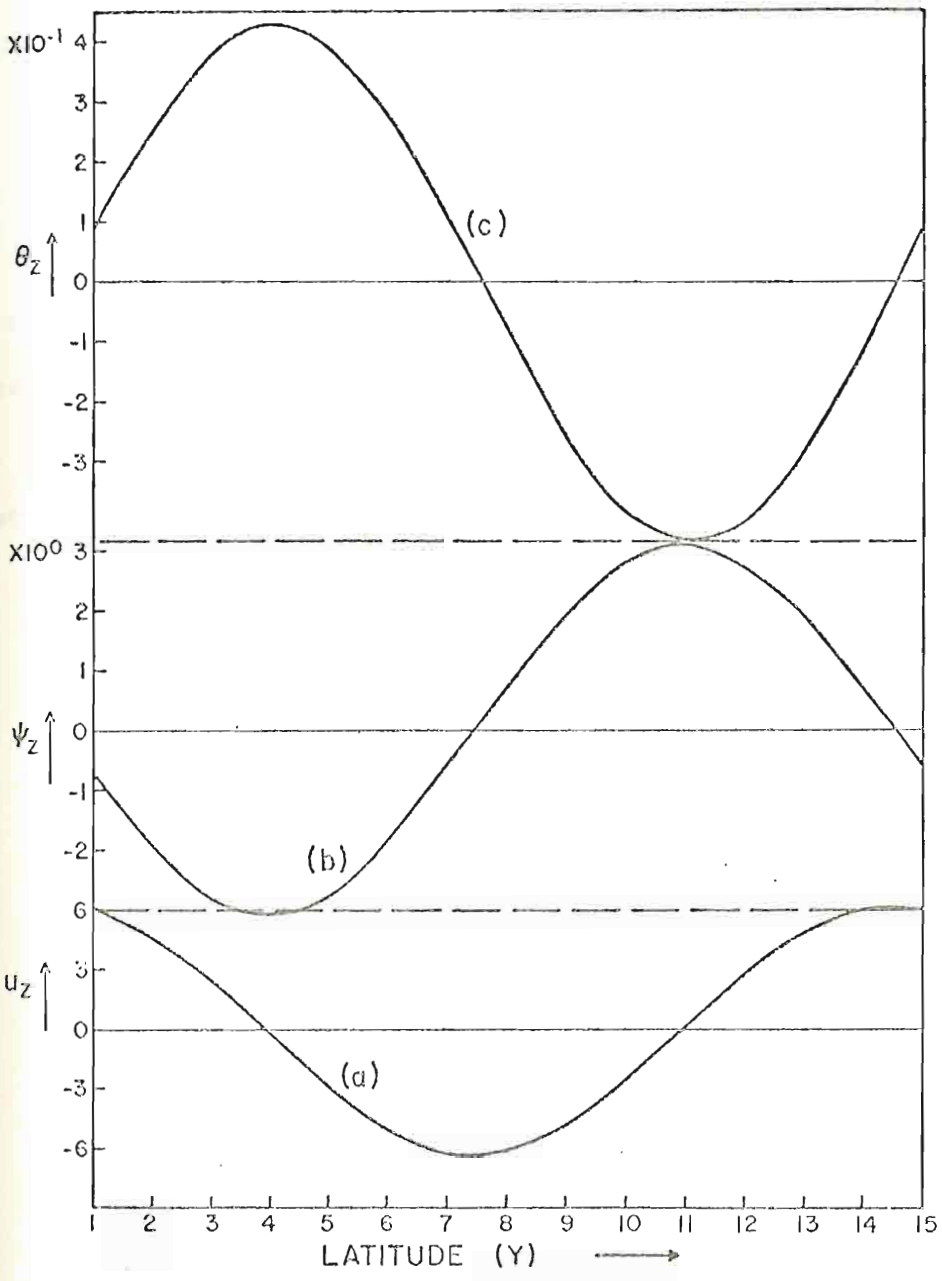

Fig. 4-Idealized initial latitudinal distributions of (a) zonal velocity u in m sec^{-1}, (b) zonal streamfunction in 10^{10} cm^2 sec^{-1}.

Fig. 4-Idealized initial latitudinal distributions of (a) zonal velocity u in m sec^{-1}, (b) zonal streamfunction in 10^{10} cm^2 sec^{-1}, (c) zonal potential temperature in °K.

The first two experiments are without heating or dissipation:

(1) Conservative experiment with

$K = 10{,}000$ km, $\quad L = \pi \times 10^3$ km

(2) Conservative experiment with

$K = 3000$ km, $\quad L = \pi \times 10^3$ km

For the remaining 6 experiments 2 sets of vertical heating profiles have been selected. These profiles are described by values of η as a function of pressure. Three experiments were done with η-profiles which decrease with pressure, and three for η-profiles which increase with pressure. In each set of experiments η is slightly varied and the response of the waves is studied. These are given in Table 2.

Table 2.-Parameters for various experiments

η-decreasing with pressure	η-increasing with pressure
(3) $K_1 = 1.4 \times 10^{-6}$	(6) $K_1 = 1.8 \times 10^{-6}$
$\eta_2 = 0.9$	$\eta_2 = 0.1$
$\eta_4 = 0.6$	$\eta_4 = 0.4$
$\eta_6 = 0.2$	$\eta_6 = 0.9$
(4) $K_1 = 2.0 \times 10^{-6}$	(7) $K_1 = 1.8 \times 10^{-6}$
$\eta_2 = 0.9$	$\eta_2 = 0.6$
$\eta_4 = 0.4$	$\eta_4 = 0.6$
$\eta_6 = 0.1$	$\eta_6 = 0.6$
(5) $K_1 = 1.8 \times 10^{-6}$	(8) $K_1 = 1.8 \times 10^{-6}$
$\eta_2 = 0.9$	$\eta_2 = 0.8$
$\eta_4 = 0.2$	$\eta_4 = 1.1$
$\eta_6 = 0.0$	$\eta_6 = 1.2$

Table 3.-Constants and variables

Quantity	Value	Definition	Units
f_0	4.51×10^{-5}	Coriolis parameter at 18°N	sec^{-1}
β_0	2.18×10^{-13}	Rossby parameter at 18°N	$cm^{-1}\ sec^{-1}$
σ_2	53.0	Static stability at level 2	$°K\ 10^{-3}$ mb
σ_4	80.0	Static stability at level 4	$°K\ 10^{-3}$ mb
σ_6	500.0	Static stability at level 6	$°K\ 10^{-3}$ mb
κ	2/7	Ratio of R/c_p	
c_p	$1.003\ \ 10^7$	Heat capacity of dry air	ergs $g^{-1}\ °K^{-1}$
g	980.665	Gravitational acceleration	$cm^2\ sec^{-1}$
$K_{1,3}$	0.1×10^{-6}	Vertical drag coefficients at various levels	sec^{-1}
$K_{1,5}$	0.2×10^{-7}		sec^{-1}
$K_{1,7}$	0.2×10^{-7}		sec^{-1}
$K_{2,3}$	0.14×10^{-7}		sec^{-1}
$K_{2,5}$	0.12×10^{-7}		sec^{-1}
h_2	0.48×10^{-6}	Radiative relaxation time	sec^{-1}
h_4	0.43×10^{-6}		sec^{-1}
h_6	0.4×10^{-6}		sec^{-1}
ρ_0	10^{-3}	Dry air density at 1000 mb surface	gm cm^{-3}
A	10^5	Horizontal eddy viscosity coefficient	$m^2\ sec^{-1}$
$\theta^{*\,2\ 0}_{1\ 1}$	1.5	Temperature in radiative equilibrium in various levels	°K
$\theta^{*\,4\ 0}_{1\ 1}$	0.7		°K
$\theta^{*\,6\ 0}_{1\ 1}$			
$\theta^{*\,4\ 0}_{1\ 1}$	0.7	Temperature in radiative equilibrium in various levels	°K
$\theta^{*\,6\ 0}_{1\ 1}$	0.3		°K
$\theta^{*\,2\ 0}_{2\ 1}$	0.2		°K

Table 3.-Continued

Quantity	Value	Definition	Units
$\theta^{*\,4\ 0}_{2\ 1}$	0.1	Temperature in radiative equilibrium in various levels	°K
$\theta^{*\,6\ 0}_{2\ 1}$	0.05		°K
Other $\theta^{*\,m}_{n}$	0.0		
ψ	units of 10^{10}	Streamfunction	$cm^2\ sec^{-1}$
ω		Vertical motion in p coordinates	dynes $cm^{-2}\ sec^{-1}$
θ		Potential temperature	°K
P		Pressure	mb
$J(\psi,\nabla^2\psi)$		Jacobian of ψ and $\nabla^2\psi$	
τ		Small-scale frictional stress	
H		Heat	
P_0	1000	1000 mb pressure surface	mb
H_L		Latent heat	
H_R		Radiation heat	
ω^*		Vertical motion at top of boundary layer	
u		Zonal velocity	$m\ sec^{-1}$
R	0.287 10^7	Gas constant for dry air	ergs g^{-1} $°K^{-1}$
K_{Uj}		Kinetic energy of ultralong wave at pressure level j	
K_{Lj}		Kinetic energy of long wave at pressure level j	
K_{Sj}		Kinetic energy of short wave at pressure level j	
K_{Sj}		Kinetic energy of short wave at pressure level j	
A_V	10^5	Vertical kinematic eddy viscosity coefficient	$cm^2\ sec^{-1}$
η_j		Latent heat parameter which varies with height	

CHAPTER V

RESULTS AND DISCUSSIONS

Results of 30 days of integration from the initial flow field described earlier will now be presented. As the model is not designed to govern the zonally symmetric flow or details of ITCZ, attention is focused upon the asymmetry of the motion field, energy cycles and relative importance of $[K_Z \cdot K_E]$ and $[A_E \cdot K_E]$, growth rates of waves at various pressure levels and the vertical variation of wave amplitudes. These will be done for the conservative and non-conservative experiments.

Motion field and its development

Maps of streamfunction ψ, vertical velocity ω, and temperature θ describe at a glance flow patterns, development of asymmetry and its scale dependence, and give indications of some instability mechanisms. Experiment 1 of the conservative case will be discussed first and experiment 5 of the non-conservative case will be presented next.

(i) Conservative case:

In experiment 1 (Fig. 5), the initial state of streamfunction represents small undulations superposed upon a basic zonal state of easterlies at levels 1 and 3. The temperature structure shows a maximum at coordinate y = 4 (Fig. 4), and is positive throughout the tropics with a minimum at y = 12 ($\phi \sim 25°N$). The magnitude of the temperature variation over 1500 km is 0.87°K at level 2, 0.8°K at level 4. The zonally averaged

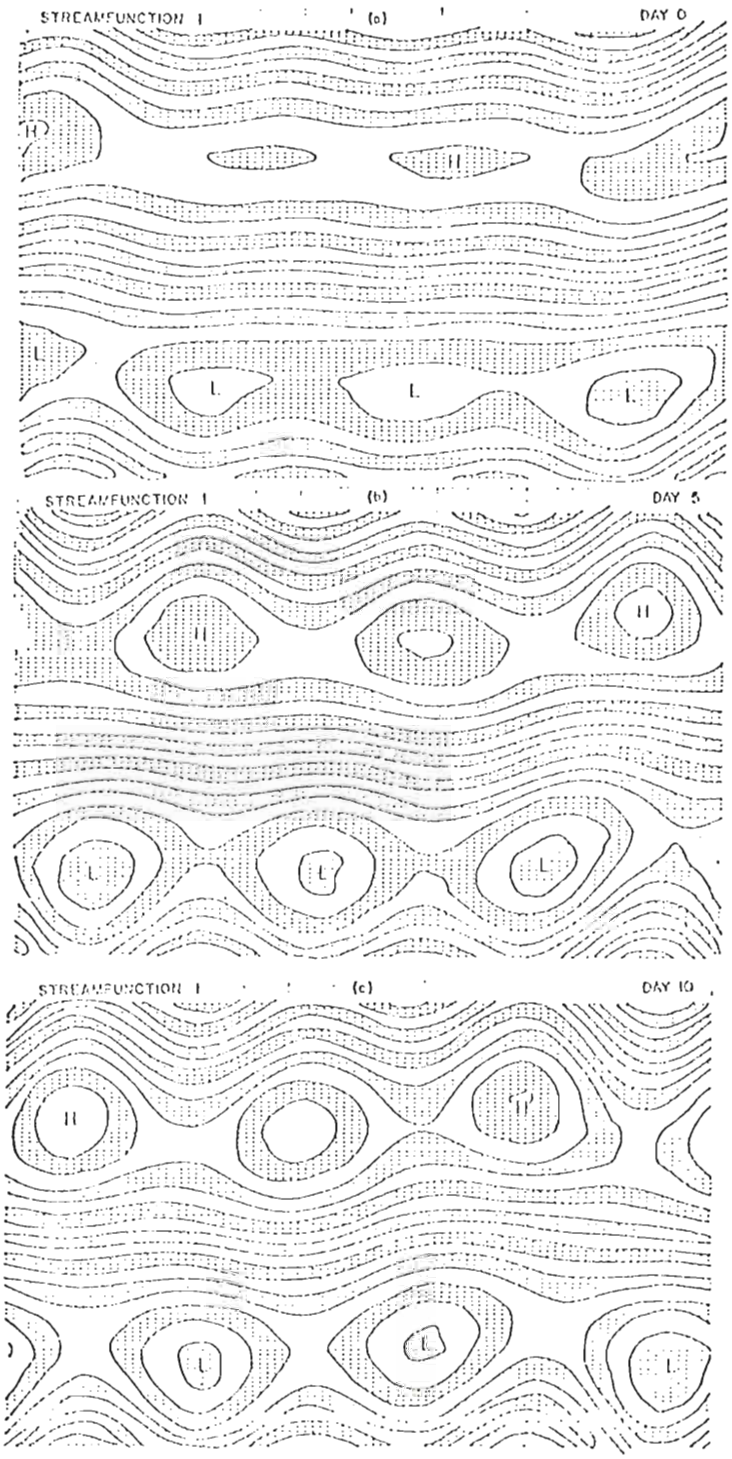

Fig. 5A-Experiment 1. Streamfunction maps at level 1 at intervals of 5 days. Isolines at intervals of 0.5×10^{10} cm^2 sec^{-1}.

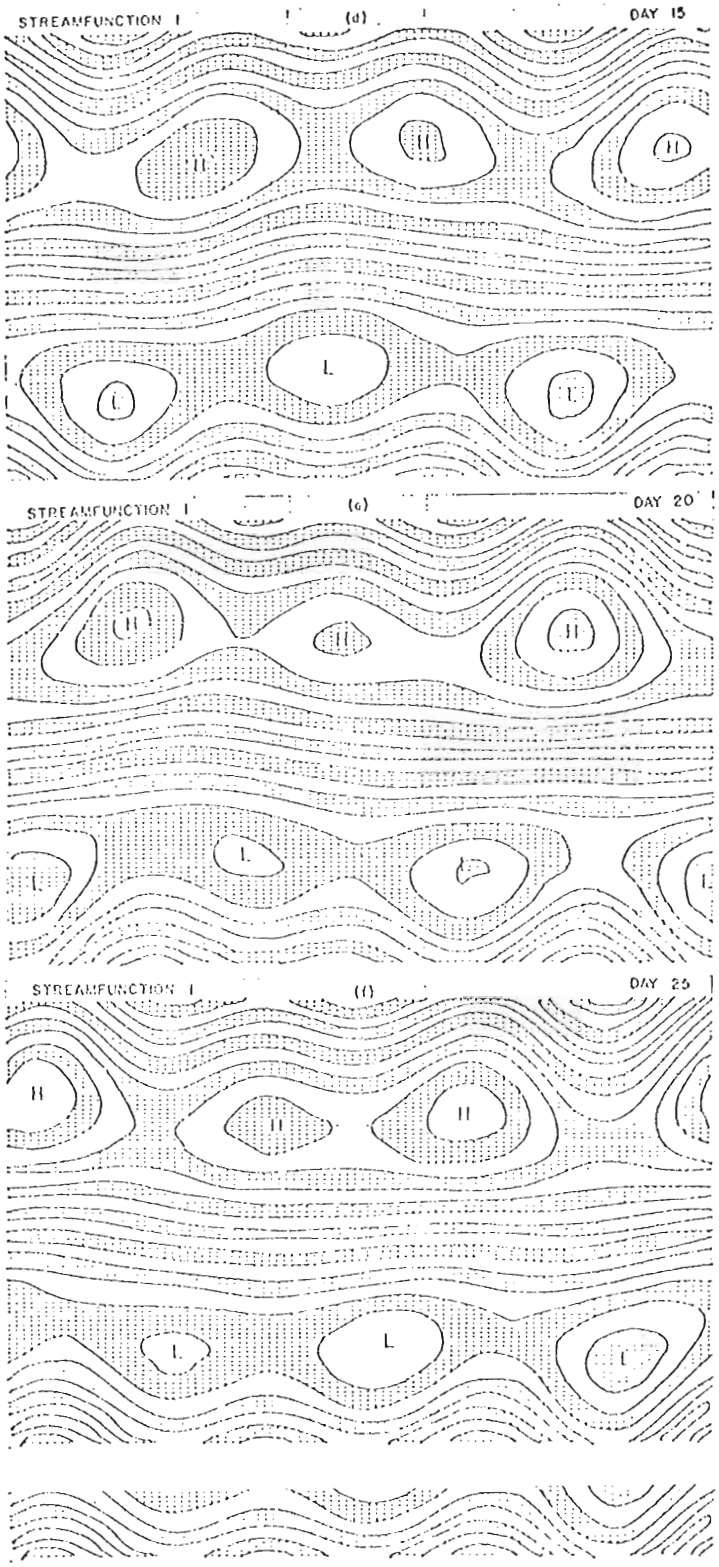

Fig. 5B-Continued. Streamfunction maps at level 1 at intervals of 5 days. Isolines at intervals of 0.5×10^{10} cm^2 sec^{-1}.

vertical motion shows a maximum at y = 3 and is quite small, of the orders of 10^{-5} and 10^{-6} mb sec^{-1}. This is a consequence of the absence of condensation and has been pointed out by Charney (1963). He found from scale analysis that the dry tropics are more horizontally non-divergent than are mid-latitude motions.

On the 5th day in Fig. 5b, the streamfunction shows a classical occurrence of barotropic interaction; the wave tilts horizontally from SW to NE and therefore amplifies. This is also verified by the value $[K_Z \cdot K_E]$ = 3.8129 at level 1. Similarly, amplification at level 3 is also indicated by an appropriate tilt of the wave. On the 10th day, we find an example of decay with SE-NW tilt of the wave. These tilts are opposite in direction to those found in mid-latitudes (Kuo, 1949), but they agree with the observed tilts of tropical waves (Nitta and Yanai, 1969). On the 15th day, the slopes of the wave at levels 1 and 3 are in opposite direction and the $[K_Z \cdot K_E]$ values are of opposite signs. Thus, the wave decays at level 1 and amplifies at level 3. No amplification of the wave at level 1 occurs until the 25th day.

Throughout the wave evolution, wave No. 3 is dominant but has not sufficiently amplified to interfere seriously with the uniform flow of the easterlies. In order to amplify and distort the easterly current, it will be seen that the CISK mechanism is of vital importance. Also observed in the maps and in Fig. 7 is the westward propagation of the waves; in particular the y-independent wave No. 3 which propagates at 3.7 m sec^{-1}, embedded in a current of maximum easterly velocity of 6 m sec^{-1}

ticular the y-independent wave No. 3 which propagates at 3.7 m sec^{-1}, embedded in a current of maximum easterly velocity of 6 m sec^{-1}.

(ii) Non-conservative case:

In experiment 5, except for the ω-field, the initial field is the same as in experiment 1. The values of ω are an order of magnitude larger

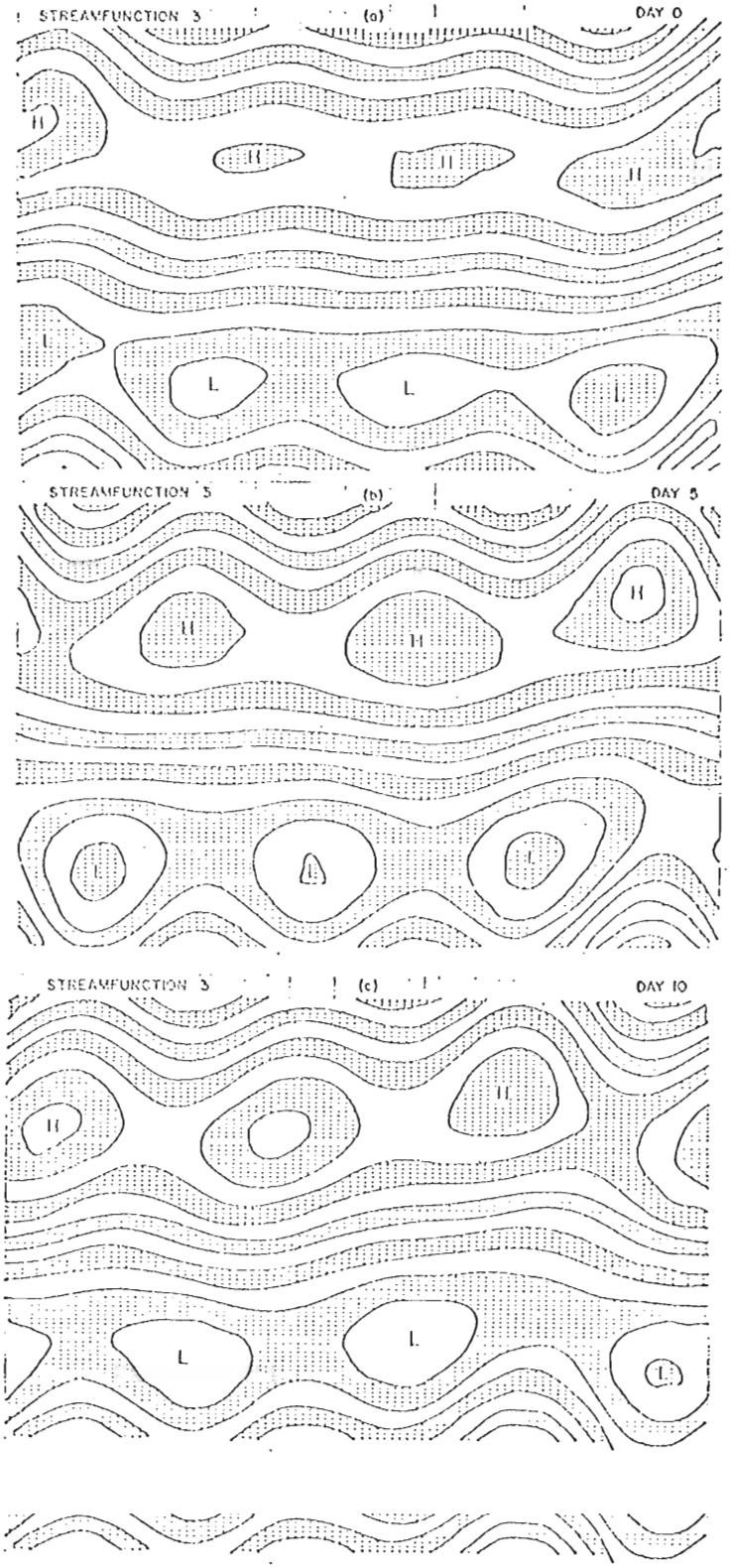

Fig. 6A-Experiment 1. Streamfunction maps at level 3 at intervals of 5 days. Isolines at intervals of 0.5x1010 cm^2 sec^{-1}.

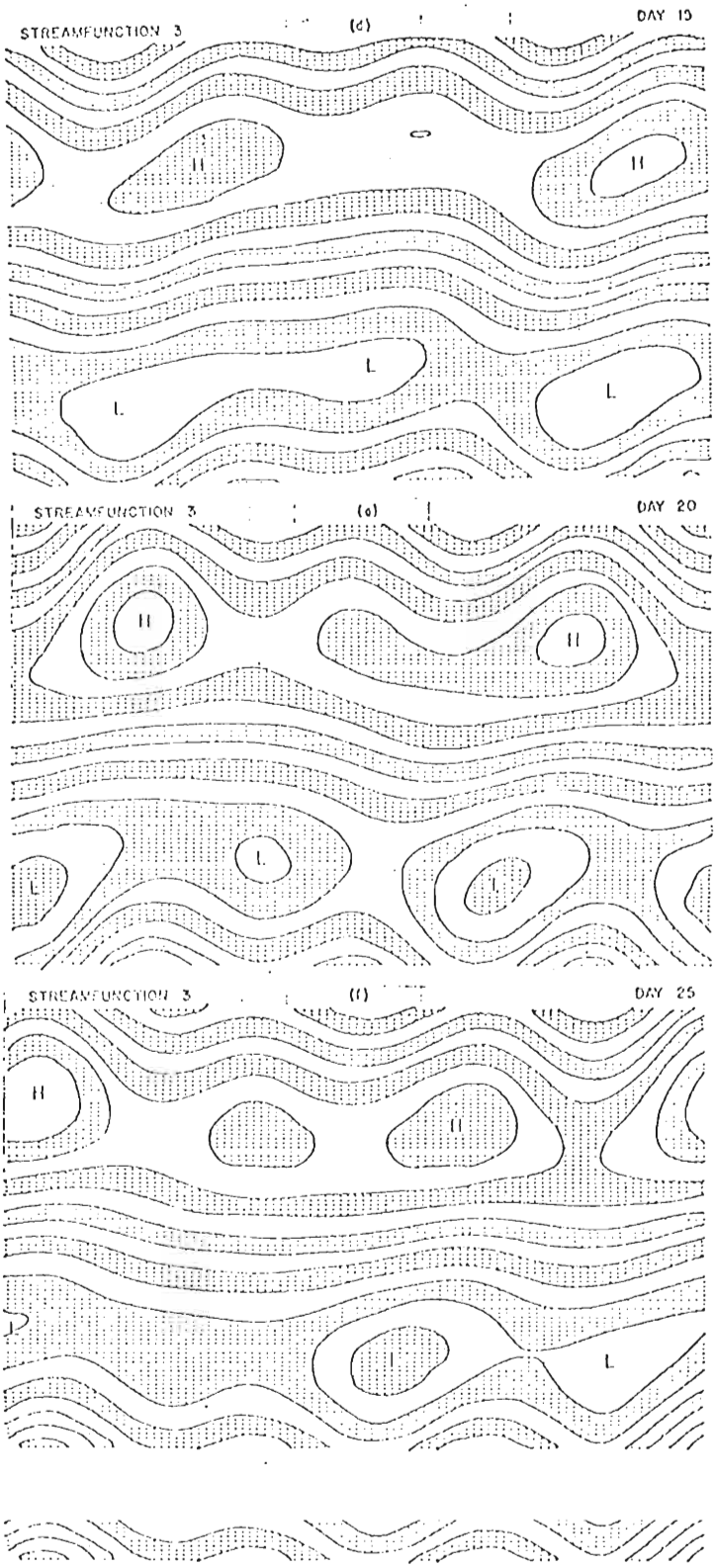

Fig. 6B-Continued. Streamfunction maps at level 3 at intervals of 5 days. Isolines at intervals of 0.5x1010 cm^2 sec^{-1}.

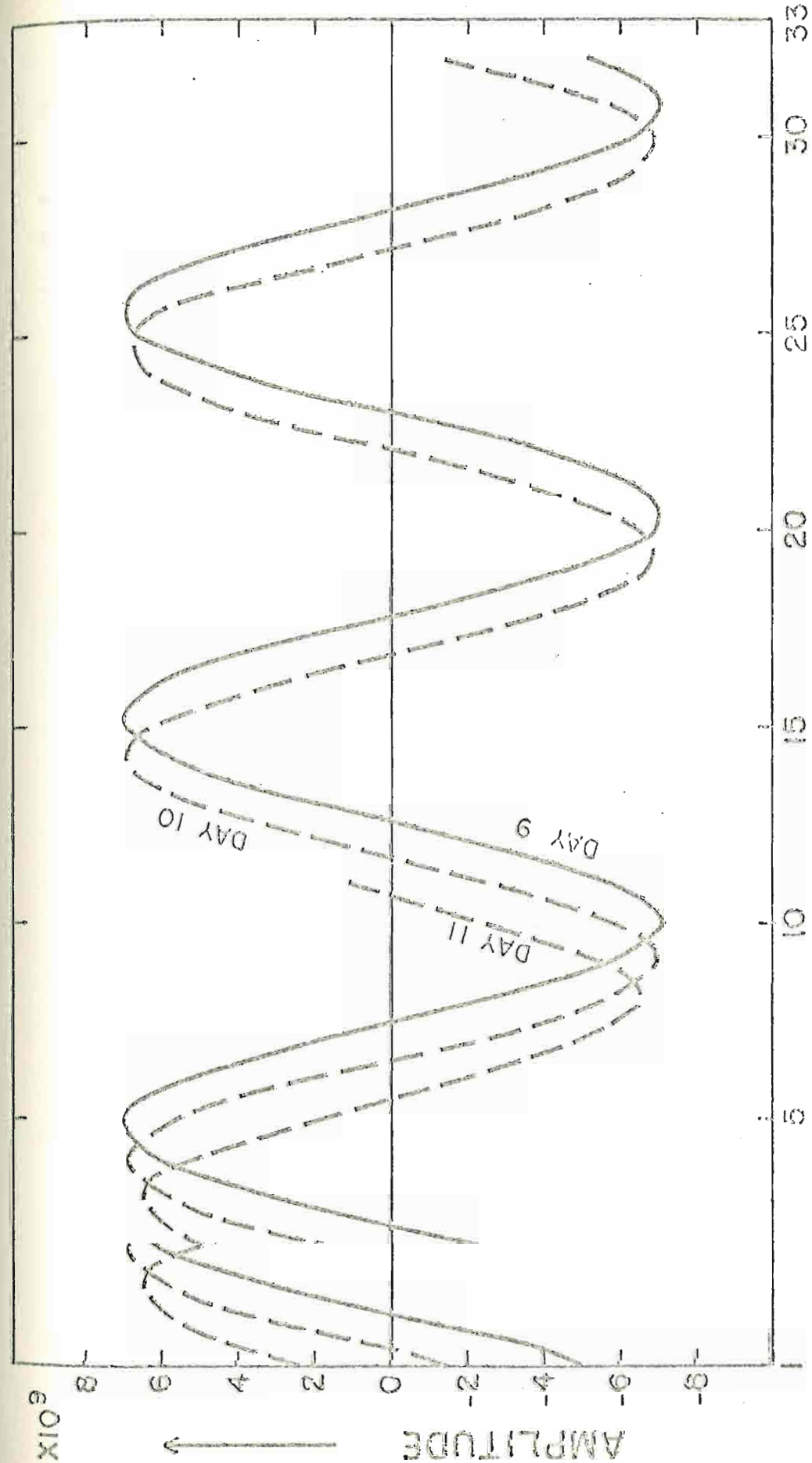

Fig. 7.-Streamfunction of component (3,0) at days 9, 10, 11. Phase speed is 3.7 m sec^{-1}.

Table 4.-Barotropic energy exchanges at levels 1 and 3 in units of ergs cm^{-2} sec^{-1} for experiment 1.

Day	$[K_Z \cdot K_E]_1$	Day	$[K_Z \cdot K_E]_1$	Day	$[K_Z \cdot K_E]_3$	Day	$[K_Z \cdot K_E]_3$
1	$+9,7147\times10^{-1}$	16	-1.2405×10^{0}	1	$+5.8347\times10^{-1}$	16	$+1.2632\times10^{0}$
2	$+2.5714\times10^{0}$	17	-1.2420×10^{0}	2	$+1.6906\times10^{0}$	17	$+1.4874\times10^{0}$
3	$+2.7259\times10^{0}$	18	-8.9062×10^{-2}	3	-1.3360×10^{0}	18	$+2.5357\times10^{0}$
4	$+4.5140\times10^{0}$	19	-1.1335×10^{0}	4	$+2.4287\times10^{0}$	19	$+1.2145\times10^{0}$
5	$+3.8129\times10^{0}$	20	-5.4711×10^{-1}	5	$+1.1505\times10^{0}$	20	$+1.4141\times10^{0}$
6	$+3.9532\times10^{0}$	21	-1.3640×10^{0}	6	$+7.8880\times10^{-1}$	21	$+1.0254\times10^{-1}$
7	$+2.4738\times10^{0}$	22	-6.2222×10^{-1}	7	-7.9386×10^{-1}	22	$+1.5057\times10^{-1}$
8	$+1.2091\times10^{0}$	23	$+2.6598\times10^{-2}$	8	$+1.8822\times10^{0}$	23	$+1.9688\times10^{-1}$
9	$+6.8268\times10^{-1}$	24	$+4.1864\times10^{-1}$	9	-1.9558×10^{0}	24	-1.1248×10^{-1}
10	-7.3634×10^{-1}	25	$+1.4879\times10^{0}$	10	-2.7657×10^{0}	25	$+6.0161\times10^{-1}$
11	-2.6253×10^{-1}	26	$+8.6560\times10^{-1}$	11	-1.6260×10^{0}	26	-3.7489×10^{-1}
12	-1.8874×10^{0}	27	$+1.8825\times10^{0}$	12	-2.4196×10^{0}	27	$+5.4266\times10^{-1}$
13	-1.4885×10^{0}	28	$+1.4847\times10^{0}$	13	-1.1889×10^{0}	28	$+4.5195\times10^{-2}$
14	-2.4213×10^{0}	29	$+2.4742\times10^{0}$	14	-1.1754×10^{0}	28	$+9.3318\times10^{-1}$
15	-1.9244×10^{0}	30	$+2.4713\times10^{0}$	15	$+6.7156\times10^{-3}$	30	$+9.6211\times10^{-1}$

Table 5.-Barotropic energy conversions at levels 1 and 3 in units of ergs cm^{-2} sec^{-1} for experiment 5.

Day	$[K_Z \cdot K_E]_1$	Day	$[K_Z \cdot K_E]_1$	Day	$[K_Z \cdot K_E]_3$	Day	$[K_Z \cdot K_E]_3$
1	$+1.2296\times10^{0}$	16	$+1.7902\times10^{2}$	1	$+1.5225\times10^{-1}$	16	$+2.5652\times10^{2}$
2	$+3.8467\times10^{0}$	17	-9.3261×10^{1}	2	$+2.0760\times10^{-1}$	17	$+5.4695\times10^{1}$
3	$+5.7815\times10^{0}$	18	-1.0583×10^{3}	3	-1.0125×10^{-1}	18	-9.1093×10^{1}
4	$+1.1142\times10^{1}$	19	-9.7963×10^{1}	4	-1.1074×10^{-2}	19	-4.6852×10^{1}
5	$+1.5113\times10^{1}$	20	$+1.5920\times10^{3}$	5	-7.8688×10^{-3}	20	$+4.5215\times10^{0}$
6	$+2.2911\times10^{1}$	21	-3.5835×10^{2}	6	-1.0202×10^{-1}	21	-2.6366×10^{2}
7	$+3.1503\times10^{1}$	22	$+7.9133\times10^{1}$	7	-6.9448×10^{-1}	22	-1.3182×10^{2}
8	$+4.6743\times10^{1}$	23	-1.8062×10^{1}	8	-1.8373×10^{0}	23	$+2.9652\times10^{2}$
9	$+7.2184\times10^{1}$	24	-1.3396×10^{3}	9	-4.3976×10^{0}	24	-2.2759×10^{2}
10	$+1.1458\times10^{2}$	25	$+2.4019\times10^{3}$	10	-9.3824×10^{0}	25	$+1.1195\times10^{2}$
11	$+1.8537\times10^{2}$	26	-9.4549×10^{2}	11	-1.7530×10^{1}	26	-1.4910×10^{1}
12	$+2.7399\times10^{2}$	27	$+5.4346\times10^{2}$	12	-2.7931×10^{1}	27	$+6.3421\times10^{1}$
13	$+3.0103\times10^{2}$	28	-1.1509×10^{3}	13	-1.2366×10^{1}	28	-6.1260×10^{2}
14	$+6.2695\times10^{1}$	29	-2.8891×10^{2}	14	$+2.2395\times10^{1}$	29	$+1.7015\times10^{2}$
15	$+1.6310\times10^{2}$	30	$+5.3959\times10^{2}$	15	$+2.7632\times10^{2}$	30	-2.0217×10^{2}

than in the conservative case, with a maximum initial zonal ascent of 2.04×10^{-4} mb sec^{-1} in low latitudes (see Fig. 8). Thus, as pointed out by Charney (1963), the effect of condensation is large and affects in important ways the dynamics of the tropics. On the 5th day $[K_Z \cdot K_E]$ at level 1 is about 4 times as much as its value on the corresponding day in the conservative case. This is due to the maintenance of K_Z by release of zonal latent heat $\overline{\eta}\ \overline{\omega^*}$. Level 1 on this day shows positive values of $[K_Z \cdot K_E]$ and an associated SW-NE tilt of the wave. Level 3, on the other hand, shows little barotropic exchange. On the 10th day, considerable amplification is observed with a very pronounced SW-NE tilt and a break-up in the symmetry of the zonal easterlies. This flow pattern resembles more closely the tropical streamfunction pattern illustrated by Krishnamurti (1971b). The level 1 ω-field also indicates the development of the asymmetry; maximum zonal ω is 3.3×10^{-4} mb sec^{-1}, while maximum rise associated with the asymmetry is as high as 5.6×10^{-4} mb sec^{-1}, which occurs at coordinate (3,5). On the 20th day, wave amplification is so large that it dominates the whole motion field. Such amplification can be controlled by incorporating in the latent heat parameterization a time-dependent stability parameter. When the environmental temperature becomes that of the convective moist element, no more heat should be released. The associated zonal ω-field on this day exhibits a maximum of 4.2×10^{-4} mb sec^{-1} at y = 3 and an asymmetric maximum of 9.8×10^{-4} mb sec^{-1} at coordinate (6,6). Thus, as pointed out by Bates (1970), asymmetries can become an important part in the description of the general circulation. We may point out that another asymmetric term which arises in non-linear latent heat parameterization $\overline{\eta'\omega^{*\prime}}$ has been omitted in the present model. This

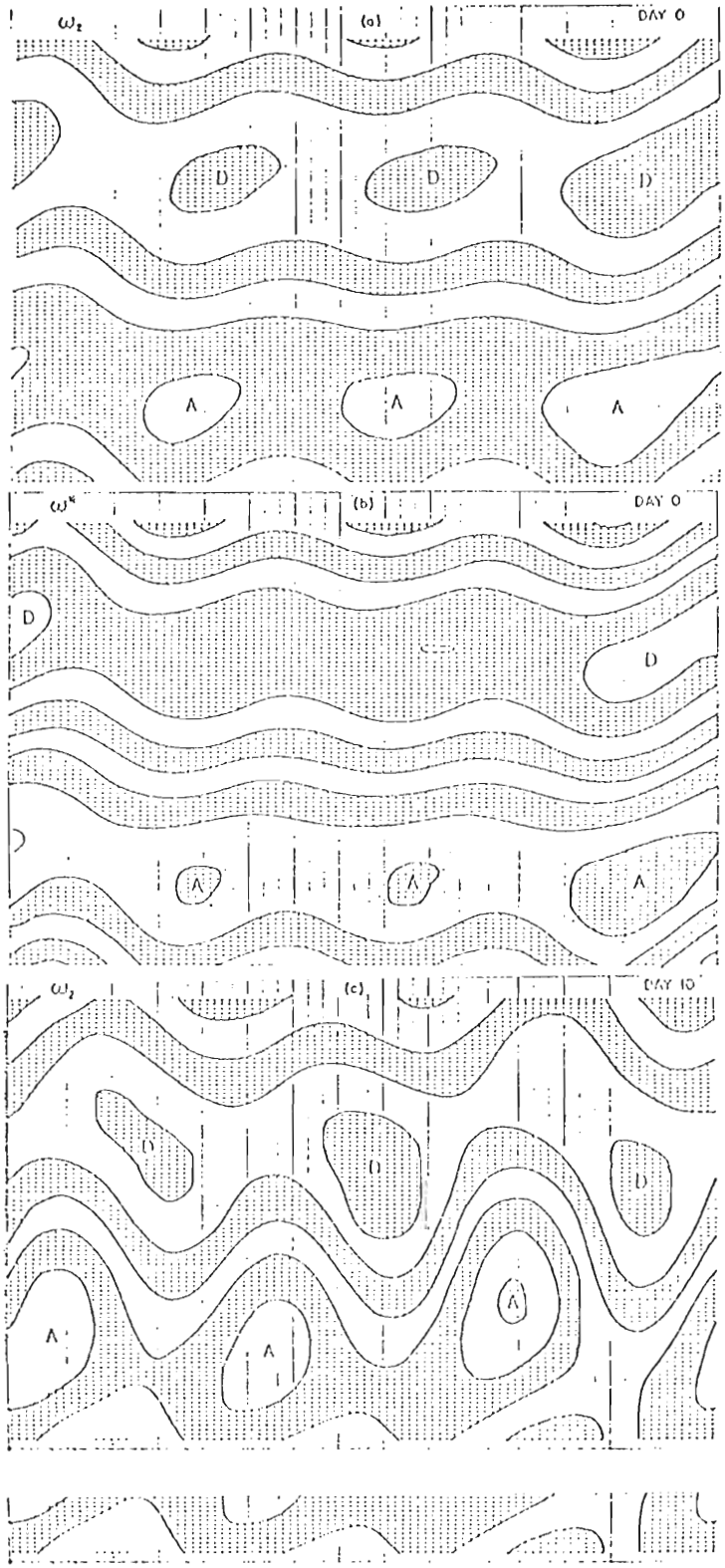

Fig. 8A-Experiment 5. Vertical motions ω and ω* for indicated days. Isolines at intervals of (i) 2×10^{-1} dynes cm^{-2} sec^{-1} for first 10 days for ω and 4.5×10^{-1} for ω*(a,b,c,d), (ii) 5×10^{-1} dynes cm^{-2} sec^{-1} for (e).

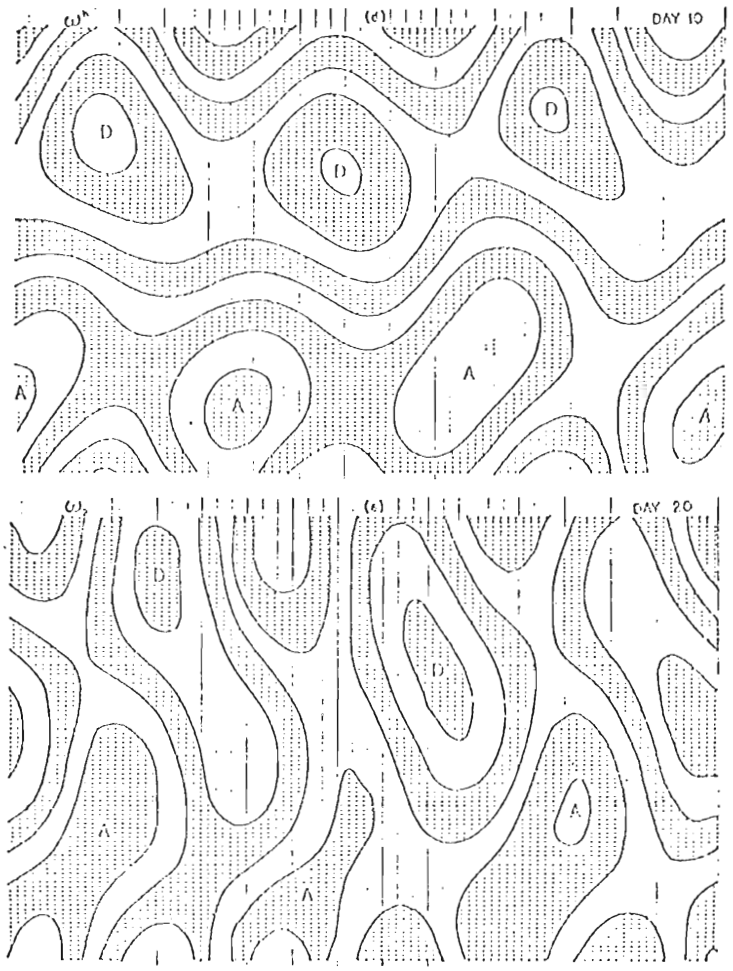

Fig. 8B-Continued. Vertical motions ω and ω^* for indicated days. Isolines at intervals of (i) 2×10^{-1} dynes cm^{-2} sec^{-1} for first 10 days for

Fig. 8B-Continued. Vertical motions ω and ω^* for indicated days. Isolines at intervals of (i) 2×10^{-1} dynes cm^{-2} sec^{-1} for first 10 days for ω and 4.5×10^{-1} for ω^* (a,b,c,d), (ii) 5×10^{-1} dynes cm^{-2} sec^{-1} for (e).

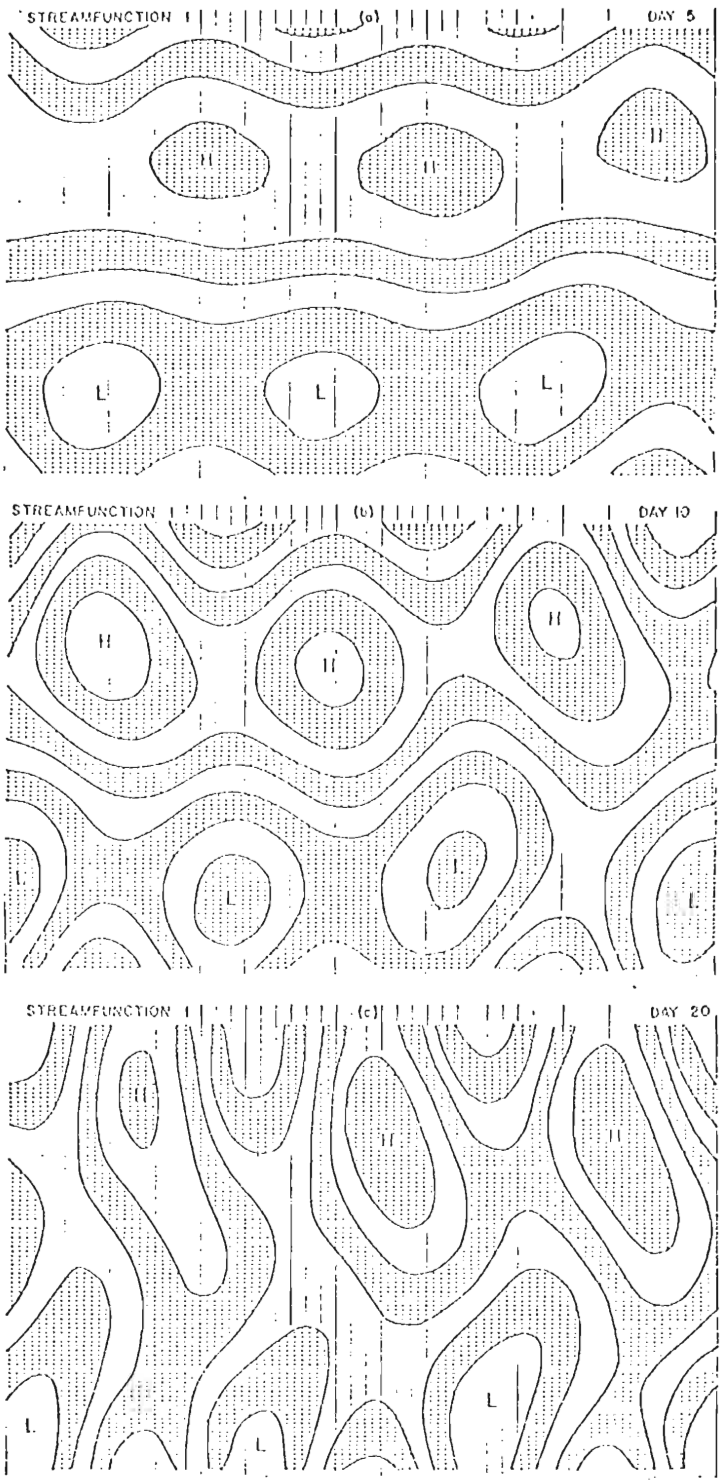

Fig. 9A-Experiment 5. Streamfunction maps at level 1 at intervals of (i) 2×10^{10} cm^2 sec^{-1} for first 10 days and (ii) 5×10^{10} cm^2 sec^{-1} for remaining days.

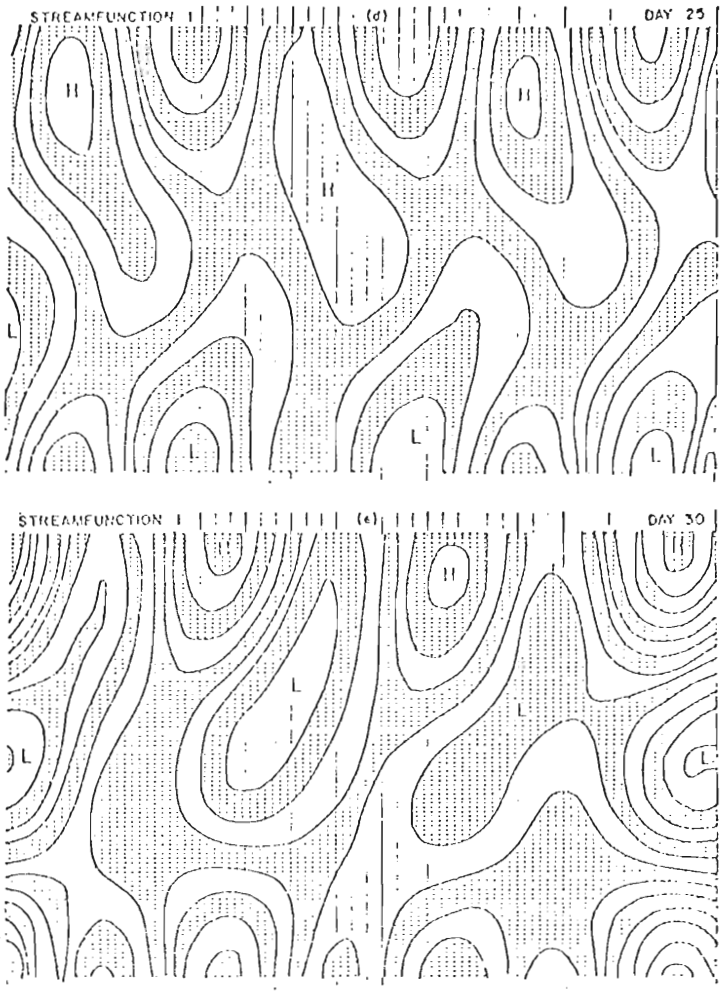

Fig. 9B-Continued. Streamfunction maps at level 1 at intervals of (i) 2×10^{10} cm^2 sec^{-1} for first 10 days and (ii) 5×10^{10} cm^2 sec^{-1} for remaining days.

term, as shown by Bates (1970), contributes to the maintenance of the zonal shear. This will be referred to again in the discussion of energy cycles. To complete this section, reference is made to the maps on days 25 and 30 for further dominance of the asymmetries in the flow patterns.

Energy cycles

The waves which appear in the maps derive their energy from various sources at various stages of their development. In this section concentration will be focused on the relative roles of barotropic and CISK mechanisms in generating and maintaining these tropical eddies. This will be done by presenting energy cycles in the manner of Phillips (1956) and figures of variation of $[K_Z \cdot K_E]$ and $[A_E \cdot K_E]$ with time. The energy cycles will be given for selected days as suggested by details in the figures of $[K_Z \cdot K_E]$ and $[A_E \cdot K_E]$.

For experiment 3, where integration is carried out for 17 days, Fig. 10a shows that for the first 10 days, the eddies are maintained mainly by barotropic gain of energy from the basic current and then by the CISK mechanism. Both processes operate at the same time, but the barotropic mechanism dominates. Two energy cycles in Fig. 11 for days suggested by Fig. 10a are constructed. The first, which represents the initial stages of the development, shows domination of $[K_Z \cdot K_E]$ over $[A_E \cdot K_E]$. The basic current is in turn maintained by $[A_Z \cdot K_Z]$ so long as A_Z can be adequately maintained by $L[H_Z \cdot A_Z]$. This conversion is due to release of zonal latent heat which builds up a N-S temperature gradi-

as A_Z can be adequately maintained by $L[H_Z \cdot A_Z]$. This conversion is due to release of zonal latent heat which builds up a N-S temperature gradi-

ent. Radiation acts as a sink for A_Z and A_E and is at least one order of magnitude smaller than latent heat release. Another interesting feature on this diagram is the dominance of $L[H_Z \cdot A_Z]$ over $L[H_E \cdot A_E]$, i.e., the

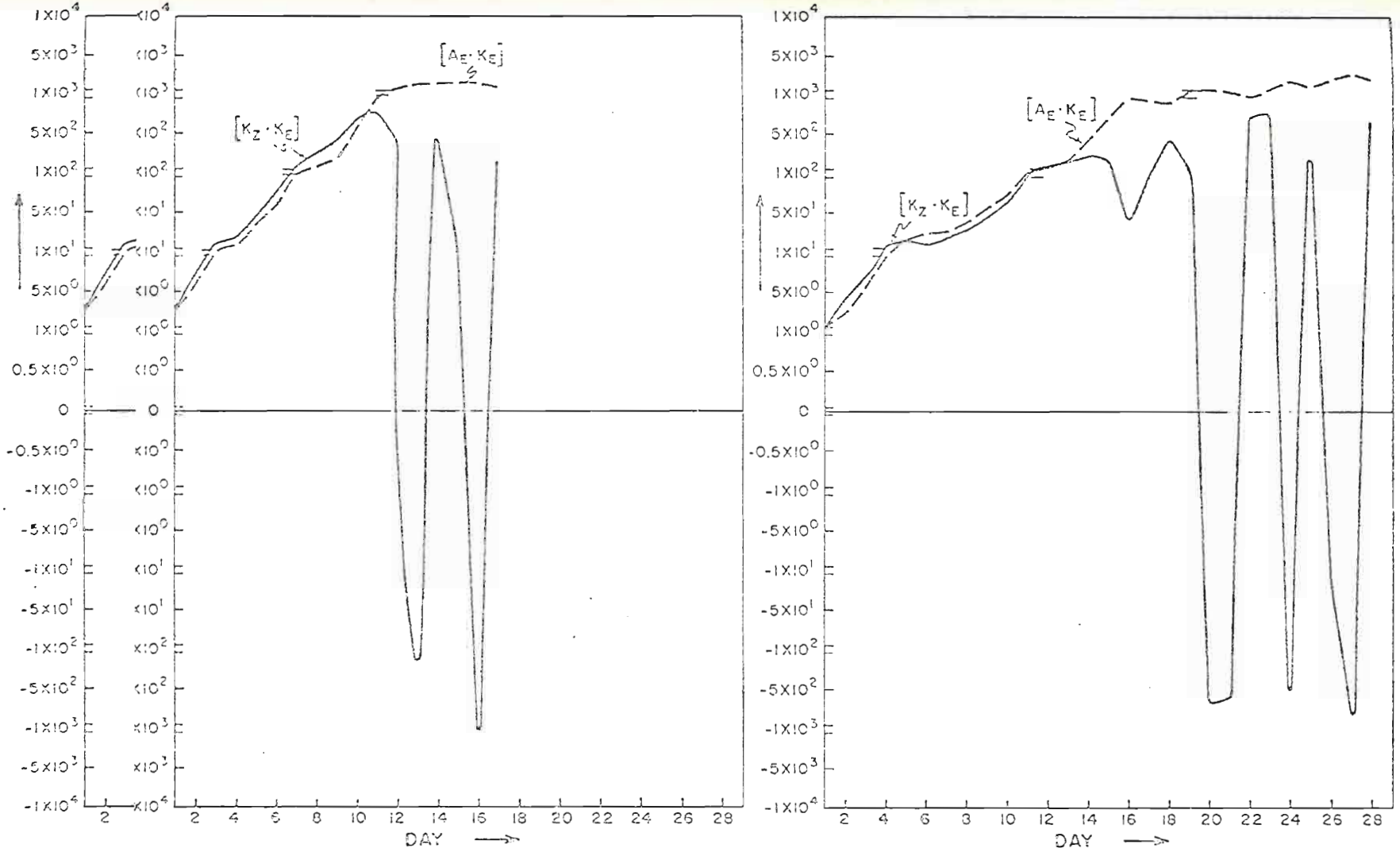

Fig. 10.-$[K_Z \cdot K_E]$ and $[A_E \cdot K_E]$ for (a) experiment 3, and (b) experiment 4. Units are in ergs cm^{-2} sec^{-1}.

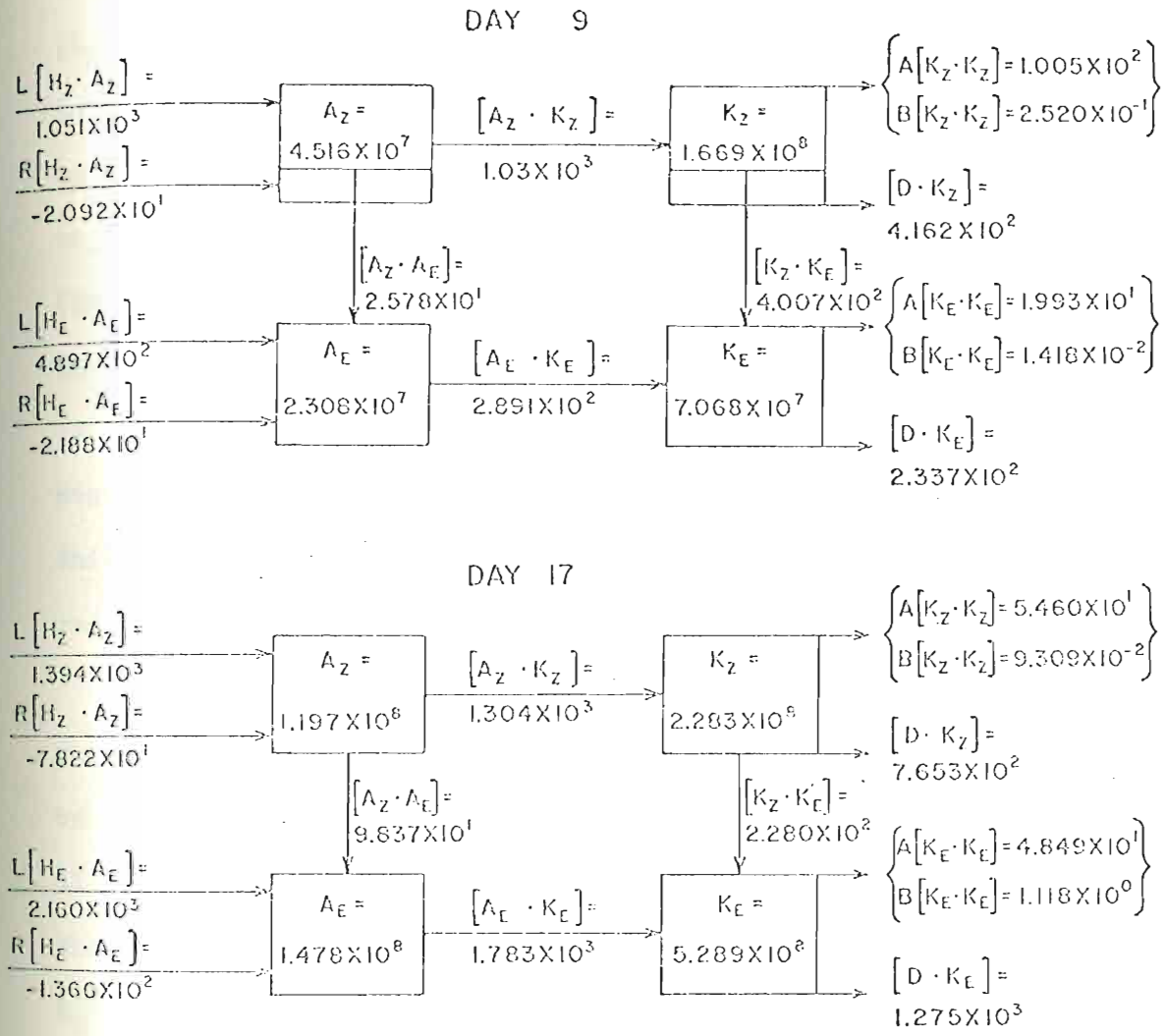

Fig. 11 - Energy cycle for experiment 3 in units of ergs cm^{-2} for the energies or ergs cm^{-2} for the exchanges.

Fig. 11 - Energy cycle for experiment 3 in units of ergs cm^{-2} for the energies or ergs cm^{-2} for the exchanges.

E-W solenoidal field has not yet been built up to a value that $[A_E \cdot K_E]$ can become the major source of eddy kinetic energy. It is for this reason that K_E is still maintained primarily by K_Z and the magnitude of $[K_Z \cdot K_E]$ is larger than in the conservative case; $L[H_Z \cdot A_Z]$ was absent in the latter case. On the 17th day, the energy cycle shows a reversal in the relative contribution of $[A_E \cdot K_E]$ and $[K_Z \cdot K_E]$, and $L[H_E \cdot A_E]$ is larger than $L[H_Z \cdot A_Z]$. Radiation, again, plays a minor role. Charney (1969) has computed from observations by Bjerknes, Venkateswaran and others that 90 per cent of the available potential energy in the tropics is obtained from release of latent heat. The cycles in Fig. 11 show negative values for radiation contribution to available potential energy; this is due to a maximum tropical temperature which is larger than the radiative equilibrium temperature.

The question of storage of $L[H_Z \cdot A_Z]$ and $L[H_E \cdot A_E]$ in A_Z and A_E, respectively, as opposed to an instant conversion to kinetic energy, can be answered by a comparison of the energy cycles for the two days in Fig. 11. Although the rates of conversion to kinetic energy are comparable to the rates of $L[H_Z \cdot A_Z]$ and $L[H_E \cdot A_E]$, there is a significant storage of A_Z and A_E over a period of 17 days. This is somewhat in disagreement with a conclusion of Wallace (1971) that "vertical motions convert potential energy to kinetic energy at almost the same rate that it is generated, i.e., there is no appreciable storage of available potential energy." The disagreement may be due to linear latent heat which accumulates small amounts of storage of A_Z and A_E over a long period of time.
disagreement may be due to linear latent heat which accumulates small amounts of storage of A_Z and A_E over a long period of time.

In experiment 4 where upper level heating has been slightly reduced, Fig. 10b shows that initially the barotropic contribution still dominates until the 4th day, remains comparable to $[A_E \cdot K_E]$ until the 14th day and

then takes second place to CISK which dominates for the rest of the period. The barotropic term is larger than CISK for a shorter period of time than in experiment 1; this is due to larger boundary dissipation and less $[A_Z \cdot K_Z]$ conversion which depends upon zonal heating (Fig. 13). A similar situation is observed in experiment 5 (Figs. 12a and 14), where upper level heating is even further reduced and dissipation assumes a value between those of experiments 3 and 4.

In all experiments, most dissipation of the zonal and eddy kinetic energy takes place at the boundary layer. It is possible, if a strong internal jet occurs, that internal dissipation would exceed boundary layer dissipation as has been computed by Charney (1968) from observations by Palmén. Such a jet does not exist in the present investigation. We may also remark that in experiment 3 energy fluxes from troposphere to stratosphere have been included in the energy cycles. These fluxes play a minor role in the energetics of the troposphere, but may be significant in the studies of the stratosphere as demonstrated by Peng (1965) and Clark (1969). Recently, Wallace (1971) has computed from observations that leakage of wave energy to the stratosphere is at least an order of magnitude smaller than the rate of energy conversion.

An important conclusion can be drawn from the energy cycles and the associated figures of $[A_E \cdot K_E]$ and $[K_Z \cdot K_E]$. Initially, the barotropic exchange of energy is important for generating and maintaining tropical eddies and latent heat becomes important at the more mature stage of the eddies. A similar and independent conclusion was reached in a two-level eddies and latent heat becomes important at the more mature stage of the eddies. A similar and independent conclusion was reached in a two-level model by Bates (1960). The additional information in the present model shows the dependence of the duration of large barotropic exchange upon the

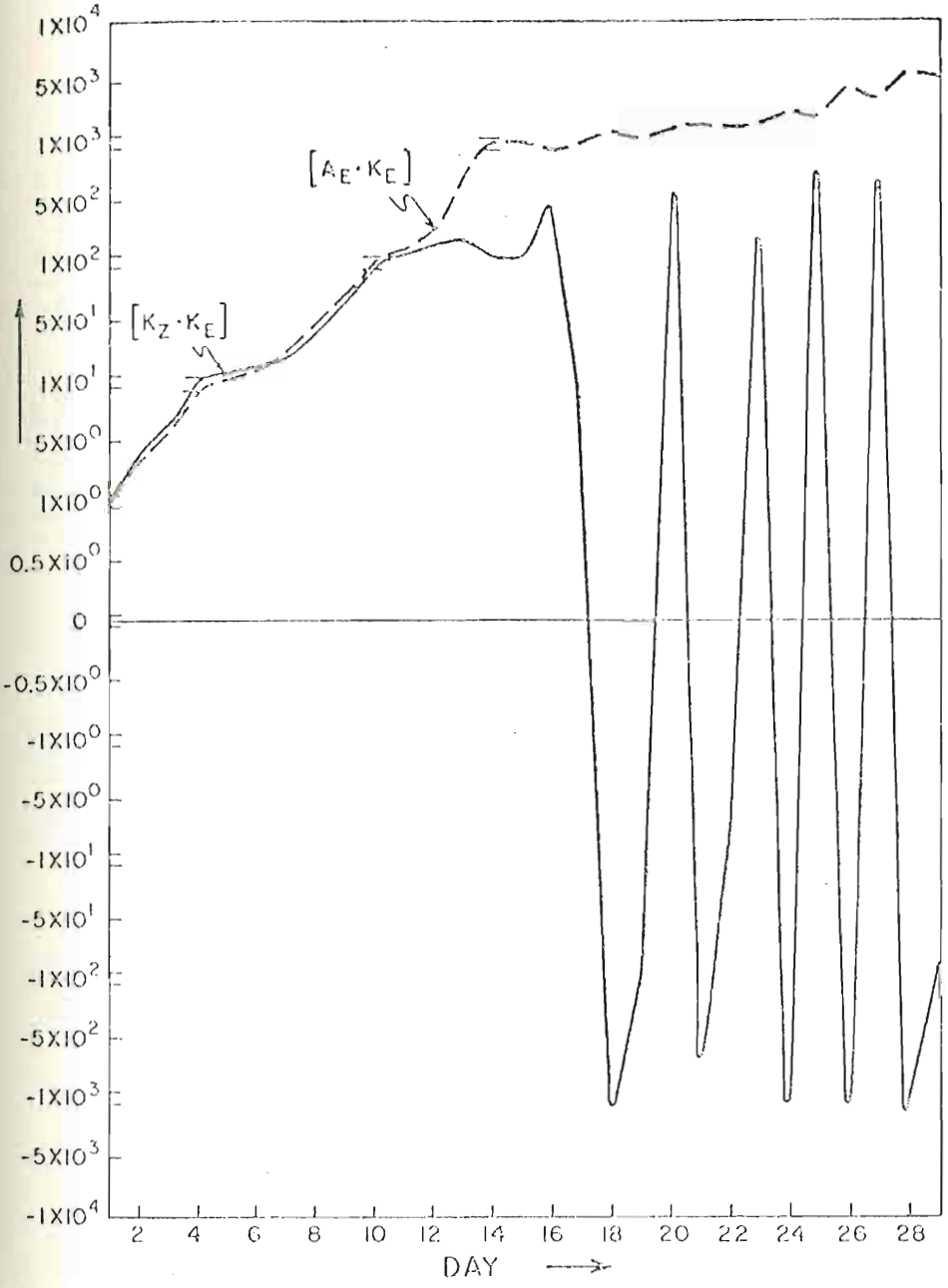

Fig. 12.-$[K_Z \cdot K_E]$ and $[A_E \cdot K_E]$ for experiment 5. Units are in ergs cm^{-2} sec^{-1}.

Fig. 12.-$[K_Z \cdot K_E]$ and $[A_E \cdot K_E]$ for experiment 5. Units are in ergs cm^{-2} sec^{-1}.

DAY 4

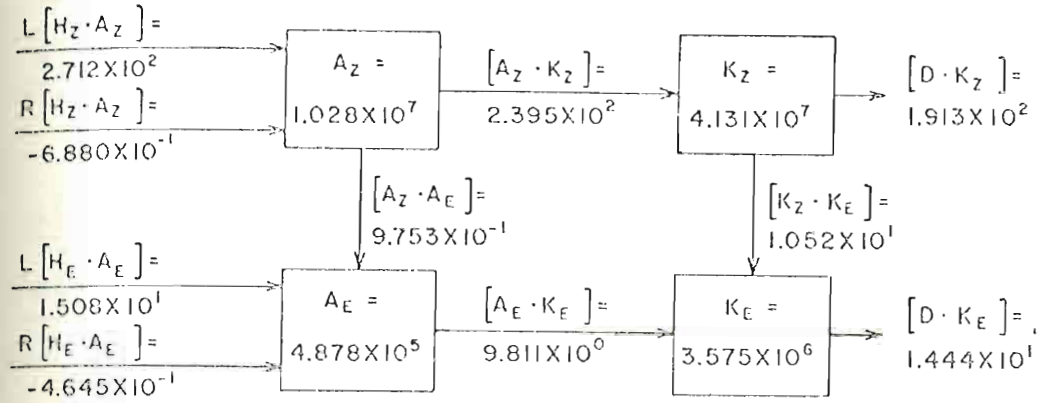

DAY 14

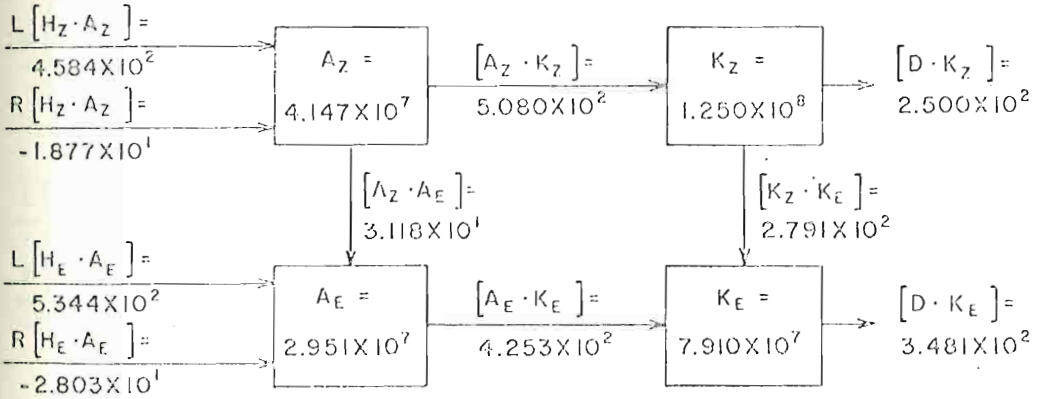

Fig. 13.-Energy cycle for experiment 4 in units of ergs cm^{-2} or ergs cm^{-2} sec^{-1}.

DAY 6

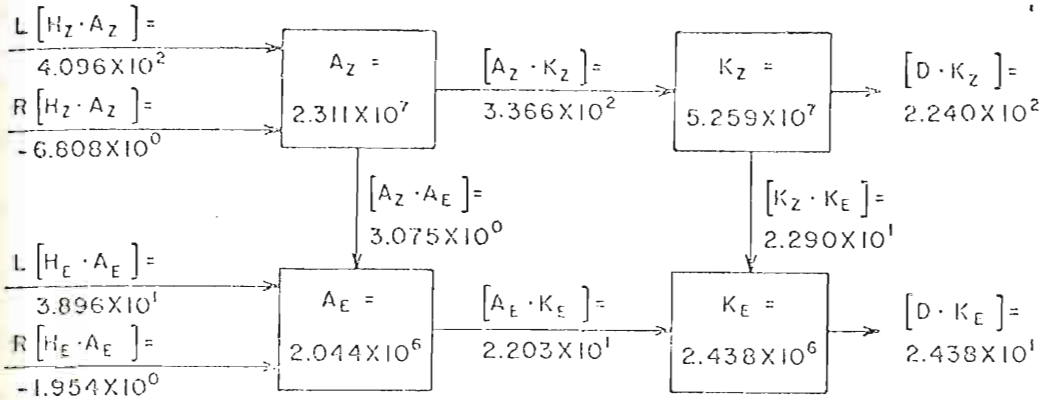

DAY 16

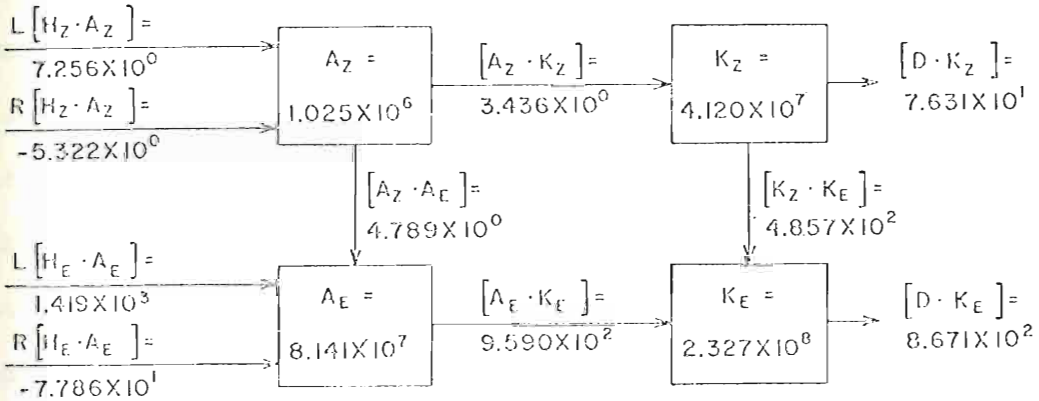

Fig. 14.-Energy cycle for experiment 5 in units of ergs cm^{-2} or ergs cm^{-2} sec^{-1}.

ergs cm^{-2} sec^{-1}.

vertical distribution of latent heat which was not possible in a two-level model.

We have stated earlier that $[K_Z \cdot K_E]$ can take place so long as K_Z is maintained. K_Z can be more properly maintained with a non-linear latent heat formulation which results in a high positive correlation between the eddy potential temperature and the vertical motion at the top of the boundary layer. It is expected that such an addition to the model would increase the small periodicity in the oscillations of $[K_Z \cdot K_E]$ which occur during the latter days of the integration (Figs. 10a and 10b). At these stages, it was found that the basic current was not sufficiently strong to maintain K_E; instead K_E was maintained by large values of $[A_E \cdot K_E]$ which makes K_E a source for K_Z. As pointed out by Lorenz (1960), such major fluctuations are common when the disturbance is very intense. Bates (1970) has utilized non-linear heating in the form of $\overline{\eta\omega^*} = \overline{\eta}\ \overline{\omega^*} + \overline{\eta'\omega^{*\prime}}$ in which the asymmetries of $\overline{\eta'\omega^{*\prime}}$ contributed to increasing the shear of the basic current in the face of drain by the growth of K_E. This does not seem to be necessary so long as K_Z is maintained by $L[H_Z \cdot A_Z]$ and the eddies can grow.

A different picture emerges from Figs. 15a and 15b and the associated energy cycle in Fig. 16 for experiments 6 and 8. In both cases $[A_E \cdot K_E]$ conversion dominates even at the early stages of the integration, but that of experiment 6 is less active. Thus, if latent heat is released in sufficiently large quantities and the shear of the zonal wind is relatively small, CISK can become the major contributor to tropical released in sufficiently large quantities and the shear of the zonal wind is relatively small, CISK can become the major contributor to tropical eddies throughout the wave evolution. In fact, in Yamasaki (1969) where barotropic instability has been completely excluded, a linearized

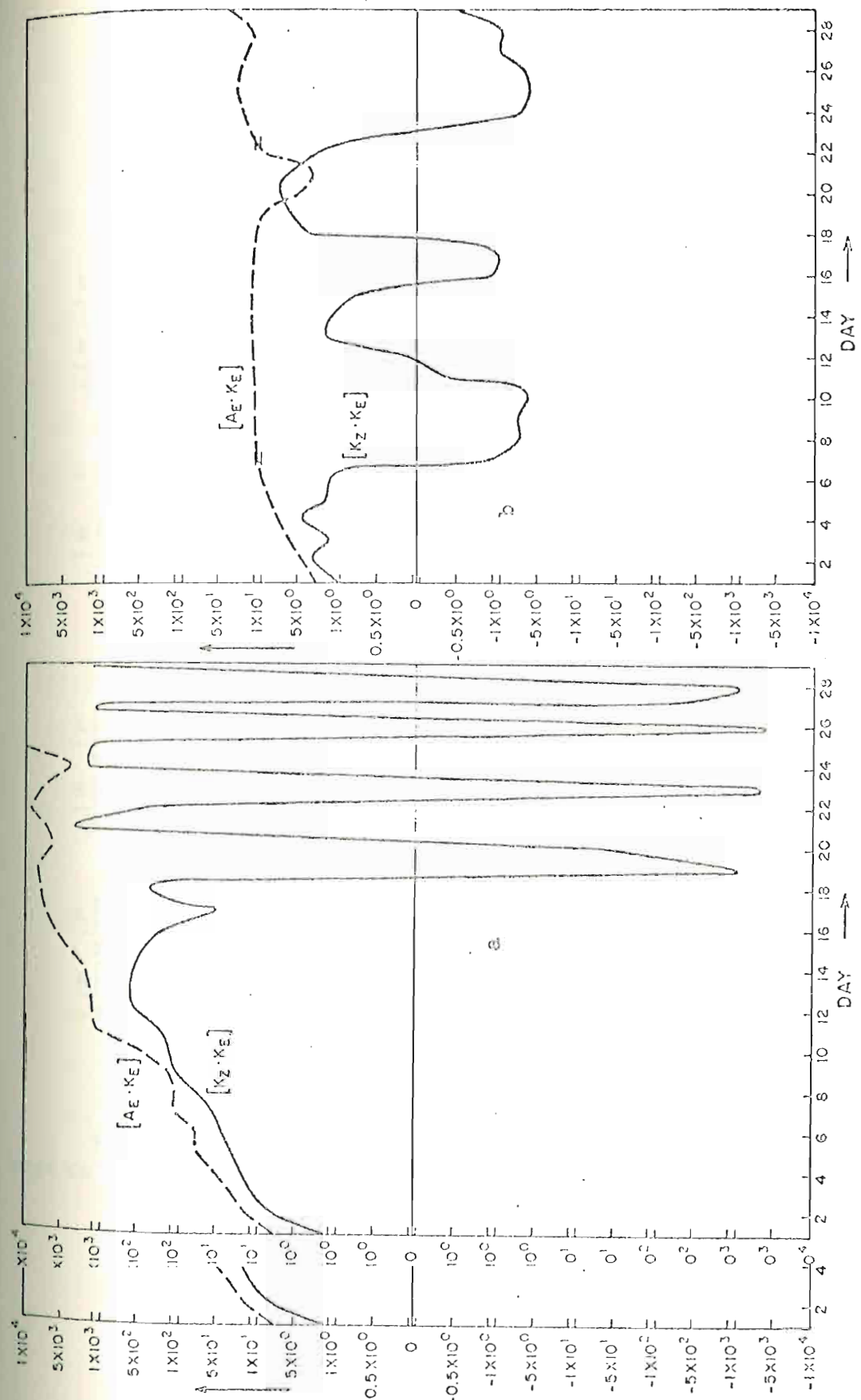

Fig. 15.-[$K_z \cdot K_\varepsilon$] and [$A_\varepsilon \cdot K_\varepsilon$] for (a) experiment 8, and (b) experiment 6. Units are in ergs cm-2 sec-1.

DAY 4

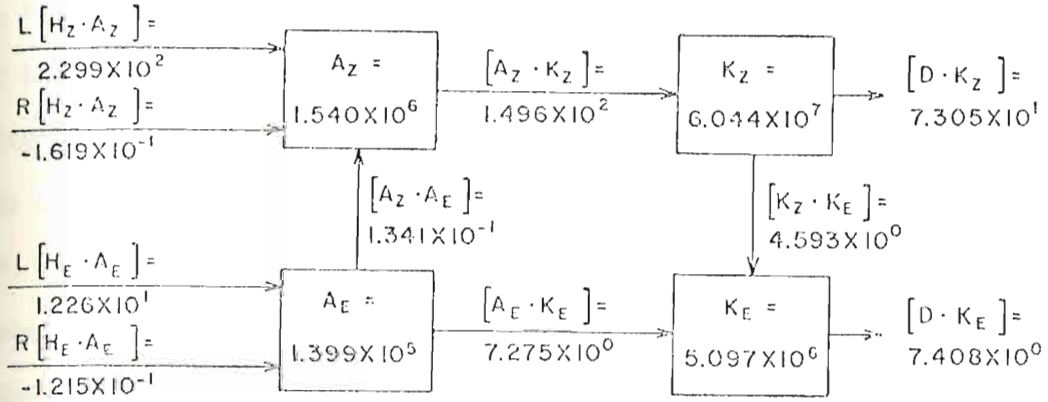

DAY 14

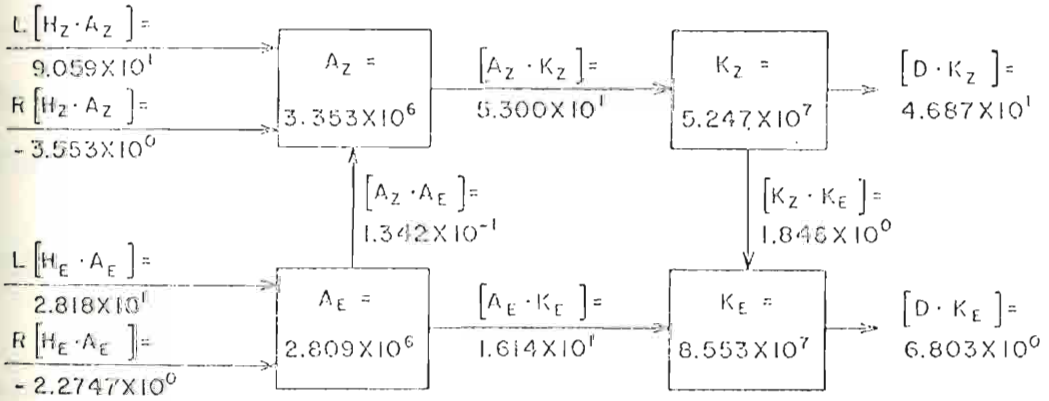

Fig. 16.--Energy cycle for experiment 6 in units of ergs cm^{-2} or ergs cm^{-2} sec^{-1}.

analysis has shown that instabilities on the synoptic and long wave scales can occur when latent heat is the sole source of energy. It may be suggested here that this is possible for very large release of latent heat at upper levels. On the other hand, we have learned from experiments 3, 4, and 5 that if latent heat is largest at the lower levels and the shear of the zonal wind can be maintained, $[K_Z \circ K_E]$ must dominate at the early stages of wave development; there exists a non-linear coupling between the CISK and barotropic processes. Since large amounts of latent heat are required in experiments 6 and 8, and this is not very likely when a wave is very weak, the results of experiments 3 and 4 may be considered more realistic.

As in previous experiments, the rapid oscillations of 2 to 3 days are also seen in Fig. 15a for experiment 8. However, both the conservative case and experiment 3 have a slow 7-day period oscillation throughout the integration, i.e., high level heating has not interfered significantly with low-level barotropic exchange of energy.

Perturbation growth rates

We have learned so far that tropical eddies can be generated and maintained. Further analysis is required to discover the most unstable waves, their growth rates, and pressure levels of maximum wave amplification. This will be done for various vertical profiles of latent heat.

(i) Conservative case:

When dissipation and heating are set equal to zero, the only

When dissipation and heating are set equal to zero, the only

sources available for eddy energy are the east-west and north-south overturnings of air and the shear of the basic current. The former is the usual baroclinic instability of the first kind and the latter refers to barotropic

exchange of energy between the basic current and the eddies. A third mechanism of wave-wave interaction is also possible. Baroclinic instability is expected to be small in low latitudes, mainly due to the small value of the Coriolis parameter. This is in agreement with the thermal wind equation used in the present model; it would require very high vertical wind shears of the zonal current to make baroclinic instability possible. In experiment 1, the predominance of $[K_Z \cdot K_E]$ exchange is shown in Fig. 17. The eddy baroclinic term $[A_E \cdot K_E]$ plays a minor role. The oscillatory pattern of $[K_Z \cdot K_E]$ yields peaks on the 4th, 14th, and 27th days.

Two conservative experiments, which we understand to be mainly barotropic, were performed. Fig. 18 of experiment 1 shows the smallest scale wave of 3300 km to have the highest growth rate, having an e-folding time of 5.5 days. Its maximum energy is attained on the 8th day. The wave has reached a finite amplitude and its further behavior is oscillatory; non-linearity is mainly responsible for this. Initially, however, the perturbation is small and its exponential growth is similar to the results obtained in Yanai's linearized barotropic analysis. In Nitta and Yanai (1969), the scale of maximum instability is 2000 km, having a growth rate in e-folding time of 5.2 days. This is also an indication that baroclinic instability in the dry tropics is small.

The two larger waves of 5000 km and 10000 km grow and decay in oscillatory fashion. Their barotropic interaction with the basic current is not large, but there exists energy exchange between the two waves themselves. In this wave-wave interaction, the long wave of 10000 km acts as is not large, but there exists energy exchange between the two waves themselves. In this wave-wave interaction, the long wave of 10000 km acts as a source for the 5000 km wave. The decay of the ultra-long wave begins at about the 12th day and contributes to the growth of the intermediate

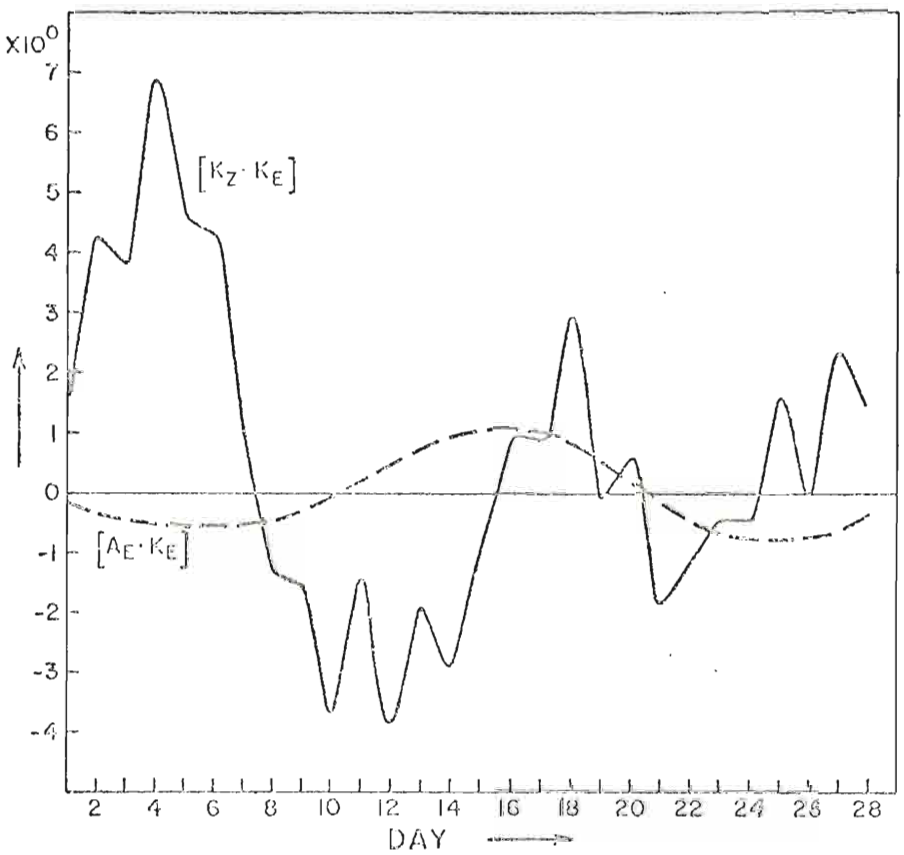

Fig. 17.--$[K_Z \cdot K_E]$ and $[A_E \cdot K_E]$ for experiment 1. Units are in ergs cm^{-2} sec^{-1}.

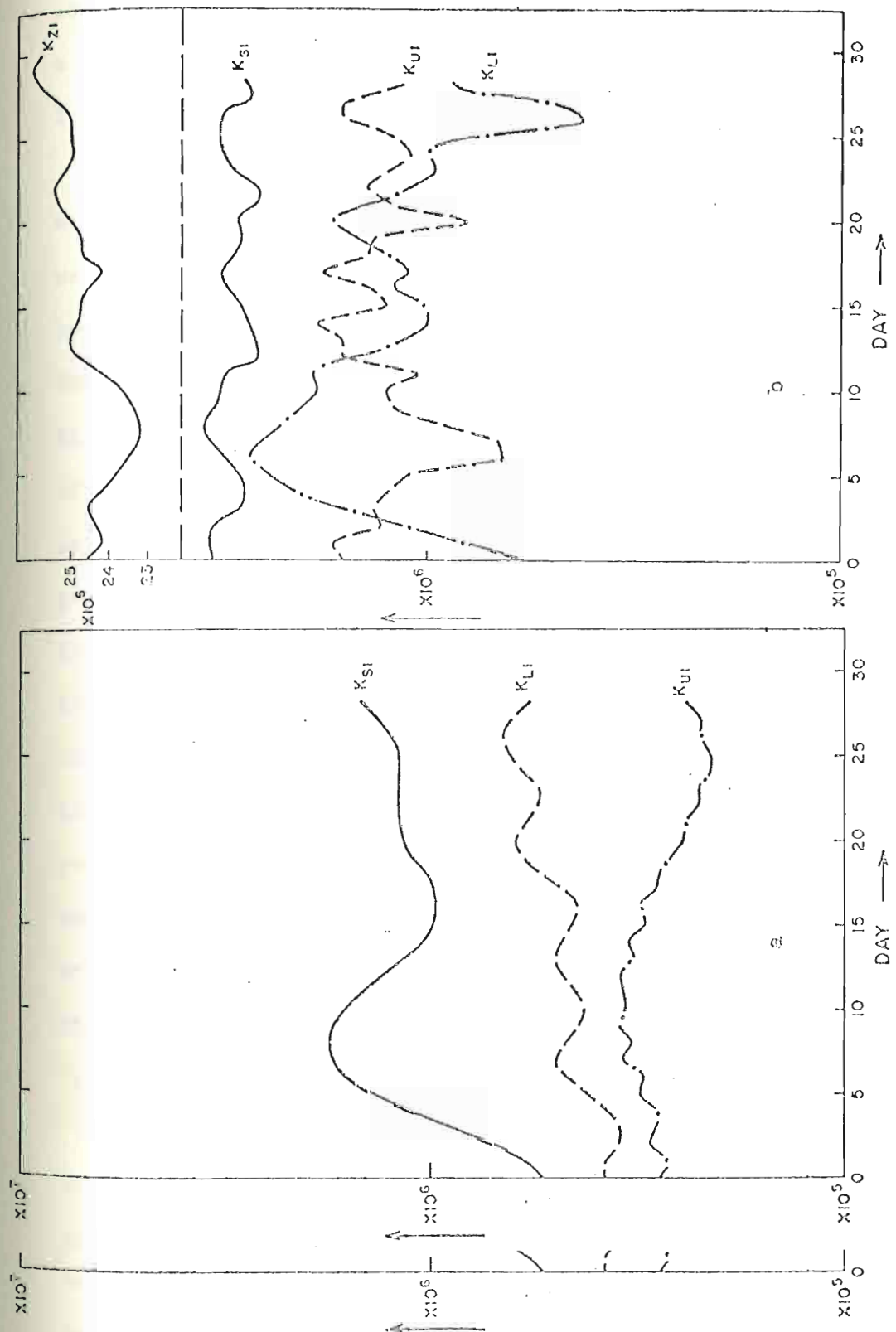

Fig. 18.-Perturbation energy changes with time at the indicated pressure levels for (a) experiment 1, and (b) experiment 2.

scale. At the upper levels, however, the same mechanisms operate, but to a smaller degree. Thus, barotropic interaction is active at the lowest level in the conservative experiment.

The objective of the second conservative experiment was to determine the instability of the 3300 km wave in a wider spectrum range of waves. We would like to ascertain if it is more unstable than other synoptic waves which approach 3000 km from the lower end of the spectrum. The other waves are of scales 1000 km, 1500 km, respectively. Once again, Fig. 18b of experiment 2 shows the most energetically active wave to be of wavelength 3000 km and the wave-wave interaction is again between the larger two waves. In its exponential growth, the 3000 km wave shows a growth rate in e-folding time of 3.5 days. This is more rapid than found in experiment 1 and is most likely due to the difference of 300 km between the unstable waves of the two experiments and the added source of wave-wave interaction between the 3000 km and 1500 km waves. The energies of the 1500 km and 3000 km waves are out of phase throughout the integration period. In Fig. 18b, the zonal energy increases while the 3000 km wave's energy decreases to a minimum on the 25th day. This is further evidence of non-linear barotropic interaction with the basic current. At level 3, the same features occur, but are less pronounced.

(ii) Latent heat profiles - increasing with height:

The picture of wave amplification changes drastically when heating and dissipation are allowed to operate. There is strong evidence that growth rates and selection of most unstable waves are height dependent.
and dissipation are allowed to operate. There is strong evidence that growth rates and selection of most unstable waves are height dependent.

In experiments 6, 7, 8 latent heat increases or remains constant with height. Towards the latter days of the integration period, the most

unstable scale is that of wavelength of 5000 km throughout the troposphere (see Figs. 19 and 20). However, this scale as well as the others are most unstable at the level of maximum heat release. Yamasaki (1969) has also shown, including scales which are not discussed here, that latent heat release at upper levels favors growth of the larger waves. Since experiment 1 shows that the barotropic mechanism favors growth of the smaller wave, and this mechanism is absent in Yamasaki's investigation, then the growth rate of the 3300 km wave in experiments 6, 7, 8 is attributed to a combined effort of CISK and barotropic exchange of energy, while that of 5000 km scale is mainly due to CISK. Unlike Yamasaki's analysis, the present investigation analyzes energy growth of waves at different pressure levels. The figures indicate that the maximum growth rate occurs at the upper troposphere where most heat is released.

Except for experiment 8 where large amounts of heat are released at the lowest level as well as larger amounts at the uppermost level, the $[K_Z \cdot K_E]$ exchange is not sufficient to balance dissipation. Thus, there exists a decrease of energy with time until latent heat becomes large enough to make a significant contribution. Of the three waves, the largest of wavelength 10000 km is least active. In experiment 8, a large low-level heating maintains a strong horizontal shear of the zonal wind and barotropic exchange is larger than in experiments 6 and 7. At level 7, in spite of large heating, the weak initial shear remains weak enough for any barotropic exchange to take place.

(iii) Latent heat profiles - decreasing with height:

barotropic exchange to take place.

(iii) Latent heat profiles - decreasing with height:

Experiments 3, 4, and 5 have been performed with heating profiles which decrease with height. Upper level heating is gradually reduced from

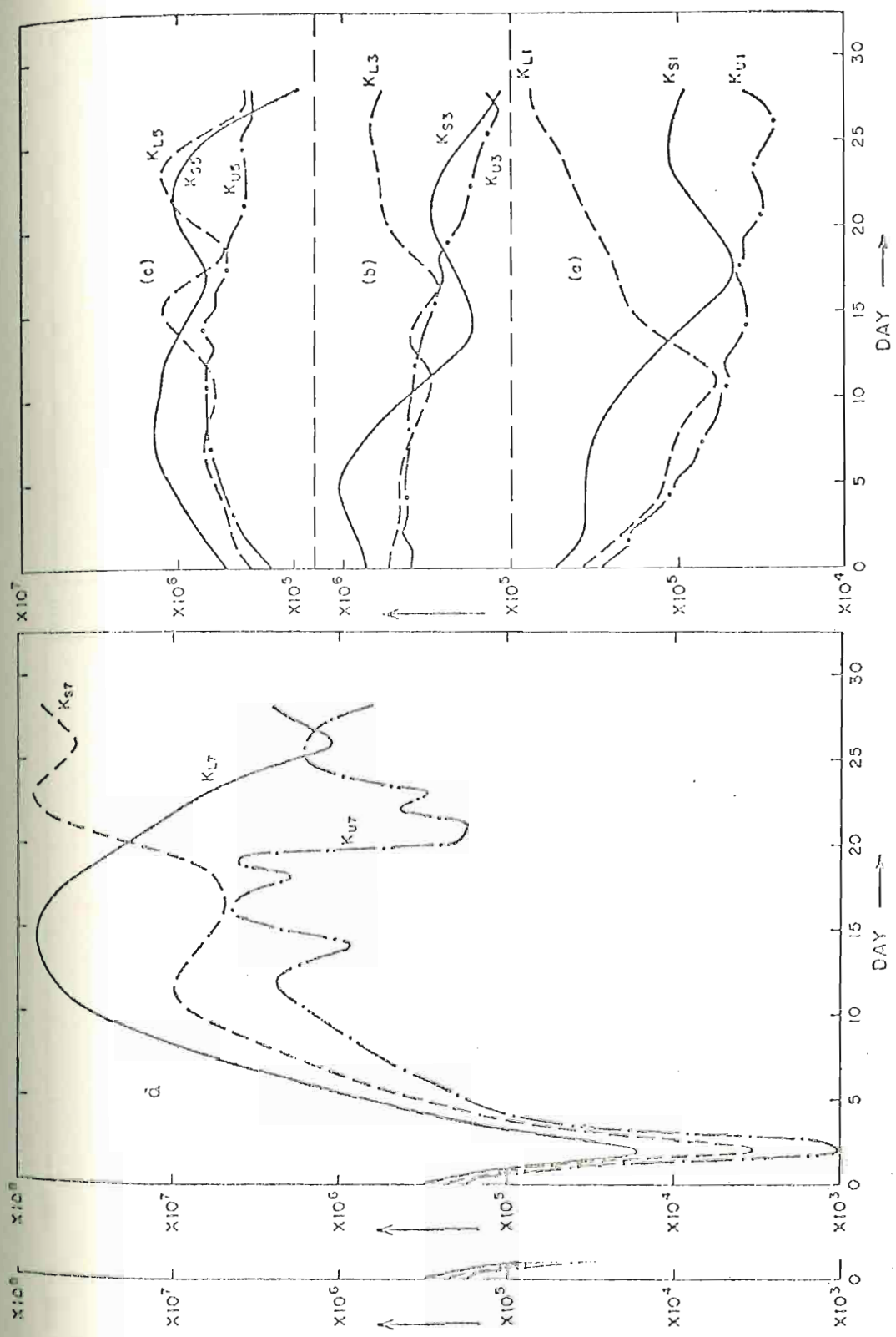

Fig. 19.-Perturbation energy changes with time at the indicated pressure levels for experiment 6.

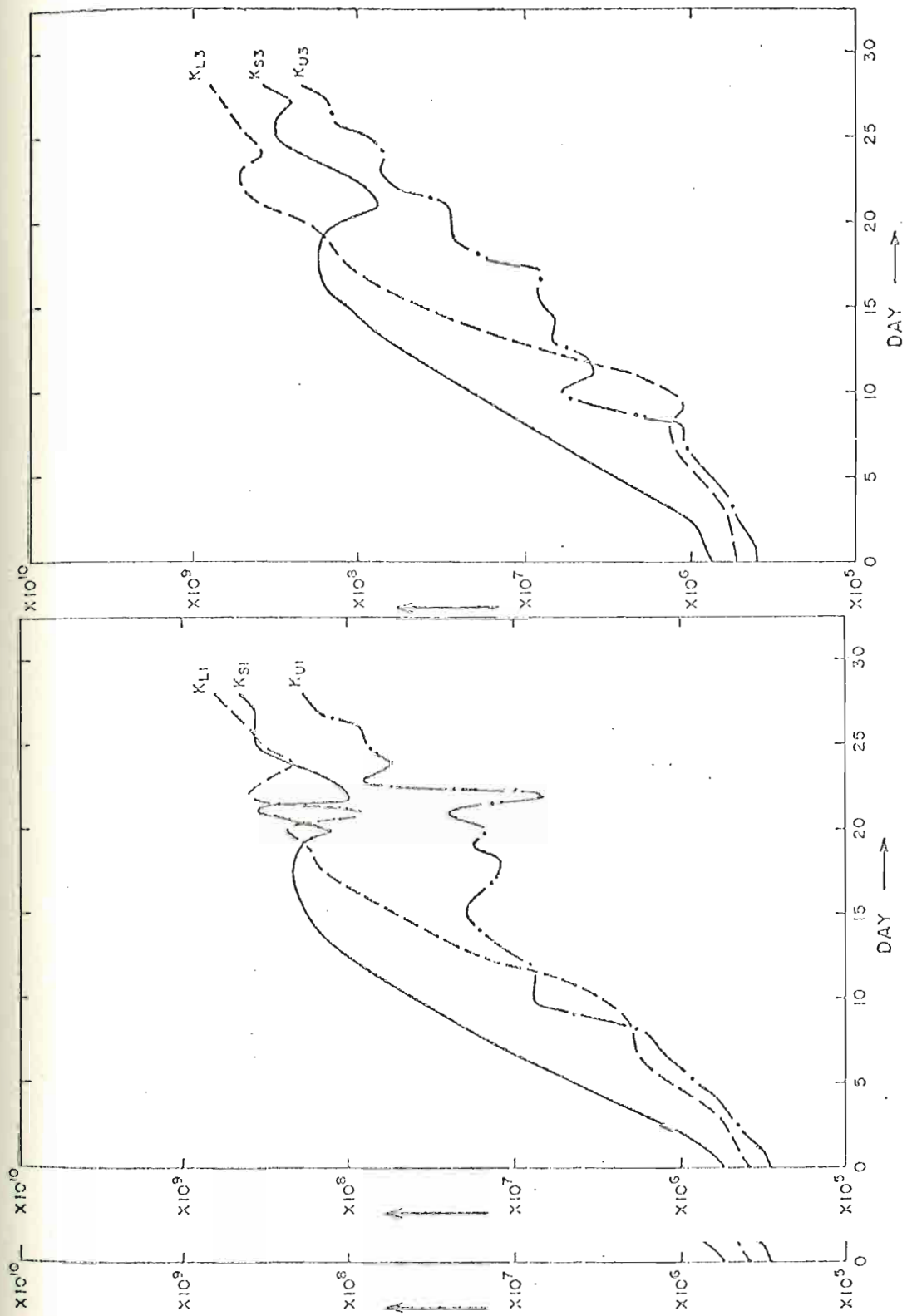

Fig. 20.-Perturbation energy changes with time at the indicated pressure levels for experiment 8.

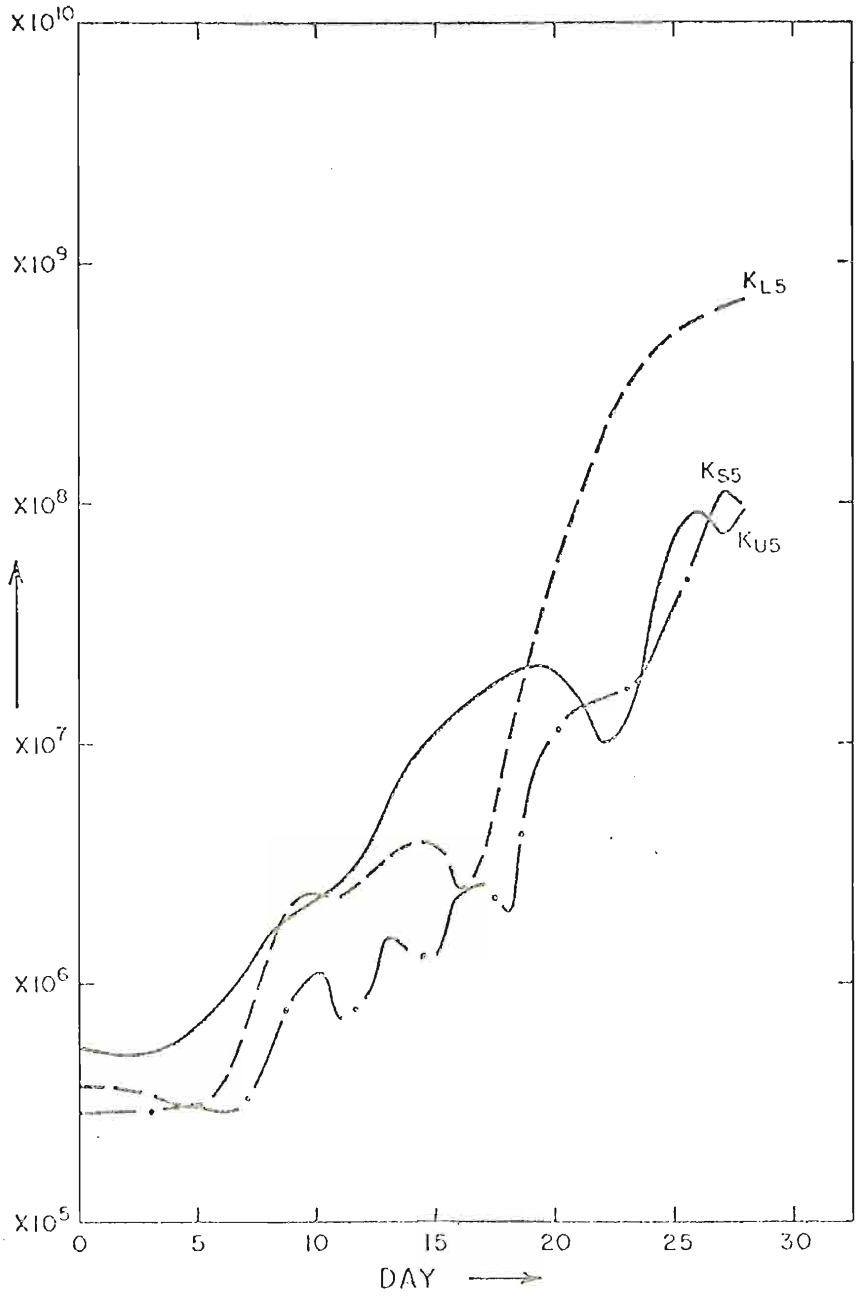

Fig. 20.-Perturbation energy changes with time at the indicated pressure levels for experiment 8.

Fig. 20.-Perturbation energy changes with time at the indicated pressure levels for experiment 8.

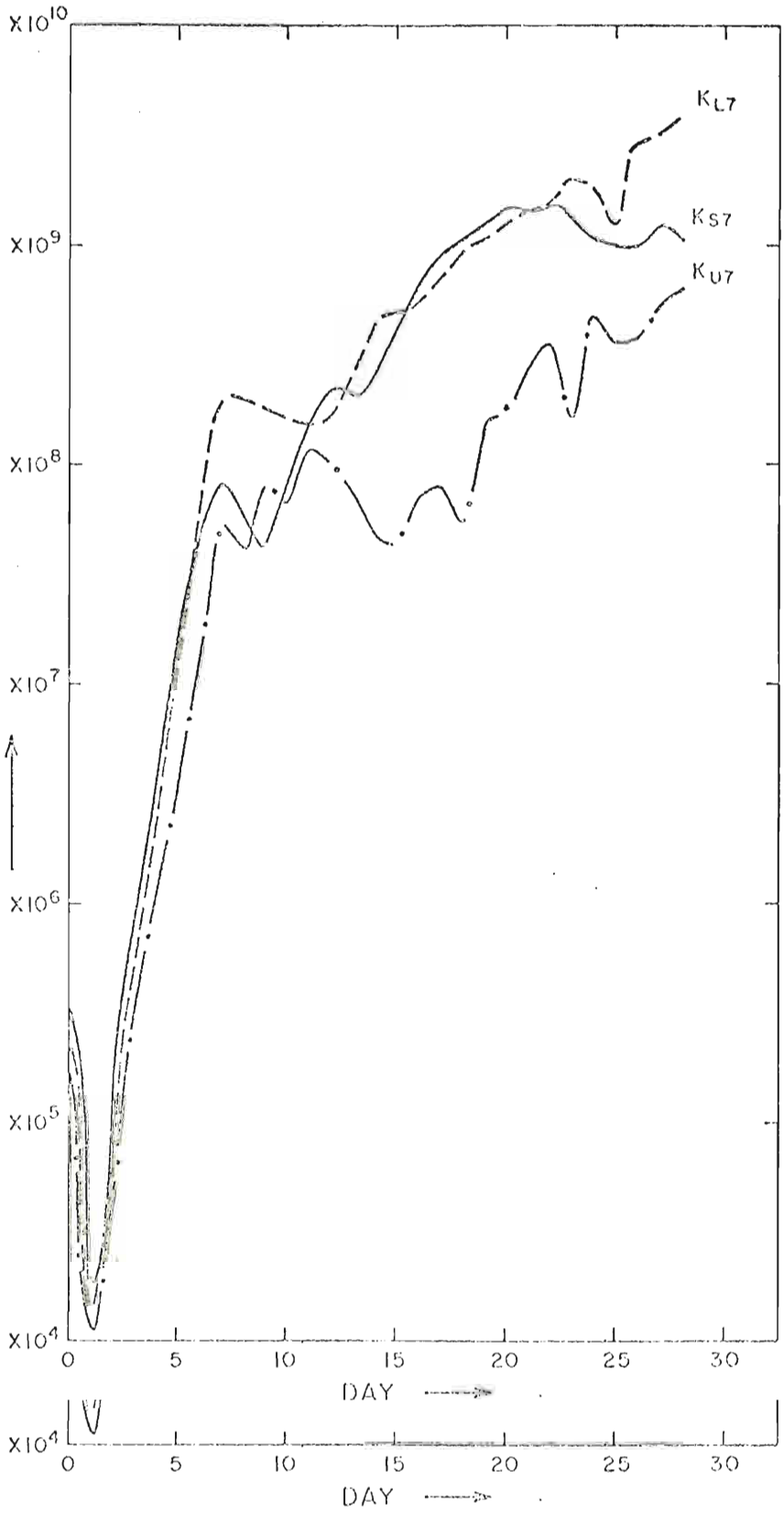

Fig. 20.--Perturbation energy changes with time at the indicated pressure levels for experiment 8.

experiment 3 to 5. In the three experiments the most unstable wave at the lowest level is the one with wavelength 3300 km. The other two waves compete equally for energy, except during the last few days of the integration period when the 5000 km wave begins to dominate the 10000 km wave. These are illustrated in Fig. 21. Growth rate of scale 3300 is largest in experiment 3. Thus, heating at upper levels can have some contribution to wave growth at lower levels.

As in Bates's (1970) investigation, the energy of the waves reaches a relative maximum sometime during their evolution. For wavelength 3300 km, this maximum occurs on the 15th day in experiment 3, 18th day in experiment 4, and 17th day in experiment 5. It is important to note that although unconditional heating with time-independent static stability has been used in the present model, a relative energy minimum for the 3300 km wave occurs on day 21 in experiment 4 and day 19 in experiment 5. This bears strong resemblance to the relative minimum achieved on the 19th day in Bates's experiment. Unlike results by Bates (1970), similar relative minima occur for the longer scales, as can be seen in Figs. 21a,b,c.

At level 3, in all three experiments and for all three waves, energy decreases for the first few days (see Fig. 22), until sufficient latent heat has been accumulated; then rapid growth occurs during the rest of the 30 days. The decrease of energy is again attributed to insufficient barotropic gain of energy to balance dissipation. However, this feature of dissipation is absent at the lowest level where the shear of the zonal wind is largest. The 3300 km wave is still most dominant at level 3 in the dissipation is absent at the lowest level where the shear of the zonal wind is largest. The 3300 km wave is still most dominant at level 3 in the three experiments.

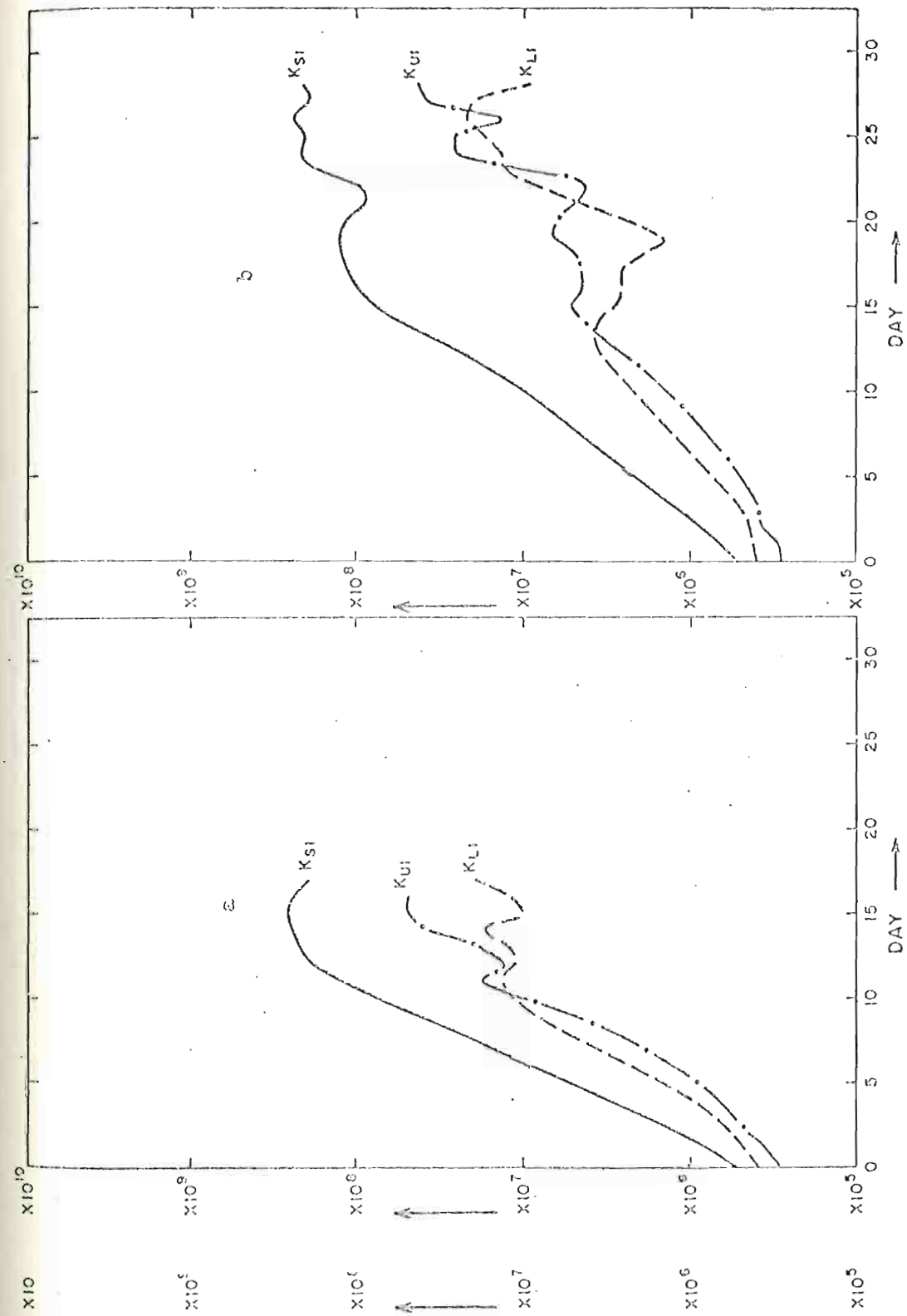

Fig. 21.-Perturbation energy changes with time at the indicated pressure levels for experiments (a) 3, (b) 4.

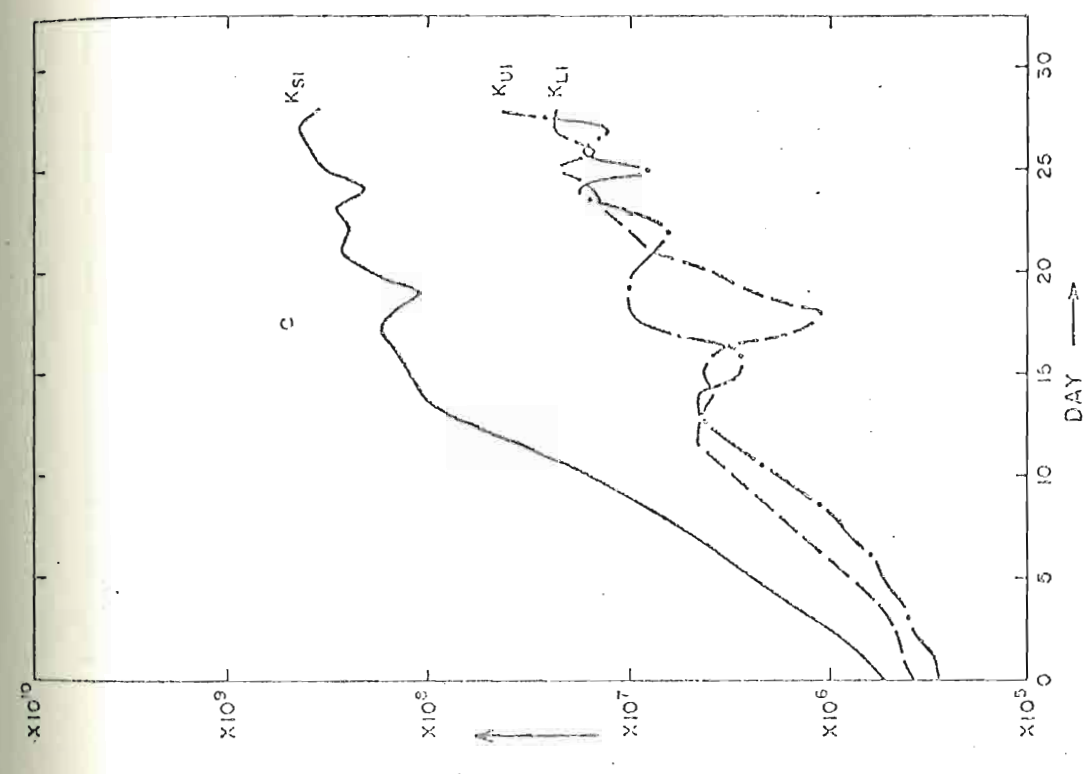

Fig. 21.-Perturbation energy changes with time at the indicated pressure levels for experiment (c) 5.

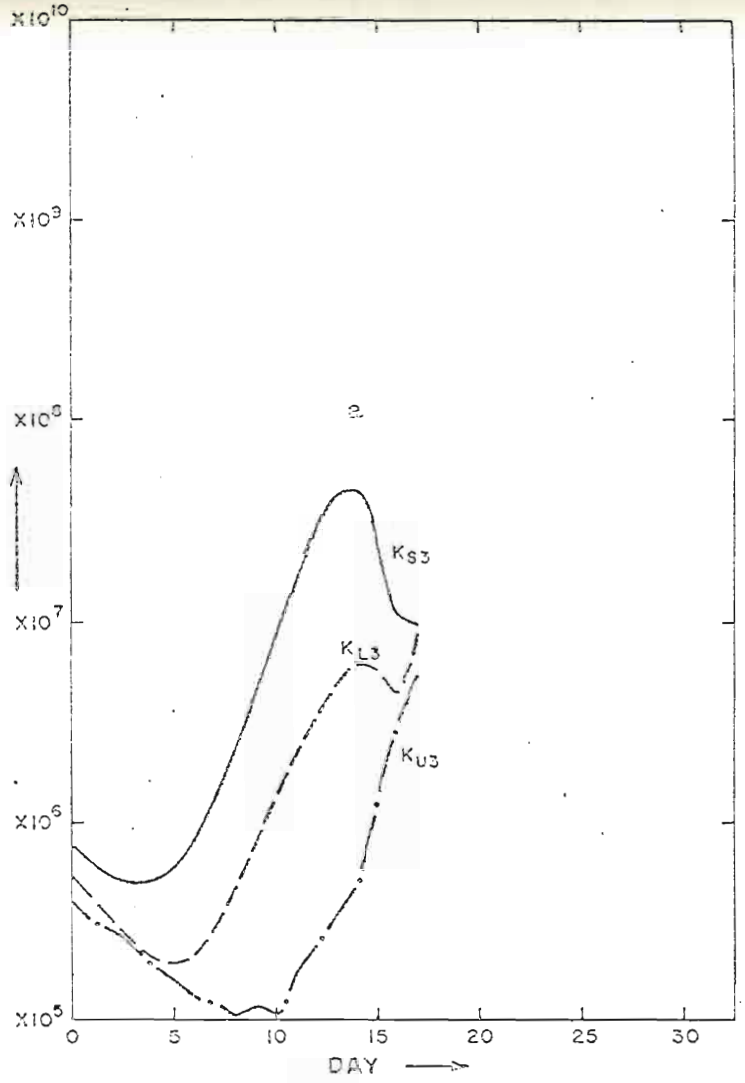

Fig. 22.-Perturbation energy changes with time at the indicated pressure levels for experiment (a) 3.

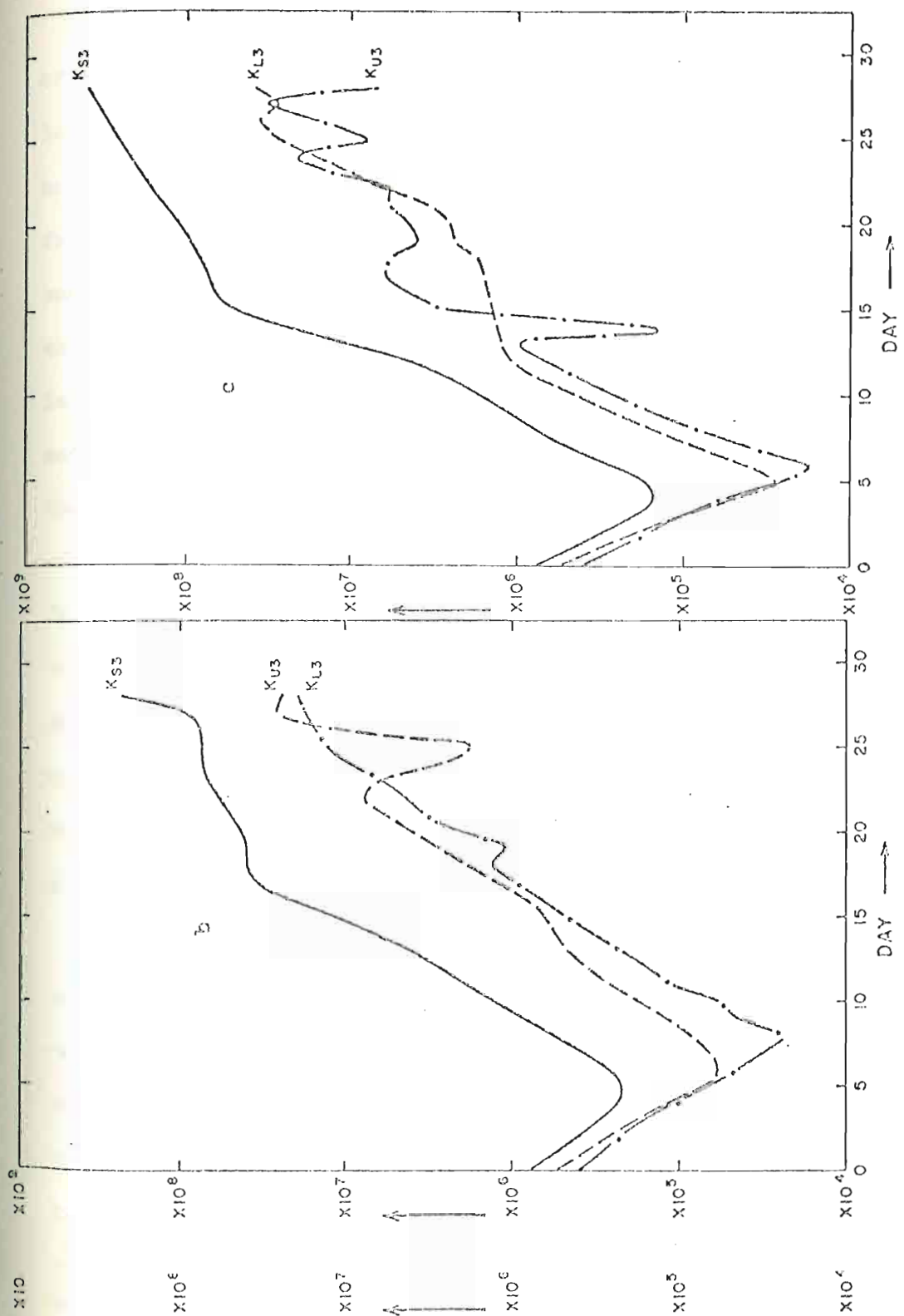

Fig. 22.-Perturbation energy changes with time at the indicated pressure levels for experiment (b) 4, (c) 5.

At level 5, a most important new feature occurs; the growth rates of the longer waves especially wavelength 5000 km are larger than at the lower levels (see Fig. 23). This happens in spite of small upper level heating. This is not true for the shortest wave. In experiment 3, in fact, scale 5000 km achieves a higher growth rate than the 3300 km wave and reaches a higher energy value. This is evidence that in the three experiments upward energy propagation exists for the larger scales, and less for the scale of the shortest wave. In a linearized study by Charney and Drazin (1961), it was found that for special vertical profiles of the zonal wind, the short waves get trapped at low levels and the long waves can propagate energy upward; this was found for mid-latitude dynamics. In the present experiments the short wave is found to have energy at upper levels, but the fact that the long waves, which have a smaller energy source at low and upper levels, do sometimes dominate at upper levels is significant information. Contribution of the upper level heating for longer waves has been discussed for experiments 6, 7, 8 but is found much less influential in experiments 3, 4, and 5.

We conclude that long waves are a dominant feature of upper levels and short waves dominate at lower levels. Further, the long wave dominance is accentuated when upper level heating is largest and short wave dominance is accentuated when lower level heating is largest. This indicates the importance of studying atmospheric wave energy changes in response to sources and sinks at individual levels rather than consider wave instabilities in the troposphere as a whole. In a paper by Yamasaki

response to sources and sinks at individual levels rather than consider wave instabilities in the troposphere as a whole. In a paper by Yamasaki (1969), we find that all the waves of the scales discussed here become unstable when upper level heating is large and when the heating increases

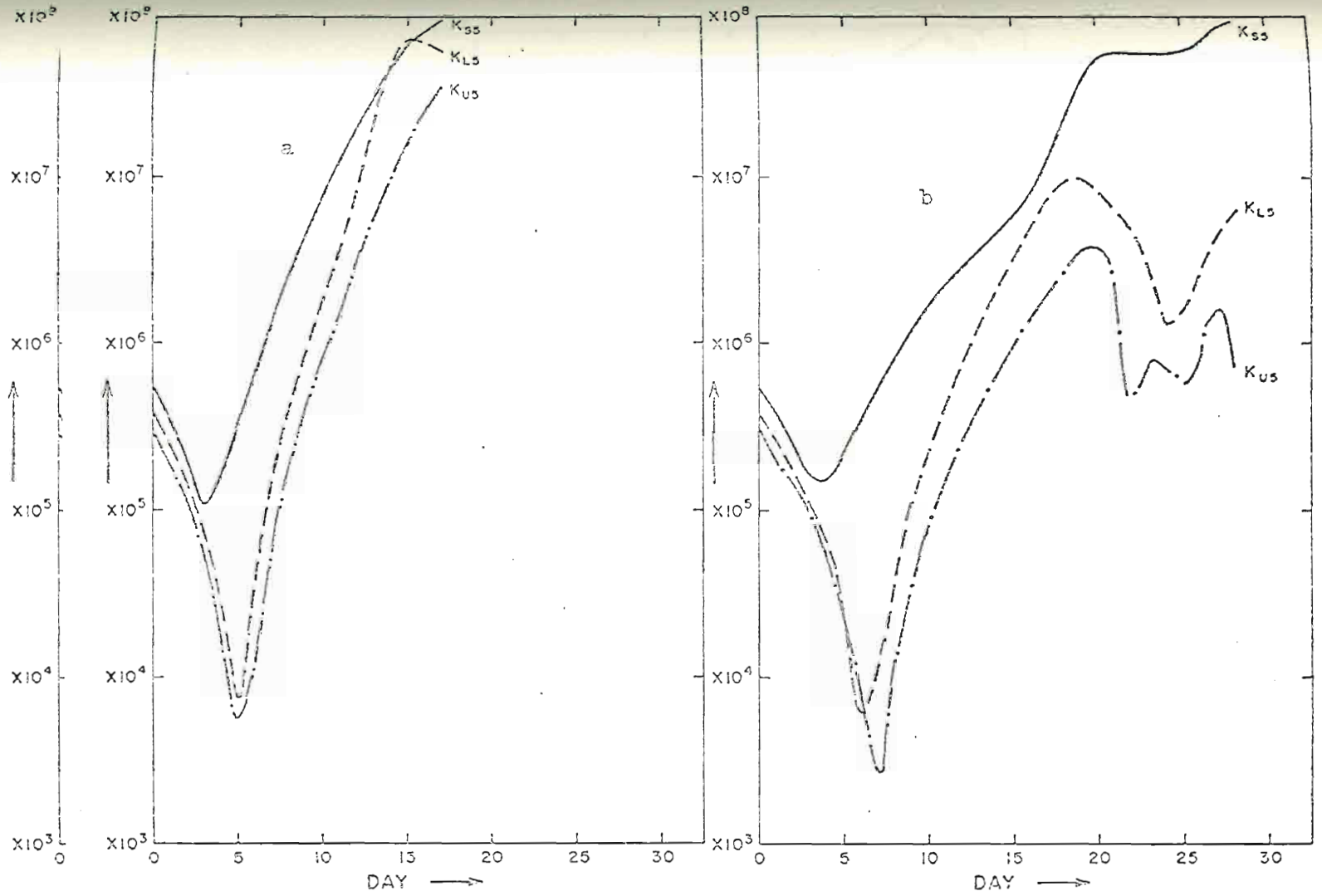

Fig. 23.-Perturbation energy changes with time at the indicated pressure levels for experiments (a) 3, (b) 4.

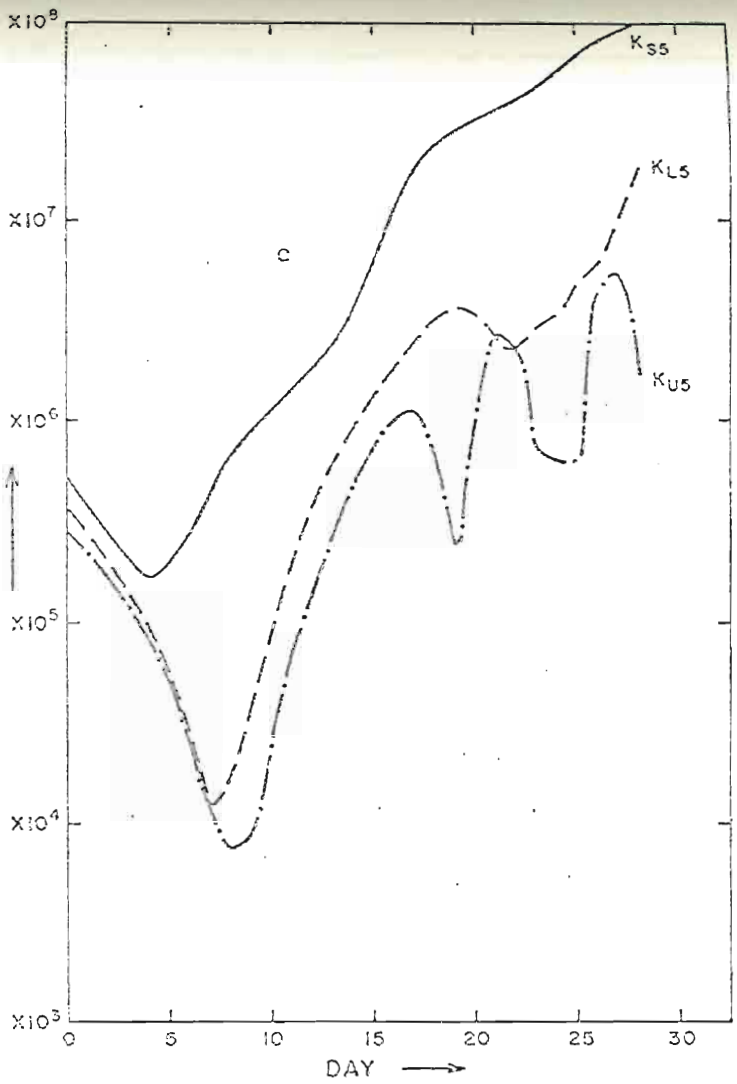

Fig. 23.-Perturbation energy changes with time at the indicated pressure levels for experiment (c) 5.

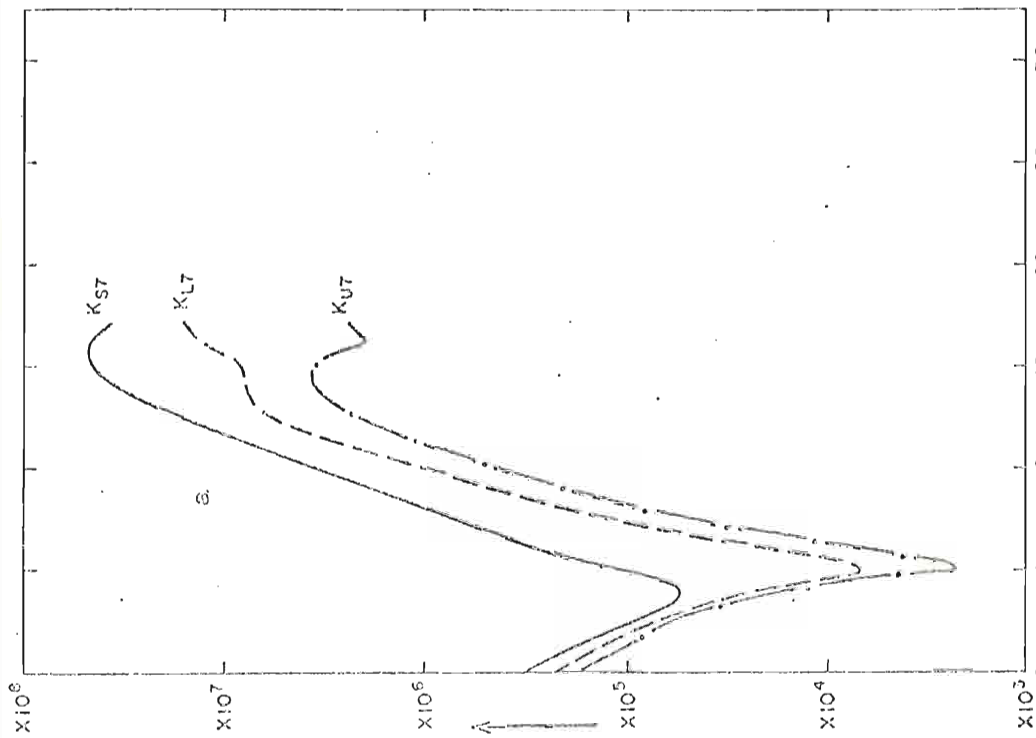

Fig. 24.-Perturbation energy changes with time at the indicated pressure levels for experiment (a) 3.

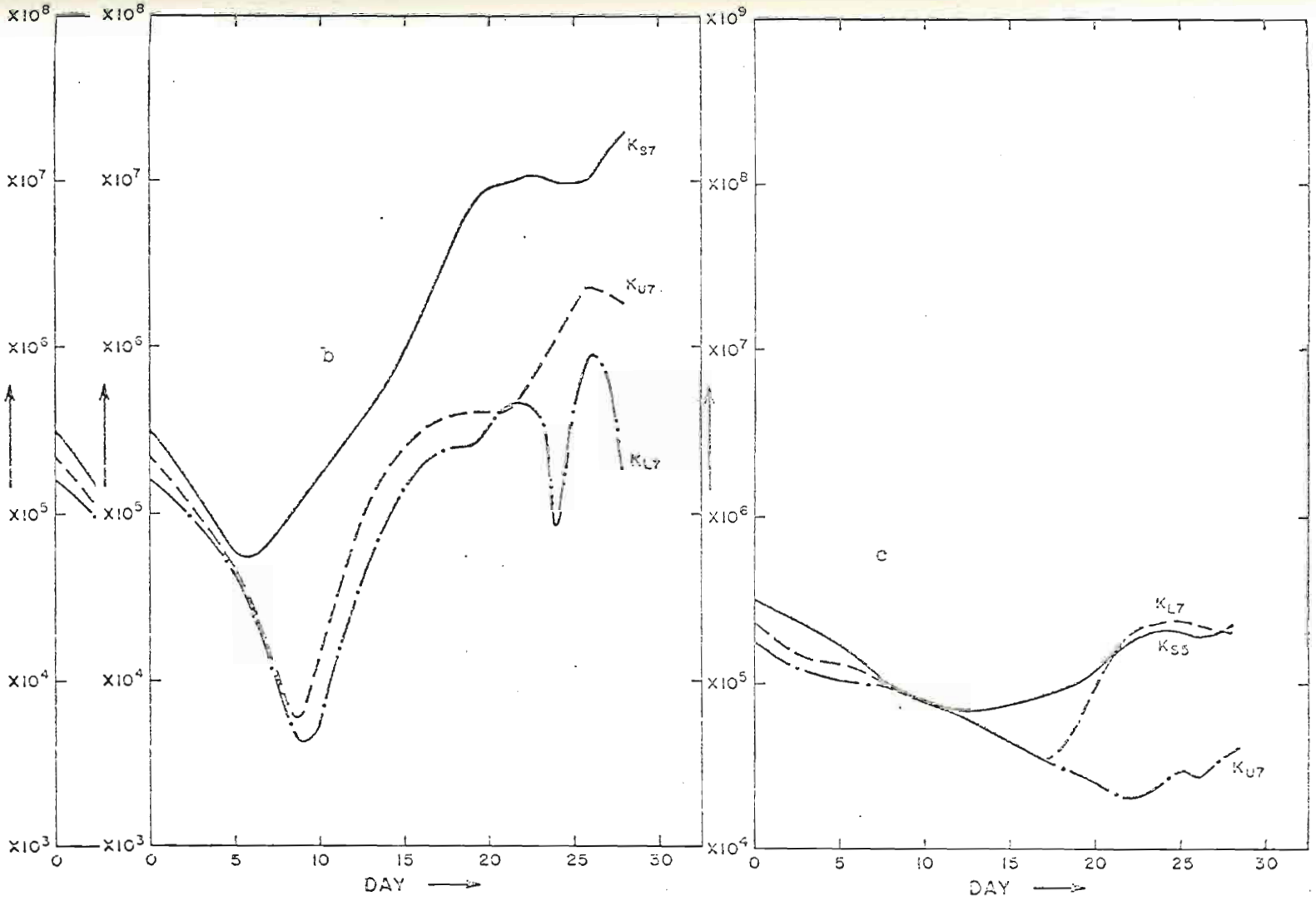

Fig. 24.-Perturbation energy changes with time at the indicated pressure levels for experiments (b) 4, (c) 5.

with height. The difference in growth rates among the waves then becomes a function mainly of vertical wind shear. No attempt has been made here to relate growth rates with vertical shear of the zonal wind; the wind shear evolves with the dynamics of the model. When we include barotropic instability, as done in the present model, a stability analysis reveals that synoptic waves can grow with large heating at low levels.

Riehl (1954) has discovered from a synoptic investigation that a wave of scale 1500 to 2000 km dominated the lower troposphere and a wave of 3000 km to 5000 km dominated the upper troposphere. Similarly, Wallace (1971) reached such conclusions from a study of time series.

Wave analysis at level 7 resembles that at level 5 except in experiment 5 where heating has been set equal to zero. Increase in energy of the longer waves is still largest among the waves, but it is quite small. It is noted in these experiments that small changes in η can cause large changes in growth rates.

The short wave at the lower levels initially feeds upon the zonal kinetic energy and the long waves at the upper levels feed upon latent heat even at the initial stages. When compared with the conservative experiments, the growth rates of the waves in the non-conservative case are larger.

Amplitude variation with height

Since integration of the equations began with equal amplitudes for all waves at all levels, amplitude analysis seems appropriate. Energy

Since integration of the equations began with equal amplitudes for all waves at all levels, amplitude analysis seems appropriate. Energy is weighted by wave number; thus shorter waves with larger wave numbers may have misleading large energies. Graphs of amplitude with height will

now be presented for waves (1, -1), (2, -1), (3, -1). Similar analysis can be done for other components.

(i) Conservative case:

In Fig. 25, day 0 shows equal amplitudes for all waves at all levels. At about the 13th day, the smallest wave (3, -1) begins to show maximum amplification at level 3 and the largest wave (1, -1) at level 5. At later stages of wave development, (1, -1) remains dominant at level 5, but wave (3, -1) attains maximum amplification at level 1 and next to maximum at level 3. This verifies that larger waves dominate at upper troposphere and shorter waves dominate at lower troposphere. It may be mentioned that in Riehl's (1954) observational analysis, the maximum amplitude of easterly waves lies somewhere between 700 and 500 mb. To determine the source for the maximum amplitude, Fig. 26a is included for day 22. The only possible source for the shorter wave is barotropic interaction with the basic current at the lower level. This is confirmed by the positive quantity of $[K_Z \cdot K_E]$ at level 3. There exists no similar source for the long waves at level 5. The remaining possibilities are wave-wave interaction between modes (2, -1) and (3, -1) to contribute to wave (1, 1) and the upward flux of energy which is observed at level 5. Both exist, as (2, -1) and (3, -1) have a minimum at level 5 and (1, -1) is a minimum at level 1, which suggests a loss of energy to level 5. At this upper level, the zonal wind variation with height, in Fig. 26b, shows a minimum easterlies (or relative maximum westerlies). Thus, the amplitude profile with height of the larger wave resembles the vertical profile of the zonal easterlies (or relative maximum westerlies). Thus, the amplitude profile with height of the larger wave resembles the vertical profile of the zonal wind. This has also been noted in the papers of Rutherford (1969) and Nitta (1967), but their analysis applies to mid-latitudes with baroclinic

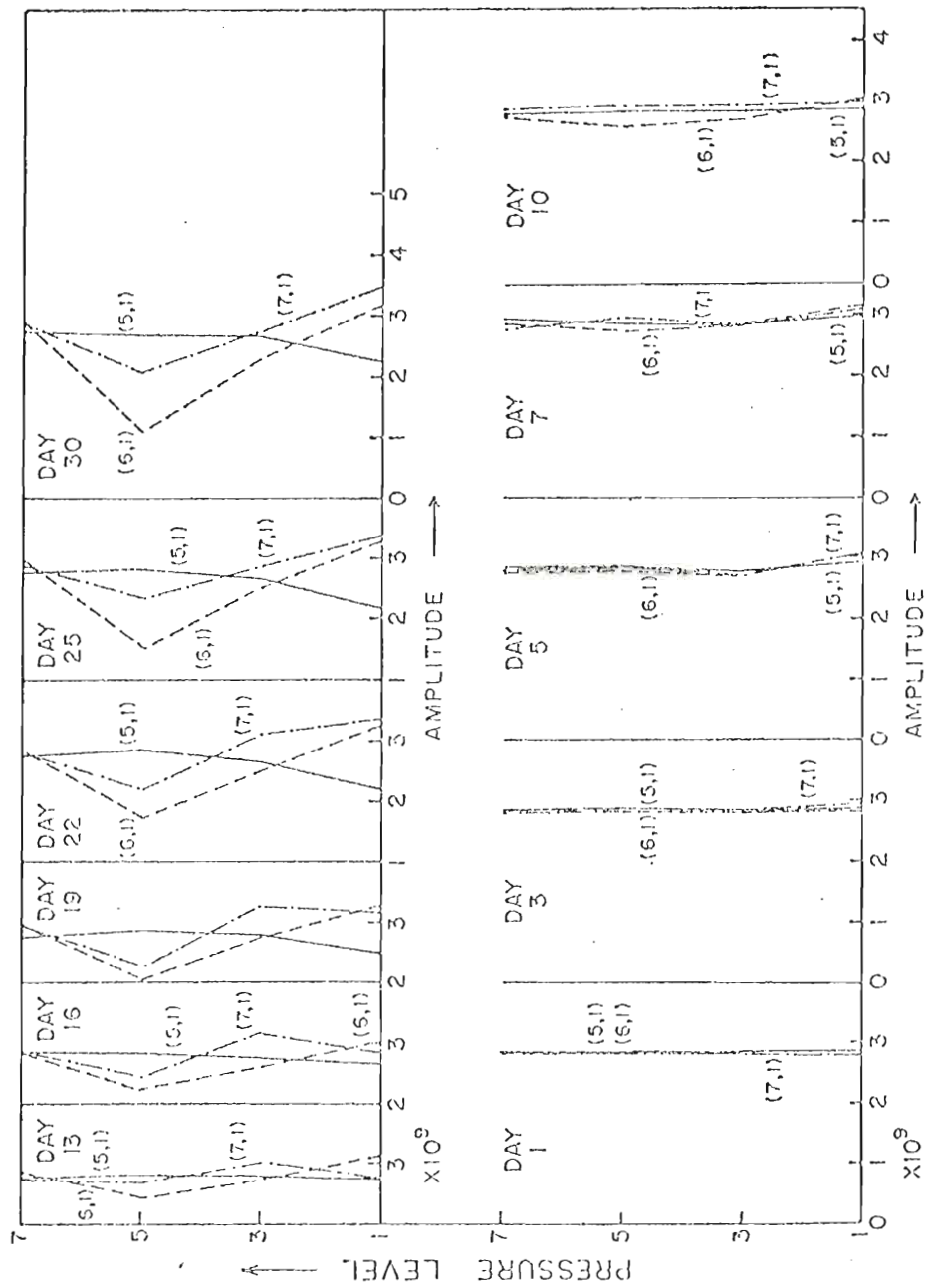

Fig. 25.-Amplitude variation of ψ ($cm^2\ sec^{-1}$) with pressure for indicated components for experiment 1.

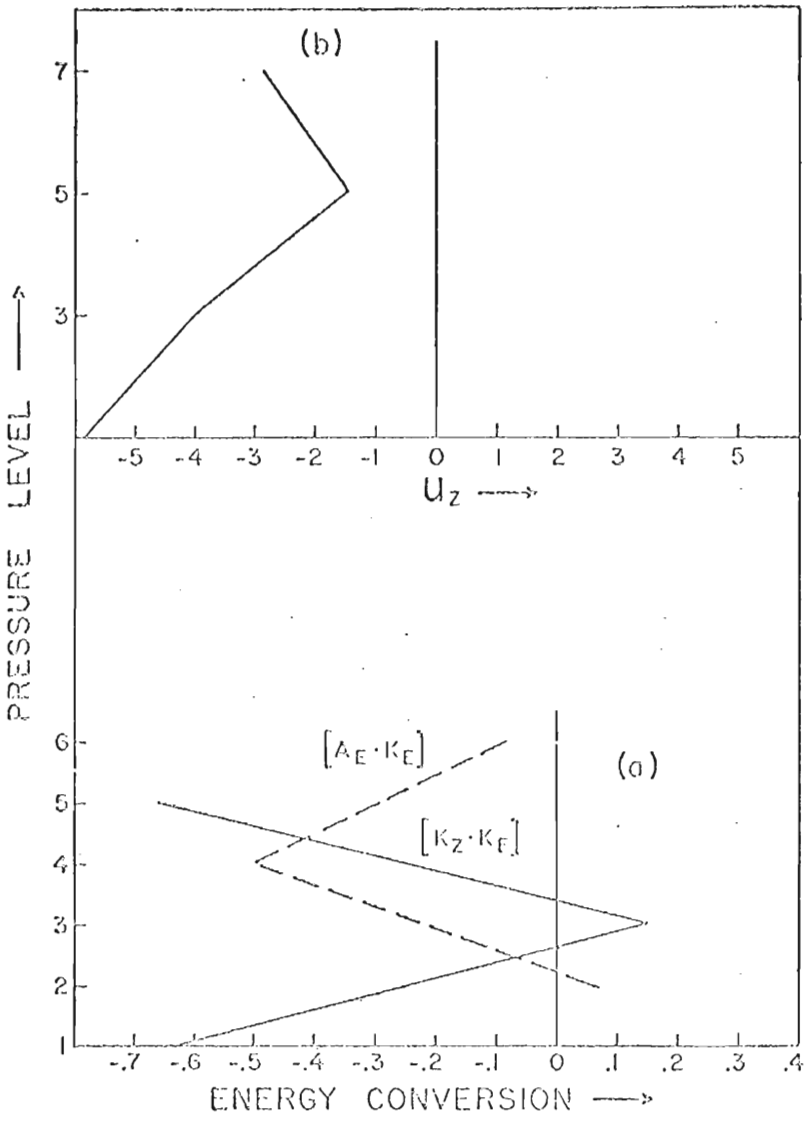

Fig. 26.-Variation of (a) $[A_E \cdot K_E]$ and $[K_Z \cdot K_E]$ with pressure and (b) zonal wind u_Z with pressure for day 22 for experiment 1.

and (b) zonal wind u_Z with pressure for day 22 for experiment 1.

sources and for higher pressure levels. They verified that for special vertical profiles of the zonal wind, the shorter waves were trapped in the lower troposphere and the larger ones propagated energy upward.

(ii) Non-conservative case:

In experiment 4, for about 18 days (see Fig. 27), the largest wave (1, -1) dominates at the upper level. Since upper level heating is small and low level is large, mode (3, -1) becomes large in amplitude throughout the atmosphere for the remainder of the integration period. This coincides with an energy minimum of the long waves which preceded the energy minimum of the short waves in Fig. 22. By contrast in the conservative case, the low-level energy source contributed greatly to the dominance of the long waves at the upper level.

In experiment 5 where upper level heating has been further reduced, Fig. 28 shows that the long waves (1, -1) and (2, -1) dominate at upper levels for a shorter duration of time. Mode (3, -1) increases in amplitude with time at all levels, but becomes most dominant at 600 mb on the 30th day. This, we recall, was found to be the level of maximum amplitude in Riehl's analysis of an easterly wave.

As a striking example of upper level heating, experiment 6 (see Fig. 29) shows that the amplitude of (2, -1) is the largest most of the time at the uppermost level. Once again, an exception on the 12th day exists and it is associated with an energy minimum of the largest waves.

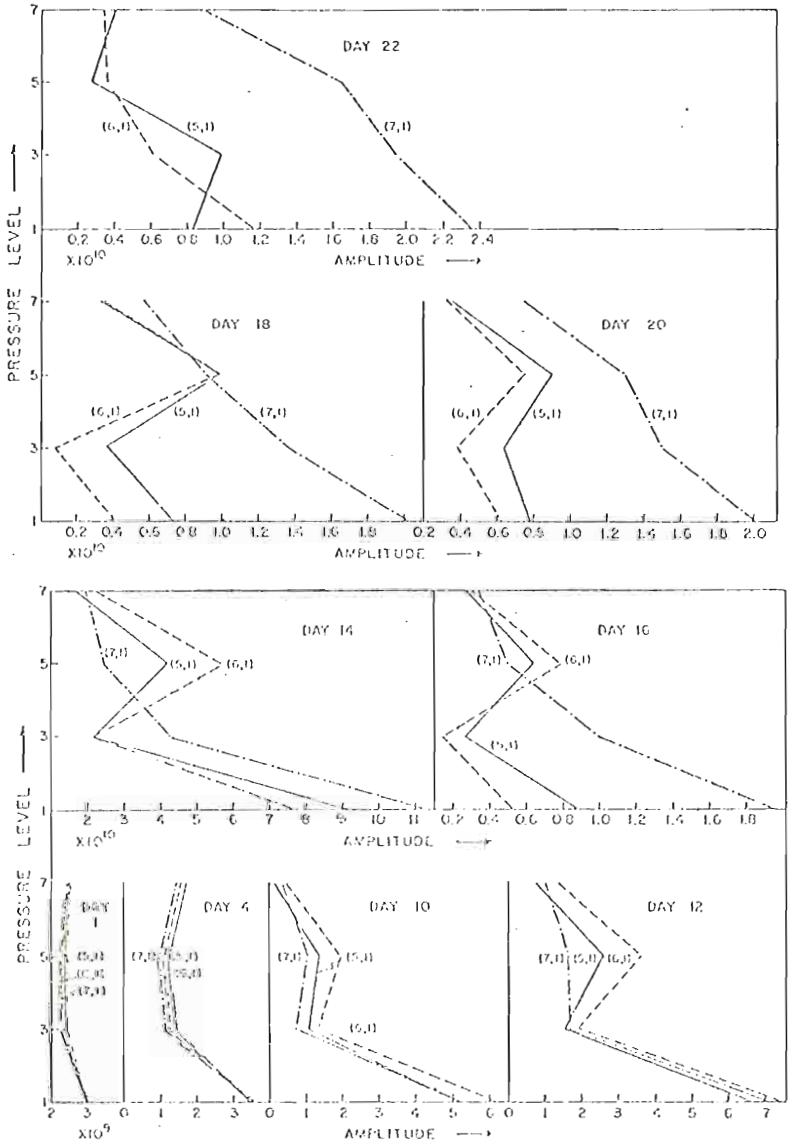

Fig. 27.-Amplitude variation with pressure for indicated components for experiment 4.

[illegible] experiment 4.

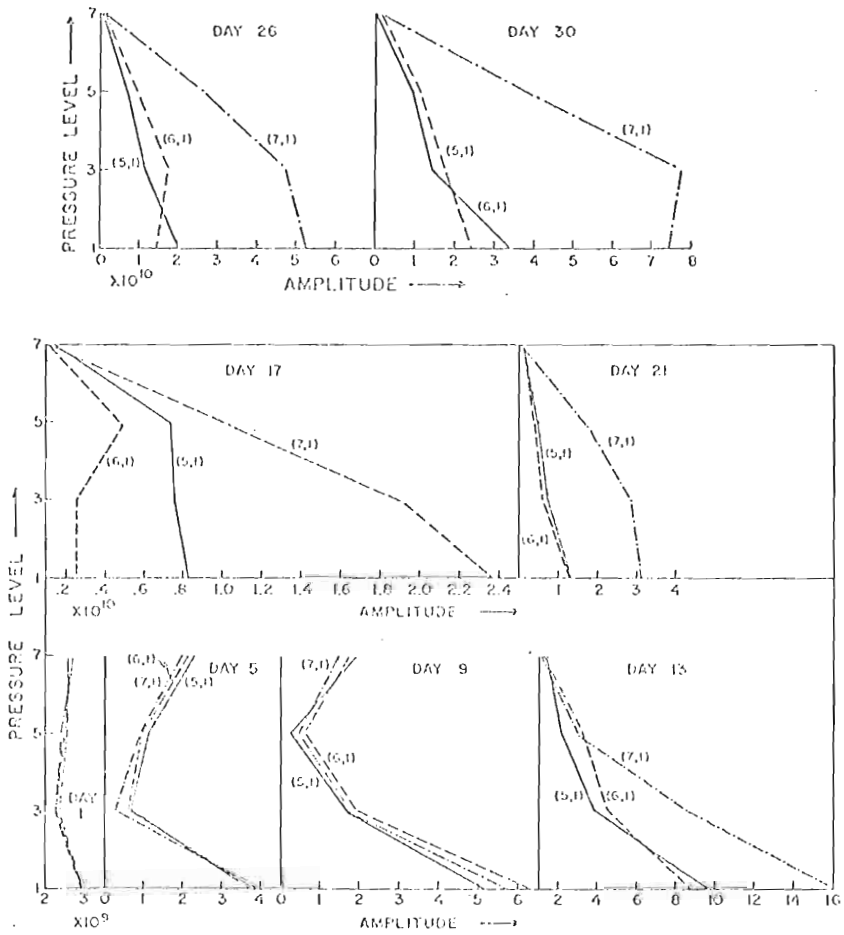

Fig. 28.-Amplitude variation with pressure for indicated components for experiment 5.

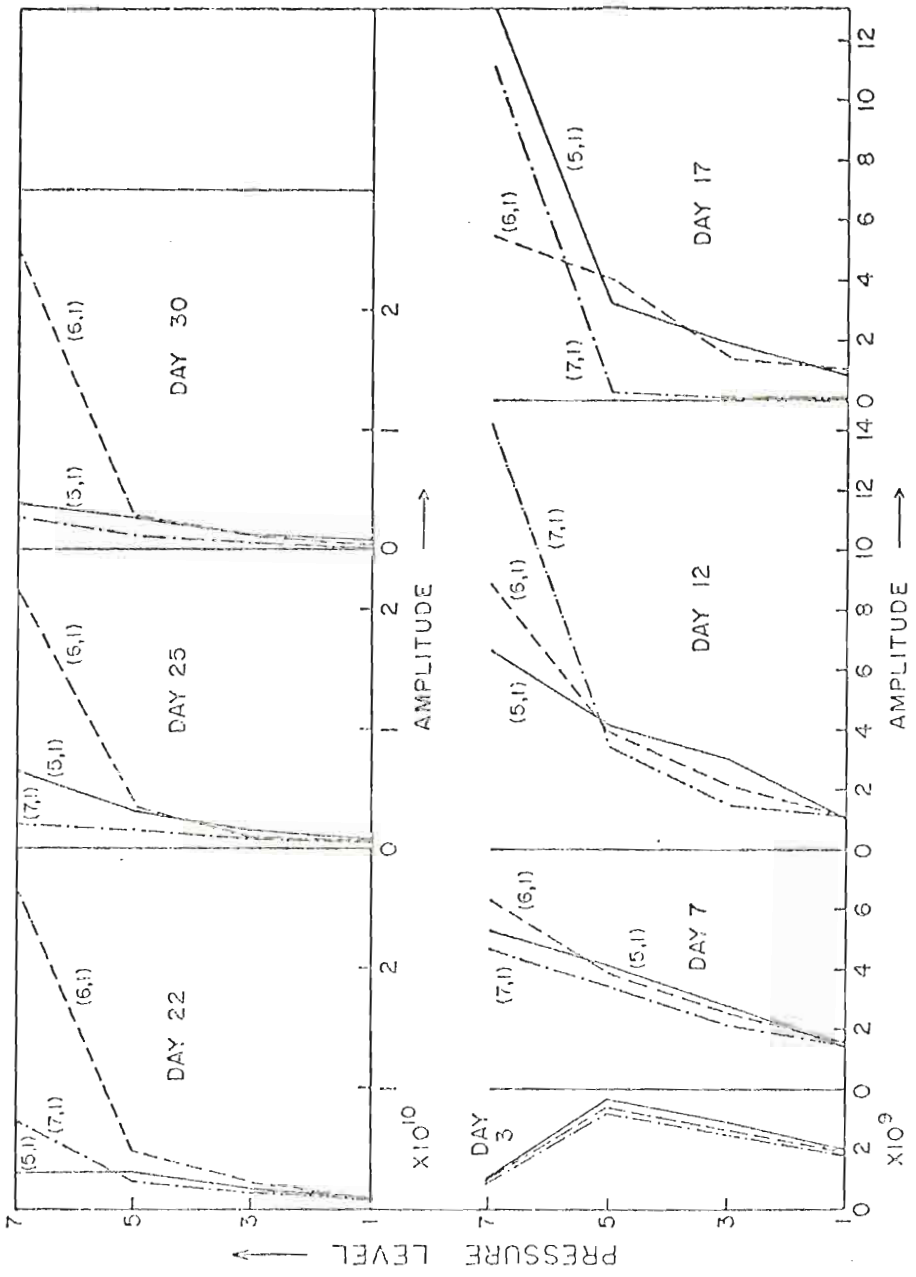

Fig. 29.-Amplitude variation with pressure for indicated components for experiment 6.

CHAPTER VI

SUMMARY AND CONCLUSIONS

The model is successful in combining both the barotropic and CISK mechanisms in order to investigate in a non-linear manner the major energy sources for tropical eddies. It also introduces some new conjectures concerning the response of the eddies to vertical profiles of latent heat. It is, however, weak in properly maintaining the basic current. This would require a broader spectrum of latitudinal scales, non-linear latent heat formulation and a different balance of terms in the equations of motion in which the Coriolis parameter is allowed to vary wherever it appears. Also, for better parameterization procedures, the vertical resolution should properly include a thin surface boundary layer. Then, a detailed ITCZ may be generated and maintained.

We may repeat the major simplifications of the present investigation. Linear heating neglects the horizontal and time dependence of the parameter η. These omissions result in larger horizontal temperature gradients and more rapid heating than would otherwise occur. The limited number of 20 Fourier components does not permit a prediction of the location and a description of the detailed structure of an ITCZ. The main features of an ITCZ that are included are the north-south zonal wind and the zonal temperature profiles. Such profiles have been observed in the vicinity of the Marshall Islands. In other regions of the tropics where these profiles do not exist, the results of the present investigation, in particular the relative roles of $[K_Z \cdot K_E]$ and $[A_E \cdot K_E]$ may be modified.

In spite of the above omissions, the quasi-geostrophic formulation is appropriate for the description of tropical waves. The results of the present model are meaningful in areas in the tropics for which the selected initial state is applicable. The most important result of the investigation describes the relative roles of $[A_E \cdot K_E]$ and $[K_Z \cdot K_E]$ in maintaining the eddies. It was found that when large amounts of latent heat are released in the lower troposphere and the heating decreases with height, $[K_Z \cdot K_E]$ is very important until the surface perturbation vorticity becomes sufficiently large for $[A_E \cdot K_E]$ to dominate. When the upper level heating is reduced, the barotropic contribution dominates for a shorter period of time. When largest amounts of latent heat are released in the upper troposphere, $[A_E \cdot K_E]$ dominates throughout the evolution of the waves, although $[K_Z \cdot K_E]$ is still important at the initial stages. The eddy available potential energy A_E is maintained by the eddy release of latent heat, while radiation plays a minor role as a stabilizing mechanism. The barotropic mechanism is most active in the lower troposphere and remains important as long as K_Z is maintained by A_Z which receives energy from the zonal release of latent heat.

When heating and dissipation are set equal to zero, $[K_Z \cdot K_E]$ makes the largest contribution toward maintaining the waves. The 3300 km wave is most unstable in the lower troposphere and has an e-folding growth rate of 5.5 days. The largest scale wave is most unstable in the upper troposphere and gaines its energy mainly from wave-wave interaction with the intermediate scale of 5000 km. Although the waves amplify
upper troposphere and gaines its energy mainly from wave-wave interaction with the intermediate scale of 5000 km. Although the waves amplify
sufficiently to weaken the zonal flow, this amplification does not destroy the uniform flow of the easterlies. When heating and dissipation

(in particular latent heat) are applied, the waves amplify sufficiently to interfere seriously with the zonal easterlies.

The growth rates of the waves are modified drastically when latent heat is released; this modification depends upon the vertical profile of latent heat. When most heat is released in the lower troposphere, the 3300 km wave is always the most unstable mode in the lower troposphere with an e-folding growth rate of 3 days. This wave also exists and sometimes dominates in the upper levels. When the largest heat release occurs in the upper troposphere, the larger scale waves in the upper troposphere are the most energetic; they sometimes dominate in the lower troposphere. The latent heat release, aided by the barotropic mechanism, chooses the scale for instability differently in different pressure levels in the troposphere.

A number of other conclusions can be drawn from the present investigation. (1) There is evidence that large scale waves propagate energy upward, while the shorter waves do not. (2) There is accumulation of energy in A_Z and A_E during a period of 17 days as opposed to an instantaneous conversion to kinetic energy. (3) Linear unconditional heating can account for the wave amplification that is observed in the tropics but fails to describe the dissipative stages. Such amplification brings about asymmetries in the tropical motion field and can play an essential role in the general circulation, particularly when mid-latitude baroclinic systems are also included.

clinic systems are also included.

APPENDIX

APPENDIX

The ω-equation for the present model which is consistent with the balance equation

$$\nabla^2\theta = -\frac{P_0^{\kappa}}{c_p} f_0 \frac{\partial}{\partial P^{\kappa}} \nabla^2\psi$$

is

$$\frac{c_p\sigma}{P_0^{\kappa}} \nabla^2\omega + f_0^2 \frac{\partial}{\partial P^{\kappa}} \frac{\partial\omega}{\partial P} = f_0 \frac{\partial}{\partial P^{\kappa}} J(\psi, \nabla^2\psi + f) + \frac{c_p}{P_0^{\kappa}} \nabla^2 J(\psi,\theta)$$

$$- A f_0 \frac{\partial}{\partial P^{\kappa}} \nabla^4\psi + f_0 g \frac{\partial}{\partial P^{\kappa}} \left(\hat{k} \cdot \nabla x \frac{\partial \bar{\tau}}{\partial p} \right) - \frac{c_p}{P_0^{\kappa}} \frac{1}{c_p} (P_0/P)^{\kappa} \nabla^2 H$$

When double Fourier series and vertical finite differencing are substituted in this equation, the ω-equation takes the spectral form given by Eq. (4) of Chapter II. The right-hand side of this spectral ω-equation is described by linear and non-linear terms involving components of ψ and θ for every pressure level. These components of ψ and θ are solved from the spectral vorticity and thermodynamic equations for every time step. If this right-hand side is denoted by SUM (j), the spectral ω-equation can be written

$$- \frac{c_p \sigma_j (P_{j-1}^{\kappa} - P_{j+1}^{\kappa})}{D(m'',n'') P^{\kappa}} \omega_{1\ n''}^{j\ m''} + \frac{f_0^2}{(P_{j-2} - P_j)} \omega_{1\ n''}^{j-2\ m''} - \frac{(P_{j-2} - P_{j+2}) f_0^2}{(P_{j-2} - P_j)(P_j - P_{j+2})}$$

$$D(m'',n'') P^{\kappa} \frac{f_0^2}{\quad} \omega_{\quad}^{j\ m''} \quad \omega_{j-2}^{\quad} \quad \text{SUM}(j) \quad (P_{j-2} - P_j)(P_j - P_{j+2})$$

$$\omega_{1\ n''}^{j\ m''} + \frac{f_0^2}{(P_j - P_{j+2})} \omega_{1\ n''}^{j+2\ m''} = \text{SUM}\ (j)$$

Superscript j denotes the pressure level and subscript 1 denotes the real part of complex ω. When level j is specified and $\omega^0 = \omega^8 = 0$, a set of three equations and three unknowns ω_1^2, ω_1^4, ω_1^6 for every m and n results, i.e.,

$$j = 2, \quad -a_1\omega_{1\ n''}^{2\ m''} + a_2\omega_{1\ n''}^{0\ m''} + a_3\omega_{1\ n''}^{4\ m''} = \text{Sum (2)}$$

$$j = 4, \quad -a_4\omega_{1\ n''}^{4\ m''} + a_5\omega_{1\ n''}^{2\ m''} + a_6\omega_{1\ n''}^{6\ m''} = \text{Sum (4)}$$

$$j = 6, \quad -a_7\omega_{1\ n''}^{6\ m''} + a_8\omega_{1\ n''}^{4\ m''} + a_9\omega_{1\ n''}^{8\ m''} = \text{Sum (6)}$$

where a_i denote the proper coefficients of $\omega_{1\ n''}^{j\ m''}$. Rearranging the algebraic equations, we obtain

$$-a_1\omega_{1\ n''}^{2\ m''} + a_3\omega_{1\ n''}^{4\ m''} + 0 = \text{Sum (2)}$$

$$a_5\omega_{1\ n''}^{2\ m''} - a_4\omega_{1\ n''}^{4\ m''} + a_6\omega_{1\ n''}^{6\ m''} = \text{Sum (4)}$$

$$0 + a_8\omega_{1\ n''}^{4\ m''} + a_7\omega_{1\ n''}^{6\ m''} = \text{Sum (6)}$$

There are 20 components (m", n") and hence 20 sets of algebraic equations of order 3 for unknowns $\omega_{1\ n''}^{2\ m''}$, $\omega_{1\ n''}^{4\ m''}$, $\omega_{1\ n''}^{6\ m''}$.

REFERENCES

REFERENCES

Bates, J. R., 1970: Dynamics of disturbances on the intertropical convergence zone. Quart. J. Roy. Meteor. Soc., 96, 677-701.

Charney, J. G., 1963: A note on large-scale motions in the tropics. J. Atmos. Sci., 20, 607-609.

_____, 1968: The intertropical convergence zone and the Hadley circulation of the atmosphere. Proceedings of the WMO-IUGG Symposium on Numerical Weather Prediction, Tokyo, Japan, Nov.-Dec. 1968, Japan Meteorological Agency. Tokyo, March 1969.

_____, and P. G. Drazin, 1961: Propagation of planetary-scale disturbances from the lower into the upper atmosphere. J. Geophys. Res., 66, 83-109.

_____, and A. Eliassen, 1949: A numerical method for predicting the perturbations of the middle latitude westerlies. Tellus, 1, 38-54.

Clark, J. H., 1969: Spectral model of the winter stratosphere. Ph.D. Thesis, Florida State University.

Dickinson, R. E., 1971: Details of the model and simulation of gross features of the zonal mean troposphere. Mon. Wea. Rev., 99, 501-510.

Frank, N. L., 1970: On the nature of upper tropospheric cold core cyclones over the tropical Atlantic. Ph.D. Thesis, Florida State University.

Holton, J. R., 1971: A diagnostic model for equatorial wave disturbances: The role of vertical shear of the mean zonal wind. J. Atmos. Sci., 28, 55-64.

Jordan, C. L., 1958: Mean soundings for the West Indies area. J. Meteor., 15, 91-97.

Krishnamurti, T. N., 1969: An experiment in numerical prediction in equatorial latitudes. Quart. J. Roy. Meteor. Soc., 95, 594-620.

_____, 1971a: Tropical east-west circulation during the northern summer. J. Atmos. Sci., 28, November issue (in press).

_____, 1971a: Tropical east-west circulation during the northern summer. J. Atmos. Sci., 28, November issue (in press).

_____, 1971b: Observational study of tropical upper tropospheric motion field during northern summer. J. Appl. Meteor., 10, December issue (in press).

Kuo, H. L., 1949: Dynamic instability of two-dimensional nondivergent flow in a barotropic atmosphere. J. Meteor., 6, 105-122.

Lorenz, E. N., 1960: Energy and numerical weather prediction. Tellus, 12, 364-373.

Mak, M. K., 1969: Laterally driven stochastic motions in the tropics. J. Atmos. Sci., 26, 41-64.

Manabe, S., J. L. Holloway, and H. M. Stone, 1970: Tropical circulation in a time-integration of a global model of the atmosphere. J. Atmos. Sci., 27, 580-613.

Nitta, T., 1967: Dynamical interaction between the lower stratosphere and the troposphere. Mon. Wea. Rev., 95, 319-339.

_____, 1970: Statistical study of tropospheric wave disturbances in the tropical Pacific region. J. Met. Soc. Japan, 48.

_____, and N. Yanai, 1969: A note on the barotropic instability of the tropical easterly current. J. Met. Soc. Japan, 47, 127-130.

Ooyama, K., 1969: Numerical simulation of the life cycle of tropical cyclones. J. Atmos. Sci., 26, 3-40.

Palmer, C. E., 1952: Tropical meteorology. Quart. J. Roy. Meteor. Soc., 78, 126-164.

_____, 1951: Tropical meteorology. Compendium of Meteorology, Am. Meteor. Soc., 859-880.

Peng, L., 1965: A simple numerical experiment concerning the general circulation of the lower stratosphere. Pure and App. Geoph. 61, 191-218.

Phillips, N. A., 1956: The general circulation of the atmosphere: A numerical experiment. Quart. J. Roy. Meteor. Soc., 82, 123-164.

_____, 1963: Geostrophic motion. Revs. Geophys., 1, 123-176.

Pike, A. C., 1971: Intertropical convergence zone studied with an interacting atmosphere and ocean model. Mon. Wea. Rev., 99, 469-477.

Pike, A. C., 1971: Intertropical convergence zone studied with an interacting atmosphere and ocean model. Mon. Wea. Rev., 99, 469-477.

Riehl, H., 1954: Tropical meteorology. McGraw-Hill Book Co., New York, N. Y., 392 pp.

Rosenthal, S. L., 1967: On the development of synoptic-scale disturbances over the subtropical oceans. Mon. Wea. Rev., 95, 341-346.

Rutherford, I., 1969: The vertical propagation of geostrophic waves in a low-order spectral model. Ph.D. Thesis, McGill University.

Saha, K. R., 1971: Mean cloud distribution over tropical oceans. Tellus, 23, 183-196.

Wallace, J. M., 1971: Spectral studies of tropospheric wave disturbances in the tropical western Pacific. Rev. Geoph. Space Phys., 9, 557-612.

_____, and C. P. Chang, 1969: Spectrum analysis of large-scale wave disturbances in the tropical lower troposphere. J. Atmos. Sci., 26, 1010-1025.

Yamasaki, M., 1969: Large-scale disturbances in a conditionally unstable atmosphere in low latitudes. Papers in Meteor. Geophys., Tokyo, 20, 289-336.

Yanai, M., 1961: Dynamical aspects of typhoon formation. J. Meteor. Soc. Japan, 39, 282-309.

_____, T. Maruyama, Ts. Nitta, and Y. Hayashi, 1968: Power spectra of large scale disturbances over the tropical Pacific. J. Meteor. Soc. Japan, 46, 308-323.

Young, J. A., 1968: Comparative properties of some time differencing schemes for linear and non-linear oscillations. Mon. Wea. Rev., 96, 357-364.

VITA

Jacob Padro, Citizen of Canada, was born March 13, 1941, in Jerusalem, Israel. He received B. Sc. degree in 1963, and M. Sc. degree in 1966 from McGill University, Montreal, Canada and Ph. D. degree from Florida State University in 1971.

His professional experience consists of work as forecaster at the Canadian Meteorological Service in 1966-1967 and as research associate with Prof. M. B. Danard at University of Waterloo, Canada for six months in 1970-1971.

In 1966 he wrote M. Sc. Thesis at the McGill University entitled "Spherical harmonic analysis of the 1000 mb surface", and a paper with Dr. T. N. Krishnamurti entitled "On wave motions in a simple tropical spectral experiment" submitted for publication to Monthly Weather Review. For project under Dr. M. B. Danard at the University of Waterloo he wrote a paper entitled "Maintenance of synoptic-scale systems in mid-latitudes."

His teaching experience includes Meteorology Laboratory course and (as substitute instructor) Dynamic Meteorology.

Laboratory course and (as substitute instructor) Dynamic Meteorology.